ASSISTIVE DEVICE FOR ELDERLY REHABILITATION: SIGNAL PROCESSING TECHNIQUES

SANGIT SASIDHAR

(B.Tech., Sardar Vallabhbhai National Institute of Technology, India)

A THESIS SUBMITTED

FOR THE DEGREE OF DOCTOR OF PHILOSOPHY

DEPARTMENT OF ELECTRICAL AND COMPUTER ENGINEERING

NATIONAL UNIVERSITY OF SINGAPORE

2013

Declaration

I hereby declare that this thesis is my original work and it has been written by me in its entirety. I have duly acknowledged all the sources of information which have been used in the thesis.

This thesis has also not been submitted for any degree in any university previously.

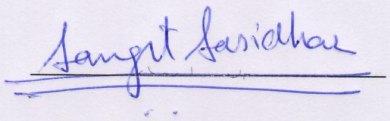

NAME: Sangit Sasidhar

DATE: 25/01/2013

Acknowledgements

I sincerely thank my supervisor, Assoc. Prof. Dr. Sanjib Kumar Panda, for offering me a challenging project that ignited my interest in Signal Processing and Rehabilitation. He has been a source of constant encouragement, necessary support and patient guidance for the entirety of my thesis work. I learnt from him to be independent, passionate, open-minded and inquisitive in research.

I would like to thank my co-supervisor, Prof. Jianxin Xu, for his invaluable help in iterative learning control and its application in biomechanical models. His wealth of knowledge and experience has helped me to sail through many difficult situations. He has been an unending source of inspiration for me to strive to be a better researcher.

I would like to thank NUS for giving me the opportunity and research scholarship to work in an environment conducive for research. I am thankful to St. Luke's hospital for inspiring me to work in an area of research that is beneficial to the society, in general and specially the elderly citizens. I would like to thank Dr. Guan Cuntai, Dr. Yen, Dr. Martin Buist, Dr. Rajesh, Dr. Sahoo and Dr. Krishna for stimulating discussions in signal processing, circuit designs, optimization techniques and biological modelling.

I am grateful to lab officers Mr. Y.C.Woo and Mr. M.Chandra for helping me with any matter, whenever necessary and ensuring a lively environment in the lab. I am thankful to Abhro, Xinhui and Haihua for their inspiring comments and discussions in the lab. I am indebted to Prasanna for helping me

design and setup the MMG measurement system. I am grateful to Prasanna, Bhunesh, Vinod, Chinh, Souvik, Parikshit, Krishna, Jeevan and Ramprakash for volunteering as subjects for the EMG and MMG data acquisition systems. I would like to thank NUS for giving me the opportunity and research scholarship to work in an environment conducive for research.

I would like to thank my dad, my brother and Jagadish for reading through my thesis umpteen number of times and helping me correct it.

I consider myself lucky to have friends who have been a surrogate family to me. A huge thanks to Jagadish, Padma, Muthu, Sudar, Nandhini and Abhilasha for listening to my rants, advising me and keeping me sane during my time here in Singapore.

Thank you Kunju, Amma and Achan for being there for me whenever I needed you and for showering me with your love and support. I would like to dedicate this thesis to my dad, my mom and my brother.

Contents

Summary

The life expectancy of human beings in general, has improved in the last decade throughout the world. With advancing age, the ageing population is likely subjected to stroke and neurological degenerative diseases like Parkinsons disease, Dementia or Alzheimers disease and, the agility of the brain to process information critical for going about daily living slows down. As a result, persons affected by these disorders lose their dexterity, reflexes and speed in performing simple day-to-day tasks.

Rehabilitation robotics is used in both in-patient and out-patient rehabilitation but it is expensive and bulky to be used for home rehabilitation. Comprehensive training for basic but necessary tasks for the elderly cannot be given sitting in a clinic or rehabilitation centre. Moreover, these tasks are a closer outlook to the elderly persons actual life; hence, using an assistive robotic system at homes for day-to-day activities could initiate a continuous recovery for the patient instead of only at rehabilitative sessions. Such assistive systems need to be scaled down in terms of the number of the sensors and actuators used, without compromising on the quality of care and end results. This is to ensure that the rehabilitation process doesn't become a burden to the elderly user.

The focus of this thesis is on developing algorithms for better processing of Electromyography (EMG) and Mechanomyography (MMG) signals, improving EMG Torque relation for the elbow joint for a reduced number of EMG electrodes and for identifying and classifying different forearm movements and exercises using MMG signals. The following problems are investigated and corresponding solutions are provided in this approach:

Adaptive Signal Processing of the EMG signal to eliminate power line interference using Hilbert-Huang Transform: Estimation and removal of power line noise in EMG is the first step in processing the EMG signal. For elderly patients, such measurements and processing becomes challenging as the actual EMG signal is at a much lower amplitude, compared to a young healthy person resulting in a much lower Signal to Noise Ratio (SNR). The problem of the power line frequency overlapping with the power spectrum of the biosignal is solved by extracting the power line frequency using Hilbert-Huang transform which then is fed into an adaptive filter utilizing the Least Mean Squares (LMS) algorithm to nullify the effect of power line frequency in the biosignal. Different conditions were simulated to ensure that the proposed filter algorithm performed satisfactorily under all conditions and a comparison was made between a LMS adaptive filter and a variable step size adaptive filter. Experimental results with measured EMG signal are presented to show the efficacy of the proposed algorithm.

Parameter Estimation of a Hybrid Muscle Model using an Iterative Learning Predictor for Estimation of the Joint Torque: Unknown parameters of the biomechanical muscle model are estimated during dynamic contractions of the hand using dual channel EMG signal by an Iterative Learning Predictor (ILP). The design of an iterative learning predictor for estimating the missing parameters of the muscle model is outlined and a pointwise ILC is proposed to ensure maximum tracking between the predicted muscle length and the measured muscle length. A hybrid muscle model is then proposed that utilizes the modified Hill's model for agonist-antagonist muscles to predict their joint torques from channels of EMG data. This predicted torque is used to train a neural network for estimating the actual joint torque from the muscle activation. The implementation of the ILC

predictor in this hybrid muscle model is presented and it is found that the error in the joint torque predicted by the hybrid model is less when compared to the fixed function and the neural network model. The ILP ensures that the maximum number of iterations for processing each data point for calculation of the contractile element length is less than 20. On a hardware platform it is possible to implement this ILC predictor with real time constraints.

Mechanomyography Feature Extraction and Classification of Forearm Movements using Empirical Mode Decomposition and Wavelet Transform: The MMG system is designed to measure data using accelerometers built into the assistive device and, hence, doesn't require any active involvement of the patient. Different muscles are evaluated for the measurement of the MMG signals for forearm and hand activity. The classification of the eight forearm movements based on wavelet transform features and Empirical Mode Decomposition (EMD) features using an Multilayer Perceptron (MLP) classifier is explored. The requisite theory is presented and two new features based on the EMD and Hilbert spectrum are defined and used for feature extraction. Experimental results for the same are presented and it is found that, the wavelet transform based and EMD based feature sets performed best for classifying movements of hand and wrist using the MMG signal.

The algorithms in this study follow real time constraints for assistive devices while the measurement protocols ensure that the biosignals were broadly representative of that measured from the elderly. Thus, the EMG and MMG signal processing techniques can be used in implementing a sensory system for an upper limb assistive device for the elderly.

List of Figures

List of Tables

List of Acronyms

CE	Contractile Element
DC	Direct Current
ECG	Electrocardiography
EMD	Empirical Mode Decomposition
EMG	Electromyography
FES	Functional Electrical Stimulation
FFT	Fast Fourier Transform
GA	Genetic Algorithm
GUI	graphical user interface
HHT	Hilbert-Huang Transform
HHT-LMS	Hilbert-Huang Transform based Least Mean Squares
HSA	Hilbert Spectral Analysis
IF	Instantaneous Frequency
IIR	Infinite Impulse Response
ILC	Iterative Learning Control
ILP	Iterative Learning Predictor
IMF	Intrinsic Mode Function
LMS	Least Mean Squares
MAV	Mean Absolute Value
MES	Myoelectric Signal

MLP	Multilayer Perceptron
MMG	Mechanomyography
MSE	Mean Squared Error
MU	Motor Unit
MUAP	Motor Unit Action Potential
MVC	Maximum Voluntary Contraction
NA	Neural Activation
PC	Personal Computer
PCA	Principal Component Analysis
PLI	Power Line Interference
PSD	Power Spectral Density
PSO	Particle Swarm Optimization
QDA	Quadratic Discriminant Analysis
RMS	Root Mean Square
SNR	Signal to Noise Ratio
SSC	Slope Sign Changes
SVM	Support Vector Machine
ZC	Zero Crossings

List of Symbols

ψ	Wavelet Basis
V_j	jth Wavelet Transform
W_{j+1}	High Frequency Subspace
$d_1(k), d_2(k)\ldots$	Detailed Wavelet Sub-Patterns
$Ag/AgCl$	Silver/ Silver Chloride
x_i^{RMS}	Root Mean Square Value
$\overline{x_i}$	Mean Absolute Value
Δx_i	Mean Absolute Value Slope
l_0	Waveform Length
W_E	Wavelet Entropy
$e_{max}(t),\ e_{min}(t)$	Cubic Spline Upper and lower envelopes
IF_n	Powerline Instantaneous Frequency
a_j	Instantaneous Amplitude
ω_j	Instantaneous Phase
v_j	Instantaneous Frequency
$r(t)$	Reference Signal
$w(t)$	Weight Vector
$e(t)$	Error Signal
$p(t)$	Power Line Noise
$d(t)$	Desired Signal
$H_{EMG}(\omega)$	EMG Transfer Function
$F_{CE},\ F_{SE},\ F_{PE}$	Force Developed by the CE, SE and PE elements
$L_{CE},\ L_{SE},\ l_{PE}$	Length of CE, SE and PE elements
f_l	Force generated by change in muscle length
f_v	Force generated by change in muscle velocity

y_d	Desired ILC Output
T	Torque
A_{RMS}	RMS of MMG Signal
W_{jk}^{RMS}	Wavelet RMS Value
W_{jk}^{MAV}	Wavelet MAV Value
W_{jk}^{H}	Wavelet Shannon Entropy
W_{jk}^{MNF}	Wavelet Mean Frequency
W_{jk}^{L0}	Wavelet Waveform Length
$Hil(IMF_i)$	Hilbert Energy of IMF
Hil_{IMF_i}	IMF Median Frequency
$H(IMF_i)$	IMF Shannon Entropy
$MNF(IMF_i)$	IMF Mean Frequency
WL_{IMF_i}	IMF Waveform Length

1

Introduction

1.1 Ageing

The life expectancy of human beings in general, has improved in the last decade throughout the world. In respect of Singapore, one out of every five people will be reaching the age of 65 by the year 2030. Today's ageing population is well educated and comparatively richer than their predecessors, and prefers living independently. The proportion of old people above the age of 65, living alone or only with their spouses, has gone up from 9.7% in 1995 to 19.9% in 2005 [1]. But with higher life expectancy, the ageing population is likely to be subjected to neurological degenerative diseases like Parkinson's, Dementia or Alzheimer's disease. With advancing age, the agility of the brain to process information that are critical for going about doing daily chores slows down, and as a result, persons affected by these disorders lose their dexterity, reflexes and speed in performing simple day-to-day tasks. The number of people suffering from dementia throughout the world may almost double every 20 years to reach over 100 million by 2050 [2].

1.2 Stroke

Stroke is another crippling condition resulting in total or partial loss of motion for the elderly. A stroke can be described as a rapid loss of brain function(s) due to disruption in the blood supply to the brain. This can be due to lack of glucose and oxygen supply, caused by blockage in the blood vessel (ischemic stroke) or due to a hemorrhage . As a result, the affected areas of the brain are unable to carry on its specific functions properly, leading to an inability to move one or more limbs on one side of the body, inability to understand or formulate speech, or inability to see one side of the visual field. A stroke is a medical emergency and can cause permanent neurological damage, complications, and sometimes, even death. It is the number two cause of death and is likely to become the leading cause of death worldwide in the near future [3]. Already it has become the leading cause of adult disability in the United States and Europe, and is a major cause of long-term disability worldwide [4]. Mortality due to stroke has reduced considerably in the last few decades but stroke survivors usually have to live with some form of disability. Fifteen million people worldwide suffer from stroke every year among which five million people are permanently disabled [5]. Disability also affects 75% of stroke survivors in some form or the other, drastically reducing their activities of daily living and deterring their employability.

Stroke can affect patients physically, mentally, emotionally, or any combination of all the three. The results of stroke vary widely, depending on the size and location of the affected lesion. Dysfunctions correspond to the specific areas in the brain that have been damaged. Some of the physical disabilities that can result from stroke include paralysis, numbness, pressure sores, pneumonia, incontinence, apraxia (inability to perform learned move-

ments), and difficulties in carrying out daily activities, loss of appetite, loss of speech, loss of vision, and pain. Prevention and early recognition of medical complications of stroke best maximizes neurologic and functional recovery.

Hemiparesis, partial weakness of one side of the body, or hemiplegia, complete paralysis of one side, commonly occurs after a stroke. If all inputs to a peripheral muscle are lost, the muscle feels soft and lax. Muscle tone is typically reduced in early stages after stroke (hypotonia) but may later become increased (hypertonia). This change happens due to sudden change from no or decreased muscle stretch reflexes to brisk muscle stretch reflexes. Spasticity is associated with spontaneous repetitive muscle contractions and the resultant loss in range of motion of the corresponding limb [6].

1.3 Neuroplasticity

Plasticity is the ability of cells to alter any aspect of their phenotype at any stage in their development in response to abnormal changes in their state and environment. Neuroplasticity is the changing of neurons, the organization of their networks, and their function via new experiences [7]. A surprising consequence of neuroplasticity is that the brain activity associated with a given function can move to a different location; this can result from normal experience and also occurs in the process of recovery from brain injury.

Neuroplasticity is the fundamental issue that supports the scientific basis for treatment of acquired brain injury and dementia with goal-directed experiential therapeutic programs in the context of rehabilitation approaches to the functional consequences of the injury. Most muscles are composed of assorted muscle units with functional difference but dominated by a particular type of muscle fibre based on the primary function of the muscle. Muscle fibres

are totally adaptable and respond entirely to any change in demand that is transmitted through the terminal synapse at the neuromuscular junction that respond by being replaced, re-innervated or by being rejuvenated. These changes release specific intra-neural hormones, which then act to modify the nervous system so that stimuli can have a different effect or in other words, the brain is physiologically restructured. This restructuring cannot happen, if the neuronal cell body itself has been destroyed and could result in the permanent loss of certain functions associated with corresponding neuron.

Physical activity proportionately increases a person's ability to perform physical work. An increasingly repetitive physical activity, known as stressing, can take the form of therapy that includes planned physical conditioning. Stressing is the repetition of a stimulus to produce an analogue effect of faithfully reproduced stimulation. Physiological stressing is the faithful repetition of a stimulus for a significant period of time to produce change in the system. Thus, it makes restructuring of the normal movement and also builds new motor pathways[8].

1.4 Rehabilitation

Rehabilitation is the process by which patients with disabling strokes or dementia undergo treatment to help them return to normal life as much as possible by relearning and regaining the skills of everyday living. Rehabilitation is a coordinated program that provides reliable, patient-centric restorative care to minimize the impairment, disability and handicap caused by stroke. Rehabilitation services can be classified as follows[6].

- **In-patient Rehabilitation**: In-patient Rehabilitation is recommended for patients who have completely lost motor function due to a stroke.

The patient is admitted to the rehabilitation cell of a hospital and the program is implemented in two stages. The initial stage known as 'acute comprehensive inpatient rehabilitation' consists of a comprehensive program aimed to maximize recovery and minimize disability and handicap. The final stage consists of medical services for the patient such as rehabilitation, therapy and hospice after acute rehabilitation programme and is known as 'sub-acute rehabilitation'.

- **Out-patient Rehabilitation**: The patient receives outpatient services at the rehabilitation facility, hospital or therapist's office either as initial or subsequent treatment. The patient goes to a facility or facilities where therapeutic services including physical, recreational and occupational therapies are provided. When facilities are in different locations, the coordination among the centers becomes a hindrance unless the patient has a strong case management system between the rehabilitation centers. This mode of rehabilitation can be used for recovering motor control for stroke patients and elderly patients affected with dementia.

- **Home Rehabilitation**: Many patients prefer treatment at home for disabling conditions because of convenience and familiarity. All comprehensive home health programs use nurses, physicians, therapists and social workers to provide for rehabilitative services. The same programmatic structure is followed at home. It could be said to be an extension of the inpatient rehabilitation with the facilities and comforts of ones own home.

Out-patient and in-patient programs try to optimize the same methodology for rehabilitation. It requires a one-to-one interaction between the therapist and the patient, with the therapist guiding the non-functioning part of the

body in exercise for recovery. The brain through visual feedback is led to believe that the arm/leg is in motion. The frequency and duration of the rehabilitation sessions vary with the severity of the disability. Motor practice consisting of simple, repetitive motions leading to a form of use-dependent plasticity that results in the brain rewiring its neurons and a re-organization of the pathways in the spinal cord and the motor cortex. With extended sessions in physiotherapy, faster recovery is a possibility.

Recently, rehabilitation centers have chosen a programmatic structure to manage specific clinical programs. In this model, a rehabilitation manager evaluates and modifies policies and procedures, service delivery and also coordinates all staff that provides stroke care.

All three traditional models of rehabilitation services are not without their drawbacks.

1. Larger number of hours for physiotherapy exercises improves the chance of recovery. This results in the patient incurring additional charges for the extra hours, that makes rehabilitation expensive.

2. Each therapist can attend to only one patient at a time during each session as each patient requires undivided attention and encouragement during rehabilitation or they may not be motivated to come for further sessions.

3. The patient is going to do the same monotonous exercise numerous times for repeatability of the motion.

4. Home rehabilitation may give the patient the comfort and familiarity of staying at home but again would be much more expensive as compared to out-patient or in-patient rehabilitation.

5. Each patient's recovery process is different and thus a different rehabilitative program is required for each patient. This can be quite time consuming and illogical for the rehabilitation manager to develop and implement in practice.

Moreover, upper limb rehabilitation requires more time and effort from the patient and the therapist as compared to lower limb rehabilitation. Though studies show similar recovery rates for both the cases within a short time period after stroke, typically 30 days, recovery rates are better for the former for a longer time period after the onset of stroke [9]. This is due to the larger functional area of the brain for the upper limb as compared to the lower limb as functions of the upper extremity requires finer motor control, for which the patient cannot readily compensate[10]. Thus, lower limb rehabilitation leads to more and faster functional improvement and less disability than upper limb rehabilitation over the similar time course.

If the therapist's role can be substituted with an assistive robotic system for conducting the repetitive tasks and exercises, it would help to overcome the above-mentioned difficulties.

1.5 Assistive Robotic Systems

There are many commercially available robotic systems that help in the rehabilitation of patients for both upper limb and lower limb paralysis. These systems concentrate on rehabilitating specific functions by repetition and feedback.

- **LOKOMAT:**The Lokomat developed by Hocoma is used by therapists for lower limb rehabilitation and is the world's first driven gait orthosis that automates locomotion therapy on a treadmill and improves the

efficiency of treadmill training[11]. A driven robotic gait orthosis guides the patient's legs on a treadmill allowing for faster progress through longer and more intensive training sessions as compared to manual treadmill training. The patient's walking activity is monitored and assessed for signs of improvement in gait. The gait patterns and the guidance force are individually adjusted as per the patient's needs. The device also provides visual feedback of the patient's performance, thus motivating them for further improvement. Clinical studies of the effectiveness of the device in stroke rehabilitation all point to an improvement in the gait of the patient[12, 13].

- **MIT-MANUS:**The MIT-MANUS robotic system learns various types of exercises from a physical therapist and guides the patient through them in rehabilitation by providing visual, auditory and tactile feedback [14]. The device can manipulate a powerless limb just like any hand-over-hand therapy or measure the speed and direction of a patient-generated movement. The robotic arm has low near isotropic inertia and reduced friction in the arm so that it gets out of the way if it senses the patient trying to move the arm. It also helps in motion if the patient is unable to move the hand and adjusts the level of assistive power, based on the person's ability to do arm movement.

  Recent works in the Institute of Infocomm Research, Singapore on a brain computer interface (BCI) using this device measures the intent of the patient by using the EEG signals and then accordingly maneuvers the robotic arm [15].

- **ARMEO:**The Armeo developed by Hocoma is used for the arm rehabilitation and is similar to the MIT-MANUS in operation. Therapists can

easily design custom training programs for each patient that address specific movements and help to promote active movement. The patient performs the pre-chosen sequence of exercises in a self-training mode. A virtual reality-training environment clearly displays the functional task and patient's performance [16]. All performance data are stored in the computer and can be used by the therapist to supervise, assess and document the patient's progress.

- **MYOMO:** An upper limb rehabilitation device developed by MYOMO, Inc. uses EMG signals to sense residual electrical muscle activity and forwards the data to a robotic device that uses it to assist the patient in performing the desired movement. The power output of the device is customized to patient's ability. EMG-driven robotics requires that patients be actively engaged throughout the therapy session. No electrical stimulation or invasive procedures are employed for limb movement. Clinical studies show an improvement in mobility of stroke patients ranging from 4 weeks to 21 years after the onset of stroke[17]. This system is the simplest and easiest for the patient for day-to-day usage.

The MIT-MANUS, ARMEO and MYOMO are functionally different from other rehabilitative manipulators. These systems don't make the patient repeat the same monotonous exercise, also known as static biofeedback, but concentrate on task specific exercises for rehabilitation, providing functional training and motivation that are key factors for successful rehabilitation. This approach known as task-oriented or dynamic biofeedback has shown better recovery rates in patients as compared to static biofeedback [18].

In systems like MYOMO, the brain through visual feedback is led to believe that the arm is in motion. The change from no movement of the arm

to assurance that the hand is moving due to the patient's efforts is highly motivational for a faster recovery.

1.6 Electromyography

The central nervous system is organized in a hierarchical fashion. Motor programming takes place in the premotor cortex, the supplementary motor area, and other associated areas of the cortex. A Motor Unit (MU) consists of a α-motoneuron in the spinal cord and the muscle fibers it innervates. The α-motoneuron is the final point of summation for all the descending and reflex inputs. The skeletal muscle is activated by the a-motoneuron at synapses called neuromuscular junction or innervation sites. The net membrane current induced in this motoneuron by the various synaptic innervation sites determines the discharge (firing) pattern of the motor unit and thus the activity of the MU. The number of MU(s) per muscle in humans may range from about 100 for a small hand muscle to 1000 or more for large limb muscles.

The Motor Unit Action Potential (MUAP), which originates at the innervation sites of each muscle, is a temporal and spatial summation of the electric potentials propagating through the muscle fibers. The Myoelectric Signal (MES) is the electrical activity of the muscles at the neuromuscular junction and is the summation of all the membrane currents in the MU. Electromyography (EMG) is the recording of the MUAP(s) of the skeletal muscles and a record of the changes in the Myoelectric Signal (MES) is called an electromyogram.

The MUAP originates at the neuromuscular junction and travels in opposite directions along the muscle fiber, with a velocity that depends on the fiber diameter and whose physiological range is between 3 m/s and 5 m/s

with an average of around 4 m/s. This propagation velocity is referred to as conduction velocity (CV) and is related to membrane properties. Such properties, which are reflected by the muscle fiber action potential, are different in different fiber types with larger muscle fibers having higher conduction velocities [19].

The conduction velocity can be measured by using an array of electrodes for measuring the EMG signal for the same muscle group. Choosing one set of electrode data as a time reference signal, the cross-correlation function for the other electrode data with respect to the reference signal is calculated. The distance between any two electrodes divided by the time delay between the peaks of the cross-correlation function gives the conduction velocity.

1.7 Adaptive Filtering of EMG Signal

The electromyogram (EMG) or the myoelectric signal has become an important input or feedback parameter in biomechanical analysis or for physiotherapy sessions. The study of EMG signals is difficult for two main reasons. Firstly, the SNR of these signals is low since the EMG signals are measured at very low amplitudes of the order of millivolts as shown in Fig.1.1. Secondly, since human body acts as an antenna, the EMG signals are corrupted by electromagnetic power line interference from the surrounding environment [20, 21]. Removing the power line interference and its harmonics from surface EMG is difficult because the myoelectric signal lacks a distinctive waveform.

For elderly patients, such measurements and processing become challenging as the actual EMG signal is at a much lower amplitude when compared to a young healthy person, resulting in a much lower SNR.

The EMG signals can be detected and recorded using invasive techniques

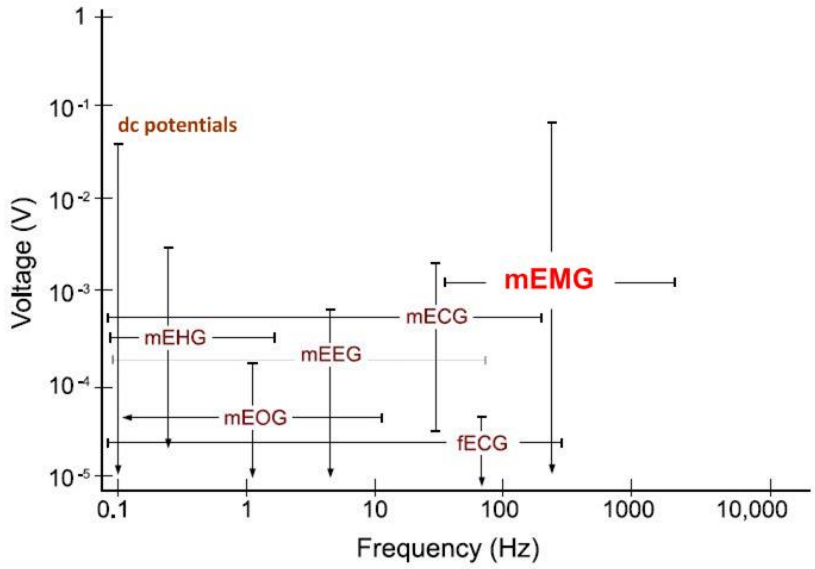

Figure 1.1: Magnitude of Different Bio-signals.

by inserting a needle electrode underneath the skin or non-invasive techniques by using electrodes on the surface of the skin. Needle electrode directly measures the firing pattern of the muscle unit it is inserted into and is more accurate compared to surface electrodes, which provides a global measure of the muscles activities [22]. But surface electrodes are much easier to use especially if measurements have to be repeated frequently or if the electrode has to be in contact during the operation of any robotic system. However, it also suffers from greater interference from the power line as the surface EMG signals bandwidth lies predominantly in the range of ***10*** to ***350*** Hz [22] and signal degradation due to an increase in impedance from the outermost layer of skin, including dead skin material and oil secretions. The issue of signal gradation due to increase in impedance can be reduced by careful skin preparation to ensure good electrical contact with the electrodes and differential amplification with common-mode rejection ratio of more than 100 dB [23].

Modern biomedical amplifiers have a very high common mode rejection ratio. Nevertheless, recordings are still contaminated by residual Power Line Interference (PLI). The removal of PLI using traditional types of digital or analogue notch filters has the inherent disadvantage of suppressing signal components in the vicinity of the power line frequency and its harmonics. The power line interference is not fixed at a frequency of 50 Hz or 60 Hz but has been found to vary between ± 2 % of the nominal frequency. Moreover, the surface EMG signal bandwidth lies predominantly in the range of 10 to 350 Hz. Hence, a fixed notch filter of 50/60 Hz would lead to ineffective filtering if there is a deviation of frequency in the power line interference and the inherent disadvantage of suppressing signal components in the vicinity of the power line frequency and its harmonics.

Adaptive techniques are preferred because the power line noise changes over the time and adaptive filters can perform satisfactorily in an environment where complete knowledge of the relevant signal characteristics is not available [24]. Different adaptive approaches have been proposed in the literature to attenuate this noise, such as adaptive FIR notch filter [25], adaptive IIR notch filter [26], adaptive notch filter using Fourier transform [27] and numerous adaptive filters training methods. An adaptive Laguerre filter for the elimination of power line noise is discussed in [28] that is a stable and is a less complex filter as compared to other FIR filters. The subtraction procedure is found to be useful in removing of power line interference from Electrocardiography (ECG) signals [29]. This procedure does not affect the signal frequency components around the interfering frequency. However, the interfering signal needs to be known for adaptive filters and for the subtraction procedure. This reference input must either be recorded in real time along with the EMG, which is expensive in terms of memory, or must be generated

synthetically such that it follows the power line frequency.

Bourdraa et.al. [30] proposed a signal filtering method based on EMD for removing the noisy Intrinsic Mode Function (IMF) to filter the signal. The authors focus on the removal of high frequency noise from standard test signals and not on signals with overlapping bandwidths. But filtering the PLI from EMG using this method is challenging as, the bandwidths of the EMG signal and the PLI overlap.

1.8 Myoelectric Control, Features Extraction and Classifier Algorithms

Myoelectric control is the preferred scheme for the control of upper limb prosthesis or orthotic devices. In these systems, the processed EMG signal is used as a control input and the generated result is used to actuate the motor controlling limb movement as shown in Fig. 1.2.

The EMG or the Myoelectric Signal (MES) of a muscle is the summation of the different Motor Unit Action Potential (MUAP). This can include the MUAP(s) of nearby muscles as well. For a single channel recording of EMG, if the muscle groups are very close to each other, it would be difficult to

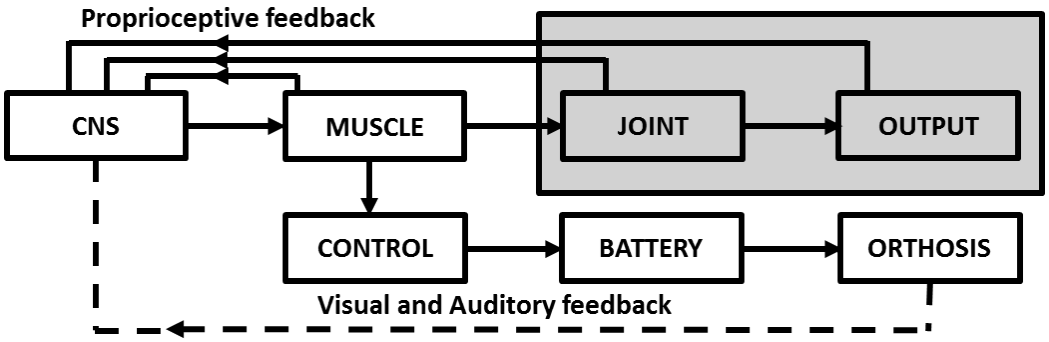

Figure 1.2: Block Diagram showing the replacement of the joint function and control by the orthosis [31].

identify the EMG corresponding to a single muscle group and, hence, difficult to identify the motion the EMG signal represents. Thus, the control system has to extract certain features that represent the user's intent of hand motion from the raw EMG data and accordingly actuate the prosthesis or orthosis. This process known as *feature extraction* is the heart of myoelectric control.

The EMG signal has to be processed keeping in mind the real time application of the prosthesis or orthotics. Thus, a maximum threshold of 300 ms for the processing of the bio-signal needs to implemented, else the user perceives a delay in the initiation of the action. The system has to acquire the EMG data, extract features, classify the intended motion based on the features and generate the control signals for actuation within this time window.

The features that can be easily extracted from a raw EMG signal are the basic time-frequency features such as *mean absolute value, mean absolute value slope, number of zero crossings, slope sign changes and waveform length.* Most of the earlier work on EMG focuses on these time-frequency features for classification of different hand motions. More recently, *auto-correlation coefficients*, *spectral measures*, and *time series models* have been used while current approaches focus on the temporal structure in EMG patterns by using the short-time Fourier transform, wavelet and wavelet packet transforms and higher order spectral analysis for feature extraction.

After features have been extracted, an efficient *classifier* has to be designed that is able to discriminate and adapt to the motions within the given time frame. The last two decades have seen tremendous interest in designing and implementing faster and more efficient classifiers. *Giuffrida et.al.* in [32] have used the k-means clustering algorithm for stroke therapy task discrimination for classifying features generated using electromyography and motion sensors.

The classifier automatically detects the task the subject is trying to do based on the gyroscope and EMG data, even when severe impairment produced movements that were visually indistinguishable from different tasks.

Chu et.al. have used wavelet packet transform for extracting features from the EMG data by using the local discriminant basis and an energy map in [33]. They have further reduced the number of features from 1024 to 8, using linear feature projection and shown the viability of this method for classifying most of the forearm movements. The classifier used is an MLP classifier.

Hudgins et.al. in [34] proposed a novel, control scheme based on the feature extraction during the onset of a contraction using artificial neural networks as a classifier and [35] developed this idea further by using pattern recognition to classify multiple classes of limb movements with focus on low storage capacity and complex sequences of manipulation involving multiple joints. The same authors have developed feature extraction algorithms for myoelectric control using time-frequency methods[36] and wavelet packet transforms [37].

Yoshikawa et.al. proposed a scheme to use Support Vector Machine (SVM) as efficient classifiers for EMG signal for robotic control in [38]. The SVM classifier takes in the feature vector and generates the output in terms of the corresponding joint angle for the manipulator. Experimental results of the estimation of seven hand motions demonstrate the effectiveness of the proposed method. *Khushaba et.al.* combine the concepts of wavelet packet transforms for feature extraction, fuzzy entropy for feature elimination and Principal Component Analysis (PCA) for dimensionality reduction in [39]. The fuzzy entropy algorithm measures the information content of the features and eliminates those features that are below a threshold value. This methodology showed 99% accuracy even when using a small subset of the original feature vector.

Thus, different classifiers have shown to faithfully discriminate different motions based on feature sets extracted, using pattern recognition techniques. Though the advantages of the above studies are mentioned, they are not without their drawbacks:

1. These schemes concentrate on reducing classification error for better classification of the myoelectric signal using multiple channels. This is better suited for use in prosthetics where the control scheme requires more precision due to the absence of the arm.

2. Their use in outpatient rehabilitation devices may be suitable but would require the patient to come to the same and/or different hospital(s) for regular physiotherapy.

3. If the same schemes were implemented for orthotic gloves for home rehabilitation, it would be rather inconvenient for the patient to put on and remove the multiple numbers of electrodes every day.

It can be concluded from the above that, the feature extraction and classification needs to focus on the use of a single channel or dual channel EMG for multi-class hand movement classification for rehabilitation of the elderly. A single channel myoelectric control of the hand movements using Empirical Mode Decomposition (EMD) for feature extraction is designed in [40] with basic features like mean and variance to achieve a better classification rate as compared to time domain auto regression features shown in [41].

Feature identification and classification alone is not a robust way for generating control signals for an assistive system. The generation of the control signal for such a case doesn't have any co-relation to the torque that needs to be produced by the actuator. A pattern recognition based system is acceptable if the torque required for the movement is not substantial. In other

words, smaller joints like the wrists and hand can be actuated using a control system shown in chapter 3. But the torque required for the actuation of the joints such as the elbow joint is high and it would be detrimental to use such a system for classifying them. The amount of time required to complete a movement is not fixed and varies from person to person. A pattern recognition based system is unable to predict the *'in-between states'* between the initial and final motions. These transient states need to be programmed into the actuator accordingly, and still there is no surety that it mimics the elderly user's intention.

1.9 Electromyography-Torque Model

If a direct relation can be established between the measured EMG and the actual joint torque or force produced, it would be beneficial for the myoelectric control of prosthetics or orthotics. Research in this area is divided into three major methods. The first methodology is to build the physiological muscle model of the human muscle and then predict the joint torque as a function of the neural activation derived from the EMG signal. The second method is to model the EMG-Torque function using some known function. The same method also involves optimizing the said function to best fit the EMG-Torque dataset. The final method is to model the EMG-Torque function using a neural network.

The earliest and most classic physiological muscle models is the Hill's model developed by *A.V. Hill* in 1938 [42]. The key finding of Hills model is the observation that a sudden change in force (or length) would result in nearly instantaneous change in length (or force) for a given sustained level of neural activation.

Herbert Hatze has contributed significantly in developing the physiological model of the muscle. He proposed two physiological control parameters, simulation rate and the motor unit recruitment, for the muscle model in [43] and provided a complete set of control equations for the the same in [44]. In [45], he provided a multivariate model for the passive human joint torque to the neural activation for articulate joints. He supported the concept of an extensor and flexor for each joint in [46].

Hof et.al. in [47] described an electrical analogue of the Hill muscle model where the surface electromyography is related to the muscle force. The joint torque was predicted by using the joint angle and the rectified EMG envelope. These results were then verified using a calfergometer in [48] and a torque plate in [49] and, the eccentric-concentric contractions were studied on a spring wheel set up in [50].

A musculoskeletal control model for the human leg was developed in [51]. This model was based on the sarcomere properties of the muscle tendons as compared to considering the muscle as a lump quantity in the classical Hill's model.

Winters and *Stark* studied the fundamental patterns of human limb movement using an *agonist-antagonist* muscle model in [52] based on the classical Hill model [42]. They further expanded their work into estimating the mechanical properties of muscles involved in different movements of a variety of human joints in [53]. The parameters estimated by combining the anatomical properties of the muscle with geometrical data on the muscle-joint anatomy, were compatible with available human experimental data.

The Hill based model was adopted by *Riener* and *Quintern* in [54], to predict the shank motion induced by neuromuscular stimulation. The muscle fatigue due to the stimulation was also modeled and the results supported

the use of functional neuromuscular stimulation for development of neural prostheses. The authors further developed this method in [55] and [56] for developing a control algorithm for Functional Electrical Stimulation (FES) supported standing.

A mathematical model for mapping EMG signal to the elbow joint torque using nonlinear regression was proposed in [57], that had greater correlation and least mean square error when compared to similar methods for both offline and online processing. *Mankala et.al.* optimized the system dynamics using an optimization function for designing an exoskeleton for gait training in [58].

A knee ankle foot orthosis powered by artificial pneumatic muscles was designed by *Sawicki et.al.* in [59] using myoelectric control and activation. The lower limb orthosis was controlled by a simple proportional controller relating the myoelectric signal of the biological extensor and flexor muscles to the artificial extensor and flexor pneumatic muscles respectively.

Hincapie et.al. in [60, 61] have studied the feasibility of an EMG-based neural network controller for upper extremity prosthesis. The focus of the study was on the use of Functional Electrical Stimulation (FES) to provide shoulder and elbow function to individuals with C5/C6 spinal cord injury.

Artificial neural networks with backpropagation were used to predict the tendon forces from EMG signal during dynamic contractions by[62, 63]. This study was focused on the prediction of the forces on a treadmill by measuring the gastrocnemius muscle of cats in different sets of experiments.

Wang et.al. in [64] have combined the neural network approach to the physiological approach by using a neural network to predict the neural activation and then using the predicted neural activation in the Hill muscle model to obtain the joint torque.

Winters et.al. described the fundamentals of varying the model complexity and the gains and losses because of the same in [65]. The input parameters of an EMG-Force model was optimized by *Cao et.al.* in [66], for constant and sinusoidal force contractions using the Monte Carlo method.

Optimization techniques such as Genetic Algorithm (GA), Particle Swarm Optimization (PSO), [67–70] have been used to estimate different parameters of the Hill muscle model. The parameters estimated in such studies were either constants or the values changed minimally during dynamic contractions. Since a changing parameter is to be estimated, which is a function of the muscle activation as well as the muscle length under consideration, optimization techniques would be complicated resulting to a huge burden on computing power.

The advantage of using neural networks or black box modelling for the EMG-Torque relation is that the governing equations or the characteristics of the system need not be known for modeling the data while the disadvantage is the requirement of multiple sensor data to ensure that the predictions are accurate.

The obvious disadvantage for the physiological modelling of the EMG-Torque relation is the need to model complicated muscle dynamics to get an accurate joint torque estimate while the advantage is that once the model is tuned, it predicts the joint torque quite accurately as it is a function of the neural activation.

1.10 Mechanomyography Signal Processing

Mechanomyography (MMG) is another method useful in assessing activities of skeletal muscles, that measures vibrations from contracting muscles. The

MMG signals produced by contracting and vibrating muscle fibers can be interpreted as a mechanical counterpart of EMG signals, since it has been shown that MMG signal informs about differences in motor units recruitment pattern [71], degenerative changes in skeletal muscles [72, 73], and mechanical properties of skeletal muscles (stiffness and vibration)[74]. Despite the difference in nature of these two signals, each of them gives information about the motor unit recruitment, firing frequency and synchronization [71] that are reflected in the amplitude and frequency of the EMG and MMG signals.

Beck et.al. in [75] estimated the relationship between MMG amplitude and frequency versus the torque for isometric and isokinetic muscle actions of the *biceps brachi*i and in [76] determined the isokinetic muscle actions of the *biceps brachii* for both EMG and MMG. They concluded that the MMG along with EMG is useful in describing motor control strategies for dynamic torque production. They also determined the MMG center frequency using the Fourier and wavelet transform procedures for fatiguing isokinetic muscle actions of the *biceps brachii* in [77] and for eccentric torque relationships in [78]. They concluded that both Fourier and wavelet transform methods can be used for examining MMG patterns during eccentric muscle actions [79], and further extended the study to the *quadriceps femoris* in [80].

Silva et.al. in [81, 82] proposed a multi-sensor data fusion system, with EMG and MMG, for prosthetic control. The authors designed a hybrid microphone-accelerometer sensor pair to simultaneously measure the EMG and MMG respectively. A strategy of multi-sensor data fusion was used for generation of binary control signals for prosthesis control. In [83], a mathematical model was derived for the the hybrid microphone-accelerometer sensor pair focussed on separation of interfering sources from the MMG signal. The authors concluded that MMG is comparable to EMG and may exceed

its functionality. This study was further extended in [84] into studying the effects of motion artifacts on MMG, measured from the extensor carpi ulnaris, using accelerometers and microphones.

Alves and *Chau* investigated forearm muscle activity using multi-channel MMG in [85]. They extract different sets of features, including wavelet transform, time-frequency features, statistical features, auto-regressive coefficients and ceptrum coefficients, from six forearm muscles. A Genetic Algorithm (GA) is used to optimally reduce the features by using the Fisher's ratio analysis. The authors discovered that using only Root Mean Square (RMS) values for classification resulted in poor accuracies while the ceptrum coefficients based features were discovered to be the feature most selected by the GA in each trial. This was compared to their work in [86] regarding the isometric contractions of hand muscles during functional grasping.

Xie et.al. explored the use of MMG for multifunction prosthetic control using MMG in [87]. Robust MMG features were extracted from the MMG signals by fusing wavelet packet transform and singular value decomposition. The best features were then selected using a distance evaluation criteria for the classification of wrist flexion, wrist extension, hand opening and hand grasping.

A human assisting manipulator for amputees, using accelerometer sensors to measure MMG, was proposed in [88]. A probabilistic neural network was used for separation and estimating the information on force and motion from the measured MMG signals with high efficiency. A MMG based pattern recognition approach was proposed in [89] for classification of, hand open, hand close, wrist flexion and wrist extension, while using a single accelerometer for measuring the MMG at the *flexor carpi ulnaris* muscle. The authors used Principal Component Analysis (PCA) for reducing the dimension of the

features and a Quadratic Discriminant Analysis (QDA) based classifier was used with an average accuracy of 79.66 %.

The advantage of using an accelerometer to measure the MMG is that, if placed properly, it can also measure the joint angle or orientation of the hand and, thus, eliminates the need to assign multiple sensors to do the same function.

1.11 Problem Statement

Rehabilitation robotics is used in both in-patient and out-patient rehabilitation but are too complicated and bulky to be used for home rehabilitation. Another aspect of task-oriented feedback is the functional training of day-to-day activities like operating a doorknob, holding and drinking water from a cup, lifting some weights etc. Comprehensive training for such basic but necessary tasks for the elderly cannot be given sitting in a clinic or rehabilitation centre. Moreover, such tasks are a closer outlook to the patient's actual life; hence, using such an assistive robotic system at homes for day-to-day activities could initiate a continuous recovery for the patient instead of only at rehabilitative sessions. The frequency of the patient going to periodic rehabilitative sessions at the hospital is reduced and recovery could be faster.

As mentioned before, the recovery of the upper limb after stroke or dementia for regaining functions of daily living is more time consuming and difficult due to its larger functional area in the brain. Losing the functionality of one or both the upper limbs can make the patient depressed and demotivated and even unresponsive to rehabilitation. If the patient can see and feel the improvement in motion and functionality, the motivation comes from within.

Rehabilitation of the elderly is particularly challenging because of the

following reasons:

a. An elderly person is set in his/her ways and would not want to believe that they are losing control of their faculties,

b. They would prefer if the rehabilitative service is available at their homes or nearby their homes and

c. They would prefer not to have too many attachments (electrodes, machines, battery packs etc.) on themselves for rehabilitation as it would be more of a hindrance than an assistive role as the process of attaching and detaching multiple electrodes everyday for measuring EMG in itself would be quite cumbersome.

This thesis presents the research work in developing signal processing techniques for implementation of Electromyography (EMG) and Mechanomyography (MMG) in such a wearable system or 'glove' for the restoration of upper limb functions. During the execution of the thesis research work, the following problems related to EMG and MMG signal processing are considered:

- The major contributor to noise in EMG signal is the power line interference. Depending on the location of the user, there may be a variable impact of the power line noise on the signal quality and discerning it from the signal is an important part of the EMG signal processing. The weakest link here is the overlapping of the energy spectrums of the EMG signal and that of the power line interference.

- Establishing a EMG-Joint Torque model for predicting the changes in the joint torque as a function of the muscle activation. The limiting factor is the complexity and quantity of the data processed along with

the need to use minimum number of electrodes to facilitate ease of use for the elderly.

- Designing a pattern recognition based classification system for the movements of hand and wrist using mechanomyography as the control input. The use of EMG for the same can be argued upon but MMG provides a simpler and less tedious way to implement the same with much less hassle.

Adaptive filtering is the preferred method for removing power line interference from the EMG signal but there is a need to identify the frequency of the PLI before the adaptive algorithm can eliminate it. Thus,it is required to estimate the frequency and amplitude of the PLI in the measured signal in real time and to design an adaptive filter that reacts to the change in frequencies in real time and removes just the noise and not the EMG data signal.

The number of sensors used for detecting the residual muscle electrical activity depends on the control algorithm that is used to differentiate the different motions of the upper limb. If the control algorithm requires the use of many sensors, the patient would find the act of putting on more sensors cumbersome and may altogether prefer not to use the glove. Thus, the secondary aim of the control algorithm is a reduction in the number of sensors used for detecting the surface EMG signals for classification of different upper limb motions.

The measurement of different bio-signals such as electromyography (EMG) and mechanomyography (MMG) and their fusion with each other is an integral part of such an orthotic glove to work seamlessly with the user to improve upon their tasks of daily living. Thus, both EMG and MMG will be studied separately and together for different day-to-day tasks for classifying them.

The physiological muscle model for different joints will be formulated and optimized for the use with minimum number of electrodes for use of the elderly. This is critical in ensuring that the system does not assume the same parameters for a healthy person and an elderly person.

A pattern recognition based system is designed using MMG for measuring the muscle vibrations for different hand movements. Different sets of features need to be extracted from the MMG to gauge its efficacy in such a system.

1.12 Thesis Contributions

The problem statement of this thesis covers different aspects of bio-signal processing for developing assistive devices for rehabilitation. Similar solutions have been provided in the literature for the same but don't provide a concrete answer for optimising the same for the elderly. The main contributions of this thesis research work are the following:

1.12.1 A Modified Hilbert-Huang Algorithm based Adaptive Filter for Elimination of Power Line Interference from Surface Electromyography

A modified Hilbert-Huang Transform based Least Mean Squares (HHT-LMS) adaptive filter is designed to eliminate the power line interference at different signal to noise ratios. It takes into account the variable nature of the power line frequency and adapts accordingly.

The HHT is an attractive solution for the estimation of PLI in a spectrum of overlapping frequencies. It eliminates the need for an a-priori defined functional basis, as is generally required for traditional signal analysis techniques. Being purely data-driven, the HHT precisely determines the most appropriate

empirical but adaptive basis for the signal. This ability to adapt is crucial, given the individualistic nature of nonlinear systems. Another key feature of the method is that, by utilizing the Hilbert transform, it operates at the scale of one oscillation and is, thus, truly able to track local changes in signals.

The variable step size LMS algorithm ensures that any changes in the frequency, amplitude and phase of the noise is adapted by using the inputs from the HHT block.

1.12.2 Parameter Estimation of a Hybrid Muscle Model using an Iterative Learning Predictor for the Estimation of Joint Torque

A hybrid model is designed that combines the muscle physiological model and the neural network to predict the joint torque of the elbow. The predicted results follow the actual joint torque faithfully and the mean square error is minimum of all the different models. Moreover, the time required for executing the hybrid model is directly proportional to the number of iterations required per data point and the constant time required by the neural network for predicting the joint torque. The accuracy of the predicted output is neither just a function of the black box neural network nor dependent on multiple muscle activation data.

Iterative Learning Control (ILC) is a simple and effective solution to the parameter identification problems of the muscle model which is highly nonlinear and multi-dimensional. The use of an Iterative Learning Predictor (ILP) can guarantee the learning process convergence even if the plant model is partially unknown or difficult to analyze. The use of an ILP ensures that the model doesn't predict unreasonable values for the parameter while

simultaneously ensuring that the time required for processing the data is minimized. This is due to the repetitive nature of rehabilitation exercises and the dependency of the predicted output on the previously predicted value and the error calculated. A pointwise ILP is implemented where the data points in the signal are iterated one-by-one till the actual output is the same as the desired system output.

1.12.3 Mechanomyography Feature Extraction and Classification of Forearm Movements using Empirical Mode Decomposition and Wavelet Transform

A pattern recognition based system is designed using the MMG as the input signal. Different feature sets are isolated and extracted based on time-domain features, wavelet features and features based on empirical mode decomposition. Two new features based on the EMD and Hilbert spectrum are defined and used in feature extraction.

A novel feature extraction technique is proposed by using the intrinsic mode functions generated by using the EMD process. The classification of the MMG signals based on different movements of the upper limb in a supervised learning environment is achieved using a Multilayer Perceptron (MLP) classifier. It is found that the wavelet based feature set and EMD based feature set performed best for classifying movements of hand and wrist using the multilayer perceptron classifier.

1.13 Organization of the Thesis

This chapter presented the fundamentals of ageing, stroke, neuroplasticity and stroke rehabilitation. It also presented the disadvantages of traditional rehabilitation and presented different assistive robotic devices available. It further introduced the concept of task-oriented biofeedback, differentiated it with static biofeedback and emphasised its importance in rehabilitation. A review of myoelectric control, different feature extraction methods and the different classifiers used by researchers is carried out. Problems associated with using EMG and MMG in an assistive system for the elderly are identified. A brief literature review of the adaptive signal processing of EMG is provided along with the description of different methods for calculating joint torque using different EMG-Torque models. The use of MMG for extracting features is explored and the corresponding literature reviewed.

Chapter 2 outlines the different EMG and MMG measurement protocols to be followed and guidelines for selecting various parameters for EMG measurement including electrode geometry, shape, size, inter-electrode distance, electrode placement, electrode configuration and skin preparation. The primary recording sites for EMG and MMG for the different motions are also identified along with their filter parameters. The different protocols followed for measuring the EMG-Torque data and joint angle measurement are also described in this chapter.

Chapter 3 is divided into three sections. Firstly, feature extraction is described using different time-frequency and wavelet features. Secondly, the control algorithm used to process the myoelectric signal which include feature extraction and classifier design is detailed. The measured EMG data is analysed and classified based on this control algorithm. Basic time domain

features are used with a multilevel perceptron classifier for pattern recognition. The final section details a prototype of a myoelectric glove along with its design specifications and the obstacles faced in implementing the hardware prototype.

Chapter 4 describes the instantaneous frequency estimation of the EMG signal using Hilbert-Huang Transform and a variable step-size adaptive Least Mean Squares (LMS) algorithm to filter out the variable Power Line Interference (PLI). The subsequent section details the simulations performed to evaluate the HHT-LMS adaptive filter under different conditions while the final section evaluates the HHT-LMS adaptive filter on experimental data.

Chapter 5 analyses the EMG-Torque relation using a physiological model of the muscle based on the modified Hill's muscle model. Preliminary tests were carried out for estimating the joint torque of the elbow using the fixed function model and neural network models. The inability of these models led to the design of a hybrid muscle model for predicting the elbow joint torque. An iterative learning predictor is proposed for estimation of the unknown parameters from the modified Hill's muscle model. The hybrid model is described in detail and evaluated using experimental data. The Mean Squared Error (MSE) is used to compare the performance of the hybrid model with the fixed function and the neural network models.

Chapter 6 describes the methodology for optimal feature extraction, selection and classification of the Mechanomyography (MMG) signal for different forearm motions. Three accelerometers are used for measuring the MMG from major forearm muscle sites. The next section extracts time-frequency features from the MMG data and classifies it using an Multilayer Perceptron (MLP) classifier. The MMG signal's time variation is also explained from measured data. The subsequent section describes the extraction of wavelet

transform based features and their classification using a MLP classifier. The final section details the decomposition of the MMG signal into Intrinsic Mode Function (IMF), used for extracting Empirical Mode Decomposition (EMD) based features and their subsequent classification using a MLP classifier.

Chapter 7 summarizes the study presented in this thesis and describes future work that can be undertaken to further develop and improve this study.

2

Electromyography and Mechanomyography Measurement Protocols

This chapter outlines the different EMG and MMG measurement protocols to be followed and guidelines for selecting various parameters for EMG measurement including electrode geometry, shape, size, inter-electrode distance, electrode placement, electrode configuration and skin preparation. The primary recording sites for EMG and MMG for the different motions are also identified along with their filter parameters. The different protocols followed for measuring the EMG-Torque data and joint angle measurement are also described in this chapter.

2.1 Electromyography

The EMG or the Myoelectric Signal (MES) of a muscle is the summation of the different Motor Unit Action Potential (MUAP). This can include the MUAP(s) of nearby muscles as well. For a single channel recording of EMG, if the muscle groups are very close to each other, it would be difficult to identify the EMG corresponding to a single muscle group and, hence, difficult to identify the motion the EMG signal represents. Thus, certain features need to be extracted that represent the user's intent of hand motion from the raw

EMG data and accordingly actuate the prosthesis or orthosis. For this study, the following hand motions are analyzed:

1. Elbow Flexion and Extension: The *biceps brachii* muscle group functions as the agonist muscle for the forearm while the *triceps* muscle groups as the antagonist muscles.

2. Wrist Flexion and Extension: The *flexor carpi ulnaris* is a muscle of the forearm, which helps to flex and extend the wrist.

3. Hand Grasp and Open: The *flexor digitorum profundus* and *flexor digitorum superficialis* are known as the flexors of the fingers and are used for grasping and opening of the hand.

Table 2.1: Different motions of the hand and the corresponding muscle groups

Motion of the Hand	Associated Muscle Group
Elbow Flexion and Extension	***biceps brachii*** ***triceps brachii***
Wrist Flexion and Extension	***flexor carpi ulnaris***
Hand Grasp and Open	***flexor digitorum profundus*** ***flexor digitorum superficialis***

2.1.1 EMG Measurement

2.1.1.1 Non-Invasive vs Invasive EMG

The EMG signals can be detected and recorded either by invasive techniques by inserting a needle electrode underneath the skin or by non-invasive techniques by using electrodes on the surface of the skin. Needle electrode directly measures the firing pattern of the muscle unit it is inserted into and is more accurate in MUAP measurements as compared to surface electrodes

which provides a global measure of the muscle unit's activities [90]. But surface electrodes are much easier to use especially if measurements have to be repeated frequently or if the electrode has to be in contact during the operation of any robotic system and are also readily available as compared to needle electrodes.

Hence for this system, non-invasive surface electrodes are used for EMG measurements, as the EMG of the patient has to be measured continuously for the time period of operation of the glove.

2.1.1.2 Electrode Material, Geometry, Size and Skin Preparation

Silver/Silver Chloride (Ag/AgCl) has certain electrochemical properties which allow it to provide a very balanced and consistent surface EMG signal that is not found with single compound electrodes [91]. Different geometry for surface electrodes exists such as rectangular, bars or circular discs. Since the MUAP propagates evenly in both directions from the neuromuscular junction, use of disc electrodes would account for maximum uniform area covered for measurement. Thus Ag/AgCl disc electrodes manufactured by *'3M'* are used for all EMG measurements.

The surface electrodes are not specific to any particular surface area of the muscle for picking up EMG signals as they provide a global measure of the muscle unit's activities. Thus, there is no ideal size for electrodes for optimum EMG measurement as each muscle unit's dimensions are different from each other. The rule of thumb is that, smaller the muscle from which the recording has to be made, the smaller is the electrode.

An electrode diameter of 1 cm is used to measure EMG for both the forearm muscles as well as the biceps muscles as both these muscle groups are relatively large as compared to muscles of fingers, which would require an

electrode diameter of about *'0.5 cm'* for faithful measurements.

Consistency in impedance is critical for the reliability of EMG measurements. Modern pre-amplifier design with high input impedance has reduced the importance of measuring EMG with a low level of electrode-skin impedance. While the absolute level of muscle impedance is not a critical factor, the stability in impedance over time and the balance in impedance between electrode sites have a considerable effect on the signal to noise ratio of the measured EMG signal, both in terms of noise levels and spatial resolution. The general rule is that the more balanced the electrode-skin impedance between electrode sites, the lower the noise, and as a result, higher the signal to noise ratio.

The electrode-skin interface generates a DC voltage potential, mainly caused by a large increase in impedance from the outermost layer of the skin, including dead skin material and oil secretions. This DC potential, common to all electrodes, can be minimized with proper skin preparation. The quality of contact is typically improved by at least a factor of 10 with proper preparation [92].

To keep the electrode-skin impedance constant, proper skin preparation is vital. The dead skin material and oil secretions on the surface are cleaned using alcohol swabs. A conducting gel *NuPrep* is applied on the skin to give uniform electrode-skin impedance during measurement.

2.1.1.3 Electrode Configuration and Inter-Electrode Distance

The bipolar electrode configuration is used for EMG measurements. In this configuration, two electrodes are used at the detection site and a third ground electrode is placed distally in a neutral electrical environment. This is because a differential pre-amplifier is used for EMG signal amplification [91]. The ground electrode site chosen for this study is the elbow joint.

Inter-electrode distance is defined as the center-to-center distance between the conductive areas of electrodes [93]. It is an important parameter when EMG signal from a single muscle is to be determined. If the inter-electrode distance is too small the surface electrodes may get short-circuited if the skin becomes moist with conducting sweat. If the inter-electrode distance is large the bandwidth of the EMG signal is reduced. The surface electrode may also pick up electrical activity of neighboring muscles or crosstalk thus leading to corrupted EMG data. The rule of thumb for small muscles is that the inter-electrode distance should not exceed one-fourth of the muscle fibre length. In this way, unstable recordings due to tendon and motor end-plate effects, can be avoided.

An inter-electrode distance of *'1.5 cm'* was chosen for EMG measurements from the biceps muscle groups while an inter-electrode distance of *'1 cm'* was chosen for the forearm muscle groups.

2.1.1.4 Electrode Placement

The goal of electrode placement is to achieve a location where a good and stable surface EMG signal can be obtained [94]. There are two general strategies for placement of electrodes. From the skin surface the electrode can be arranged longitudinally with respect to the long axis of the muscle where it is recommended to place the electrode on the mid-line of the muscle belly such that the innervation site is avoided during motion. Transversely, it is recommended to place the electrodes such a way that they are away from the boundary of the muscle recording area of interest i.e. perpendicular to the long axis of the muscle so that neighboring muscle groups are avoided in measurement.

A longitudinal arrangement of the electrodes is chosen and the electrodes

are placed on the mid-line of the muscle belly and the electrode contacts lie parallel to the muscle fibers and not across them. For each of the muscle groups used, the electrodes are centered as follows:

1. *biceps brachii* and *triceps brachii*: The mid-line of the muscle belly.
2. *flexor carpi ulnaris*: Proximal one-third point on a line drawn from the posterior portion of the medial epicondyte to posterior portion of the styloid process of the ulna.
3. *flexors of the fingers*: Midway point on a line drawn from the medial epicondyte to the styloid process of the ulna.

Table 2.2: EMG Parameters used for measurement in this study

EMG Parameter	Value
EMG Detection	Non-Invasive Surface Electrodes by 3M
Electrode Material	Silver/Silver Chloride (Ag/AgCl)
Electrode Geometry	Circular Disc
Electrode Size	Diameter: 1cm
Skin Preparation	Alcohol Swabs Conducting Gel NuPrep
Electrode Configuration	Bipolar Electrode Configuration with Ground Electrode Ground Electrode Site: Elbow Joint
Inter-Electrode Distance	Biceps: 1.5 cm Forearm muscles: 1 cm
Electrode Placement	Longitudinal along the long axis of the muscle

2.1.2 EMG Signal Processing

2.1.2.1 EMG Equipment

The equipment used to measure EMG for this study on a Personal Computer (PC) is the CleaveMed BioCapture Research System. The measuring unit is wirelessly connected to the PC unit. The system is capable of simultaneously

measuring eight channels of EMG and has adjustable sampling rates with a maximum value of 960 Hz.

A joint torque measurement system has been developed in the laboratory for simultaneous use along with the EMG equipment. The system is based on the dSPACE hardware platform and can be used to implement real time signal acquisition and processing to generate appropriate control signals for the actuation of the rehabilitative device. The joint torque measurement system provides visual feedback on the current level of Maximum Voluntary Contraction (MVC) for the motion analyzed.

Sampling Frequency: 960 Hz

The selected bandwidth of the EMG signal for our system lies in the range of 10 - 350 Hz. According to Nyquist Theorem, the sampling rate chosen should be at least twice the bandwidth of the EMG signal for faithful representation of the signal. Hence a sampling rate of 960 Hz is chosen for all the experiments.

2.1.2.2 Filtering

The electrode-skin interface generates a DC voltage potential, mainly caused by a large increase in impedance from the outermost layer of skin, including dead skin material and oil secretions. The mean value in the data is removed to filter out this DC offset. The Power Spectral Density of the measured EMG data processed offline shows that the EMG signal lies predominantly in the range of 10 to 350 Hz as shown in Fig. 2.1 [95].

A low pass filter with a cut-off frequency of 350 Hz and a High Pass Filter with a cut-off frequency of 10 Hz were designed to process the EMG data both in real time and for offline processing. A second order Butterworth filter was chosen as it gave a flat magnitude response in the pass band. The high

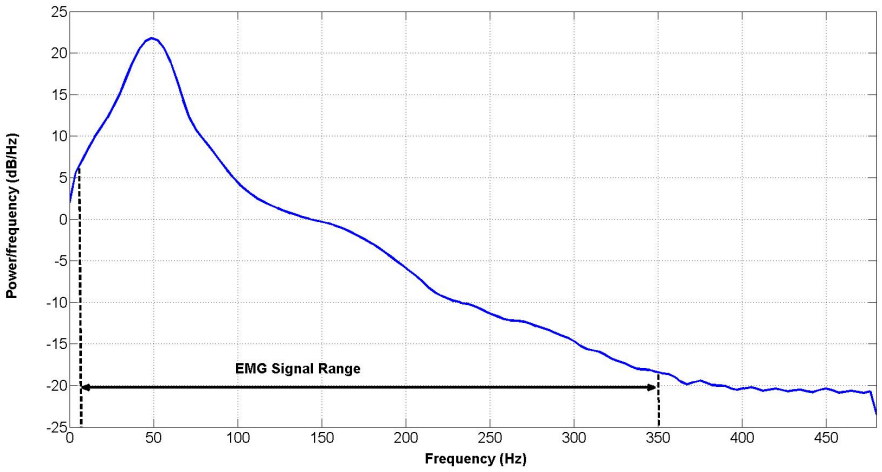

Figure 2.1: The Power Spectral Density of measured EMG signal.

pass filter helps removing the noises due to motion artifacts and random firing of motor units while the low pass filter acts as an anti-aliasing filter.

2.1.2.3 EMG Crosstalk

Crosstalk is the EMG signal detected over a muscle but generated by another muscle close to the first one [96–99]. The phenomenon is present in surface recordings, when the distance of the detection points from the sources may be relevant and similar for the different sources. Crosstalk is one of the most important sources of error in interpreting surface EMG signals. This is because crosstalk signals can be confounded with the signals generated by the muscle, which thus may be considered active when indeed it is not. The problem is particularly relevant in cases where the timing of activation of different muscles is of importance, such as in movement analysis. Just because two muscles lie close to each other or are separated by a thin layer of fascia does not mean that crosstalk can occur at any given pair of surface or indwelling recording sites. A set of guidelines is utilized to prevent crosstalk as mentioned in [100]. The selection of the electrode size, geometry, inter-

electrode placement in this study has been carried out keeping in mind the problem of crosstalk.

Table 2.3: Filter Parameters used for EMG processing in the study

Filter Parameter	Value
Low Pass Filter	Type: 2nd Order Butterworth Filter Cut-Off Frequency: 350 Hz
High Pass Filter	Type: 2nd order Butterworth Filter Cut-Off Frequency: 10 Hz
Sampling Rate	960 Hz
EMG Equipment	Clevemed BioCapture Research System

The focus of this study is on elderly rehabilitation and to ensure that the data measured is representative of that measured from the elderly, the following protocol is strictly followed while measuring EMG from healthy young subjects:

1. **The Maximum Voluntary Contraction (MVC) of the volunteer is measured in terms of the torque and is related to the corresponding EMG.**

2. **A set of weights are chosen such that the MVC % is between 15% to 30% for the motions analyzed.**

3. **A visual feedback is given using the dSPACE Torque measurement system to maintain the MVC(s) at the aforementioned levels.**

2.2 Mechanomyography

Another method that is useful in assessing activities of skeletal muscles is mechanomyography (MMG) that measures vibrations from contracting muscles. The MMG signals produced by contracting and vibrating muscle fibers

can be interpreted as a mechanical counterpart of EMG signals, since it has been shown that MMG signal informs about differences in motor units recruitment pattern [71], degenerative changes in skeletal muscles [72, 73], and mechanical properties of skeletal muscles (stiffness and vibration) [101]. Despite the different natures of these two signals, each of them gives information about the motor unit recruitment, firing frequency and synchronization [71] that are reflected in the amplitude and frequency of the EMG and MMG signals.

However, an apparent advantage of MMG over EMG is that MMG reveals mechanical properties of the muscles [71, 72]. Thus, simultaneously recorded EMG and MMG signals can be used in monitoring relations between electrical and mechanical properties of skeletal muscles [58, 71] and may potentially provide useful information in sports, medical, and neuroscience research. The MMG can be measured either by a microphone, a piezoelectric sensor, laser detection sensors or by an accelerometer.

A MMG data acquisition system has been developed in the laboratory for this study. The system is based on the dSPACE hardware platform and can be used to implement real time signal acquisition and processing to generate appropriate control signals for the actuation of the rehabilitative device. The following sub-sections describe the MMG data acquisition system in detail.

2.2.1 MMG Measurement

2.2.1.1 Sensor Type

The MMG can be measured either by microphones [83, 102], a piezoelectric sensor[103], laser distance sensors[74] or by an accelerometer. Use of microphone for data collection would lead to lot of post-processing to isolate the

MMG from the measured signal as the sensor would record all surrounding noise. Laser detection sensors are an expensive proposition for use in a practical low cost system. Piezoelectric sensors are a good choice for measuring MMG but there are inherent advantages while using accelerometers for measurement of MMG.

- If aligned properly, it can also measure the joint angle or orientation of the hand along with the MMG, thus eliminating the need to assign multiple sensors to do the same function.
- The accelerometer can be embedded into the rehabilitative device to assuage the discomfort and redundancy of attaching and detaching electrodes to the elderly user.
- The accelerometer signal data can also provide the velocity and acceleration of the hand during different movements.
- Low-cost of the sensor.

2.2.1.2 MMG Measurement Protocol

For this study, the following hand movements are analyzed:

(a) Wrist Pronation and Supination

(b) The Wrist Flexion and Extension

(c) Hand Open and Close

(d) Wrist Ulnar and Radial Deviation

MMG data from the following muscle groups of the forearm were used to analyse the above hand movements:

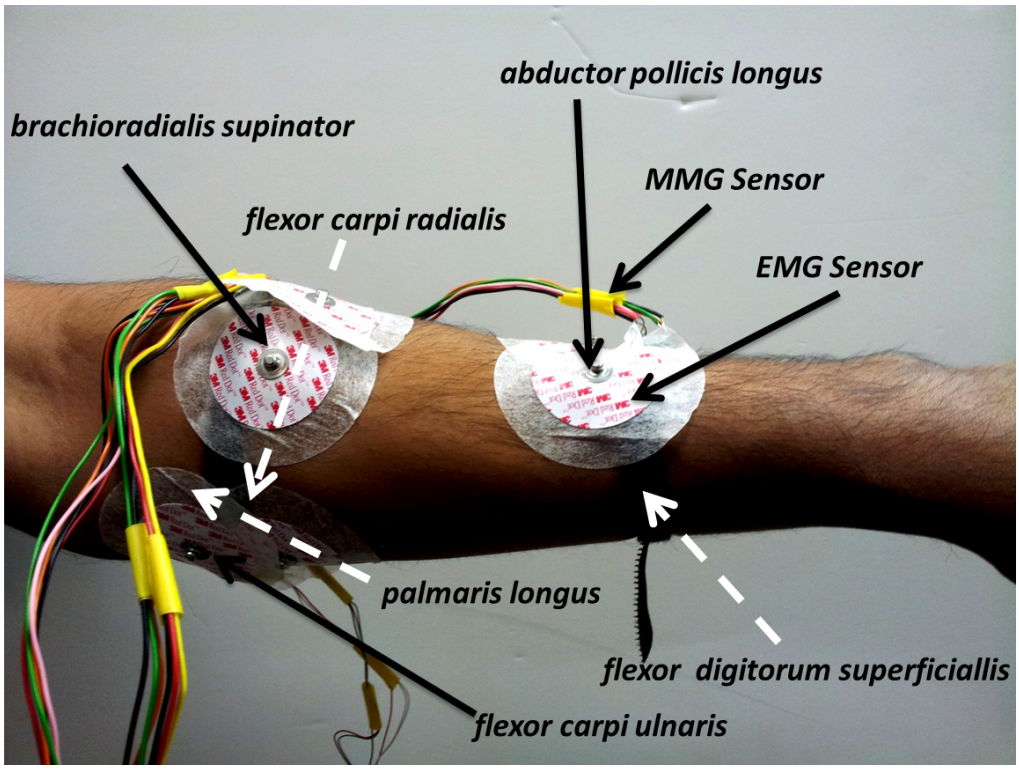

Figure 2.2: The different muscle groups for MMG measurement. The solid lines point to the muscles measured, while the dotted lines point to the nearby muscle groups.

(a) *flexor carpi ulnaris*

(b) *brachioradialis supinator*

(c) *abductor pollicis longus*

Fig. 2.2 shows the different muscle sites for MMG measurement. Simultaneous EMG measurement sites can be identified by the use of the *'3M'* electrodes. The MMG sensor is hidden under the EMG electrodes. It can be observed that the muscles in the forearm are densely located and it is difficult to isolate exact muscle groups corresponding to each hand movement. **Hence, the crosstalk from surrounding muscle groups is abundant in the measured data.**

2.2.1.3 Sensor Placement

The goal of sensor placement is to achieve a location where a good and stable surface MMG signal can be obtained. From the skin surface the sensor can be arranged longitudinally with respect to the long axis of the muscle where it is recommended to place the sensor on the mid-line of the muscle belly such that the innervation site is avoided during motion.

2.2.2 MMG Signal Processing

2.2.2.1 MMG Equipment

The equipment used to measure the MMG for this study on a personal computer (PC) is designed inhouse using accelerometers and the dSPACE hardware platform. The system is capable of simultaneously measuring upto eight channels of MMG and has adjustable sampling rates.

Accelerometer

The MXA2500G/M is a low cost, dual axis accelerometer fabricated on a standard, sub-micron CMOS process. It is a complete sensing system with on-chip mixed mode signal processing. The MXA2500G/M measures acceleration with a full-scale range of 1.7g and a sensitivity of 500mV/g at 5V at 25C. It can measure both dynamic acceleration (e.g. vibration) and static acceleration (e.g. gravity). The MXA2500G/M provides two absolute analog outputs. The typical noise floor is 0.2 mg/Hz allowing signals below 1 mg to be resolved at 1 Hz bandwidth.

There are two identical acceleration signal paths on the accelerometer, one to measure acceleration in the x-axis and one to measure acceleration in the y-axis.

Sampling Frequency:960 Hz

The selected bandwidth of the MMG signal for our system lies in the range of *5 - 100 Hz*. To keep the sampling rate consistent with the EMG acquisition system a sampling rate of 960 Hz is chosen. The sampling frequency chosen, also satisfies the Nyquist criteria.

2.2.2.2 MMG Filtering

The accelerometer sensor has an inherent DC voltage potential in the measurement. The mean value in the data is removed to filter out this DC offset.

The Power Spectral Density of the measured MMG data processed offline shows that the MMG signal lies predominantly in the range of 5Hz to 100 Hz as shown in Fig 2.3 .

A low pass filter with a cut-off frequency of 100 Hz and a High Pass Filter with a cut-off frequency of 5 Hz is designed to process the MMG data both in real time and for offline processing. A second order Butterworth filter is chosen similar to EMG filtering. The high pass filter helps removing the noises due to motion artifacts while the low pass filter acts as an anti-aliasing filter. The motion artifact noise can be further sub-divided into involuntary muscle movement and the joint angle. This is addressed in the next section.

2.2.3 Joint Angle Measurement

One of the applications for the accelerometer is tilt/inclination measurement for the dynamic contractions of the elbow joint. An accelerometer uses the force of gravity as an input to determine the inclination angle of an object. This feature is exploited upon to measure the joint angle of the elbow during different movements or exercises of the hand. The accelerometer is most sensitive to changes in position, or tilt, when the accelerometer's sensitive

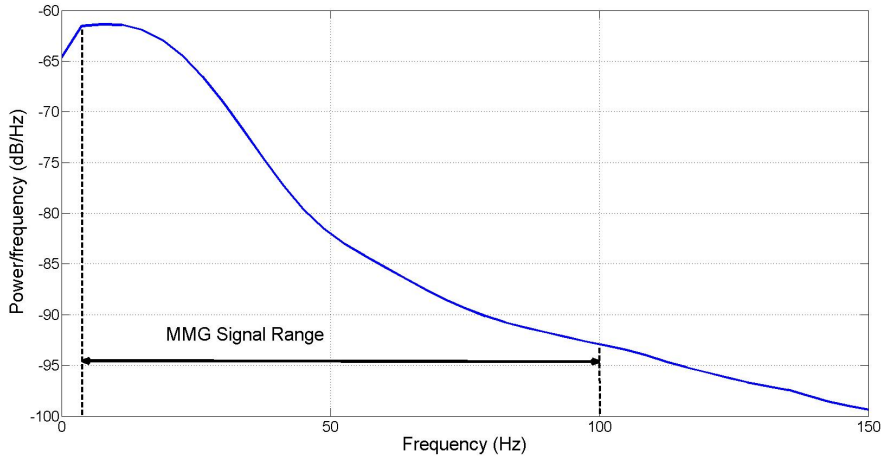

Figure 2.3: The Power Spectral Density of measured MMG signal.

axis is perpendicular to the force of gravity, or parallel to the Earth's surface. Similarly, when the accelerometer's axis is parallel to the force of gravity (perpendicular to the Earth's surface), it is least sensitive to changes in tilt.

Figure 2.4 helps to illustrate the position of the accelerometer for measurement of the elbow joint angle. An external low pass filter is useful in low frequency applications such as tilt or inclination. The low pass filter limits the noise floor and improves the resolution of the accelerometer. The joint angle is extracted from the data using a low pass filter of 2 Hz. The cut-off frequency can be tuned based on the speed of motion of the hand for different movements.

Table 2.4: Filter Parameters used for MMG processing in the study

Filter Parameter	Value
Low Pass Filter	Type: 2nd Order Butterworth Filter Cut-Off Frequency: 100 Hz
High Pass Filter	Type: 2nd order Butterworth Filter Cut-Off Frequency: 5 Hz
Sampling Rate	960 Hz
MMG Equipment	dSPACE Hardware Platform
Joint Angle Measurement	Low Pass Filter: Cut-Off Frequency: 2 Hz

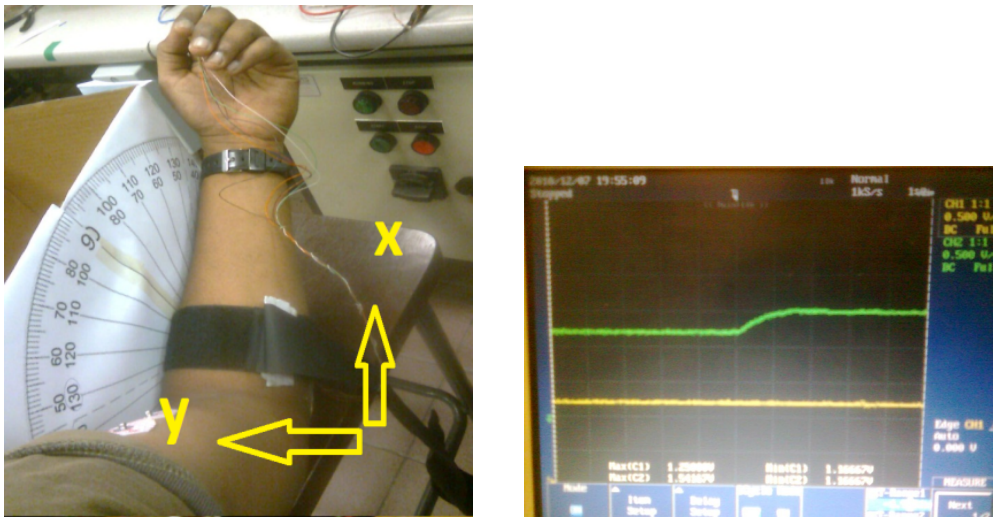

(a) (b)

Figure 2.4: Accelerometer Angle Measurement Setup

2.3 Summary

This chapter lists out the different protocols followed for EMG and MMG measurement. Firstly, the protocol for measuring EMG from different muscle sites is described. The muscle groups to be analysed for the different motions of the hand are identified and the different parameters for EMG measurement such as electrode size, material, shape, geometry, inter-electrode distance, skin preparation, electrode placement on the muscle groups and electrode configuration have been appropriately selected keeping in mind the issue of EMG crosstalk. The issues of noise, filter selection and sampling rate for the EMG signal have also been addressed. The measurement protocols ensure that the biosignals were representative of that measured from the elderly.

The MMG measurement protocol is described in detail in the next section. The muscle groups to be analysed for the different motions of the hand are identified and the different parameters for MMG measurement such as sensor placement, hardware platform, sensor selection are identified. The different

protocols for set up and measurement of mechanomyography signal using accelerometers and the measurement of joint angle or hand inclination using the same sensor are explored. The issues of noise, filter selection and sampling rate for the MMG signal have also been addressed.

3

Preliminary Tests: A Real Time Control Algorithm for a Myoelectric Glove

This chapter details the theoretical background for feature extraction and pattern classification of different movements of the upper limb using Electromyography (EMG) as a control signal along with the experimental results of the same. Two different sets of features were extracted from the EMG signals, that are classified using three different classifiers.

3.1 Methodology

The EMG measurement protocols have been discussed in detail in Chapter 2. The following sections describe the subjects participated and the specific tasks performed by them for this study. Data was collected from two muscle sites represented in this study as shown in Table 3.1. The overview of the system is shown in Fig. 3.1.

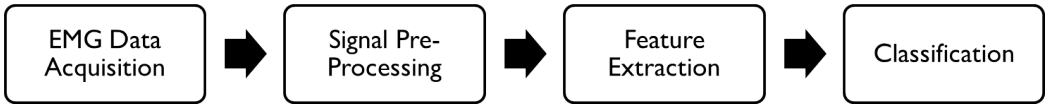

Figure 3.1: Overview of the pattern classification based system

Table 3.1: Electromyography Electrode Notation and Muscle Sites

Muscle Site	Notation
biceps brachii	E1
triceps brachii	E2

3.1.1 Subjects

Data was acquired from two able-bodied individuals, aged 23 ± 6 years. The subjects were healthy and reported no physical or mental disorders. Each subject had access to the full range of forearm motions with no previous history of musculoskeletal illness.

3.1.2 Experimental protocol

All subjects were instructed not to perform fatiguing upper limb exercise one day prior to the sessions. The CleaveMed BioCapture system was used to start data acquisition and the participants were visually cued by the operator of the BioCapture System to perform the elbow flexion and elbow extension movements. A numerical index is used for each class of the hand motion for identification during pattern recognition as shown in Table 3.2.

Table 3.2: Index for different hand motions for classification

Hand Motion	Index
Elbow Flexion	I
Elbow Extension	II
Wrist Flexion	III
Wrist Extension	IV
Hand Open	V
Hand Close	VI

Subjects performed repetitions of each of the above motions. Each motion was comprised of the full range of motion from the resting position to the

final position, followed by the limb being held in the final position for 5-10 seconds. The first motion performed is '*elbow flexion*' while the next motion is *'elbow extension'*. This sequence is then repeated for the rest of the session. The data was collected on multiple sessions, each session lasting not more than 2 minutes to avoid muscle fatigue.

3.1.3 Signal Pre-processing

The measured and filtered surface EMG signals were stored and analysed on a PC using MATLAB software. Each channel of the EMG data was processed and analysed separately. The Direct Current (DC) offset was removed by filtering the mean value in the EMG data while the 2nd order Butterworth high pass and low pass filters, with cut-off frequencies of 10 Hz and 350 Hz respectively, were applied to filter out the noise and motion artifacts including changes in forearm joint angles.

3.2 Feature Extraction

The measured and filtered surface EMG signals were stored and analysed on a PC using MATLAB software. Each channel of the EMG data was processed and analysed separately. The DC offset is filtered by subtracting the mean value of the data set in each time window. The 2nd order Butterworth high pass and low pass filters, with cut-off frequencies of 10 Hz and 350 Hz respectively, were applied to filter out the unwanted noise and motion artifacts.

As mentioned earlier, for real time applications, the response time threshold of the system should be less than 300 ms, so that the user does not perceive a delay between the initiation of a hand movement and the generation of the

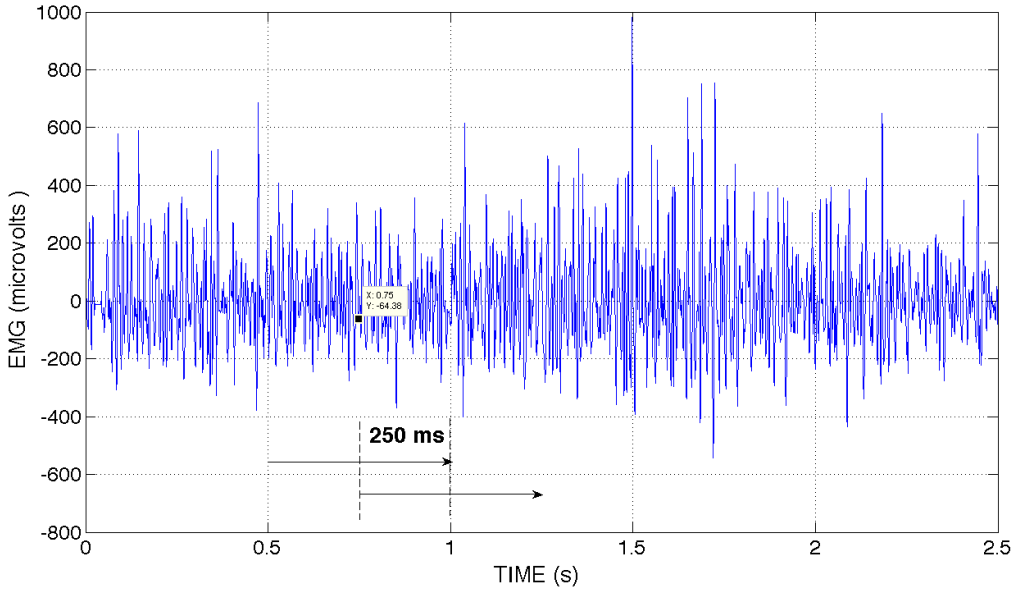

Figure 3.2: Different Time Analysis Windows for the the EMG data.

control signal. In the applied control algorithm, a decision window of 250 ms is chosen. The EMG signal continuously changes during the progress of a contraction. The motion can be identified truly only if the relation between the current and the previous EMG analysis window is known. Thus, the algorithm extracts features from two different time analysis windows (Fig. 3.2) as follows:

1. An analysis window of 250 ms consisting of 240 samples is chosen as the current active time window (kth window) and a feature set is computed based on this segment.

2. An analysis window of 500 ms with 480 samples is chosen consisting of the current time window (kth window) and the previous time window (k-1th window) and the feature set is computed based on this time window. For feature extraction in this time epoch, a moving window scheme is implemented with the moving time window of 250 ms.

3.2.1 Feature Extraction using Time Domain Features

The following time domain features for the EMG signal were computed for both the analysis windows called *'Feature Set-I'*. These features are extracted for motions corresponding to the elbow and wrist movements:

- Mean Absolute Value (MAV) : The mean absolute value of the signal x in segment i that has N samples is calculated as

$$\overline{x_i} = \frac{1}{N}\sum_{k=1}^{N}|x_k| \tag{3.1}$$

- Mean Absolute Value Slope: The difference between the mean absolute values of adjacent segments over the entire sampled signal is given by

$$\triangle\overline{x_i} = \overline{x_i} - \overline{x_{i-1}} \tag{3.2}$$

- RMS Value: The Root Mean Square (RMS) is a measure of energy of the signal. The acRMS of the signal x in segment i that has N samples is calculated as

$$x_i^{RMS} = \sqrt{\frac{1}{N}\sum_{k=1}^{N}|x_k^2|} \tag{3.3}$$

- Zero Crossings (ZC): It provides the frequency measure of the signal by counting the number of times the waveform crosses zero. A threshold (σ) is included to reduce noise induced zero crossings. Given two consecutive samples x_k and x_{k+1}, the ZC count is incremented if,

$$\begin{gathered}\{x_k > 0 \text{ and } x_{k+1} < 0\} \text{ or } \{x_k < 0 \text{ and } x_{k+1} > 0\} \\ and \\ |x_k - x_{k+1}| \geq \sigma\end{gathered} \tag{3.4}$$

- Slope Sign Changes (SSC): A change in the slope sign provides another measure for the frequency content of the signal. A threshold (ϵ) is included to reduce noise induced slope sign changes. Given three consecutive samples x_{k-1}, x_k and x_{k+1}, the ZC count is incremented if,

$$\begin{gathered}\{x_k > x_{k-1} \text{ and } x_k > x_{k+1}\} \text{ or } \{x_k < x_{k-1} \text{ and } x_k < x_{k+1}\} \\ and \\ |x_k - x_{k+1}| \geq \epsilon \text{ or } |x_{k-1} - x_k| \geq \epsilon\end{gathered} \tag{3.5}$$

- Waveform Length: A feature which provides information on the waveform amplitude, frequency and duration. It is the cumulative length of the waveform over each analysis window.

$$l_0 = \sum_{k=1}^{N}(x_k - x_{k-1}) \tag{3.6}$$

3.2.2 Feature Extraction using Wavelet Transform

Different sets of features are extracted using wavelet transform for both the analysis windows. A wavelet transform characterizes the signals locally in the time domain in the analysis window and is useful for approximating non-stationary signals like EMG. The wavelet decomposition of a signal V_0 is given by,

$$V_0 = \sum_{j=-\infty}^{\infty}\sum_{k=-\infty}^{\infty} d_j(k)\psi(2^{-j}t - k) \tag{3.7}$$

where, $d_1(k)$, $d_2(k)$, $d_3(k)$,... are the wavelet coefficients and ψ the wavelet basis. Let the j_{th} wavelet transform of an EMG signal V_0 be denoted by V_j. According to the wavelet orthonormal decomposition, first V_j is decomposed orthogonally into a high-frequency sub-space W_{j+1} and a low frequency sub-

space V_{j+1} using wavelet transform. The low-frequency sub-space V_{j+1} is further decomposed into W_{j+2} and V_{j+2}.

The feature selected for representing each of the wavelet transform sub-patterns is its wavelet entropy. If a wavelet sub-pattern has L coefficients, then the wavelet entropy W_E is defined as,

$$W_E = \sum_{j=1}^{L} |d_j(k)|^2 \tag{3.8}$$

The wavelet entropy for each sub-pattern is calculated for both the time analysis windows and put together, to form a feature vector, *'Feature Set-II'*.

3.3 Classifier Algorithms

The EMG signal is not consistent for different individuals for similar hand motions. The repeatability of the signal for an individual is high but is not exactly the same [104]. Moreover, training an individual to use the glove would improve their motor skills resulting in variations in subsequent Myoelectric Signal (MES) recordings of the same muscle group. A classifier that is able to adapt to these variations in features for different individuals as well as to accommodate each individual's MES change over the course of time is required for faithfully classifying the different hand motions.

3.3.1 k-Nearest Neighbor Classifier

A k-nearest neighbor classifier is initially used for classification of the EMG patterns into hand motions based on feature set I. The k-nearest-neighbor classifier is based on the Euclidean distance between a test sample and the specified training samples [105]. Let x_i be an input sample window with 'q'

features (x_{i1}, x_{i2} ,..,x_{iq}) and 'n' be the total number of input samples. The Euclidean distance between sample x_i and x_l (where l=1,2,3,... n) is defined as,

$$d(x_i, x_l) = \sqrt{(x_{i1} - x_{l1})^2 + (x_{i2} - x_{l2})^2 + \ldots + (x_{iq} - x_{lq})^2} \tag{3.9}$$

With 1-nearest neighbor rule, the predicted hand motion of the test sample *'x_i'* is set equal to the true hand motion (ω) of its nearest neighbor, where m_i is a nearest neighbor to *'x_i'* if the distance is

$$d(m_i, x_i) = min_j \{d(m_j, x_j)\} \tag{3.10}$$

For k-nearest neighbors, the predicted hand motion of the test sample *'x_i'* is set equal to the most frequent actual hand motion among *'k'* nearest training samples.

3.3.2 Linear Discriminant Classifier

To identify which hand motion a sample window belongs to, a linear classifier makes a classification decision based on the value of a linear combination of the different features [105]. If the input feature vector to the classifier is '$\mathbf{x}_i$', then the output y is,

$$y = f(\overrightarrow{w} \cdot \overrightarrow{x}) = f\left(\sum_j w_j \cdot x_j\right) \tag{3.11}$$

where, *'w'* is a real vector of weights and *'f'* is a function that converts the dot product of the two vectors into the desired output. The weight vector *'w'* is estimated from a set of labeled training samples. Often *'f'* is a simple

function that maps all values above a certain threshold to the first class and all other values to the second class. For a multiple class problem, multiple thresholds are present for classification into different classes.

3.3.3 Multilayer Perceptron Classifier

A MLP classifier [105] is used for pattern classification from the input *Feature Vector-II* as shown in Fig.3.3. These networks have an input layer, one or more hidden layer and an output layer. The weights of the neural network for the different layers are initiated to zero before training.

- Input Layer: The 24-dimensional feature vector generated from the EMG data is presented to the input layer. The input layer normalizes these values so that the range of each variable is -1 to 1. The input layer distributes the values to each of the neurons in the hidden layer. The number of neurons in the input layer is equal to dimension of the feature vector; hence, there are 24 input neurons *(N_{in})*.

- Hidden Layer: At a neuron in the hidden layer, the value from each input neuron is multiplied by a weight *(w_{ji})*, and the resulting weighted values are added together producing a combined value u_j. The weighted sum *(u_j)* is fed into a transfer function, σ_h, which outputs a value h_j. The outputs from the hidden layer are distributed to the output layer. A single hidden layer consisting of sixteen *(N_{hid})* neurons is used and a sigmoid function is chosen as the activation function for the hidden layer. Thus, the weighted sum is given by

$$u_j = \sum_{i=1}^{N_{in}} w_{ji} * x_i \tag{3.12}$$

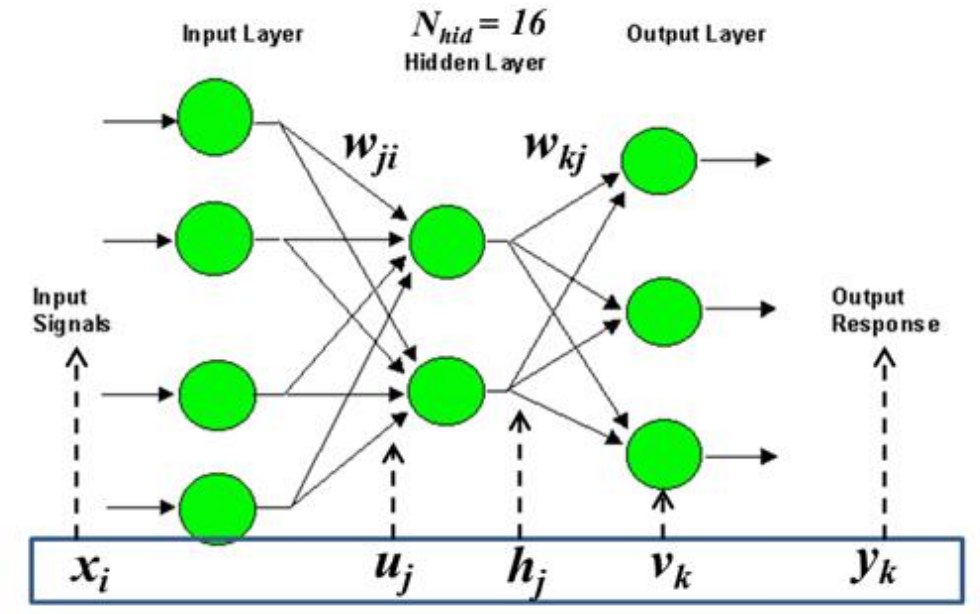

Figure 3.3: Layer structure of the Multilayer Perceptron classifier for the pattern classification of MMG signals

and the hidden layer output h_j is

$$h_j = \sigma_h * u_j \tag{3.13}$$

- Output Layer: At the neuron in the output layer, the value from each hidden layer neuron is multiplied by a weight *(w_{kj})*, and the resulting weighted values are added together producing a combined value v_k. The weighted sum *(v_k)* is fed into a transfer function, σ_o, which outputs a value y_k. The output layer has six neurons corresponding to the six motions to be classified and a linear function is used, as the activation function. Thus,

$$v_k = \sum_{i=1}^{N_{hid}} w_{kj} * h_j \tag{3.14}$$

and the output y_k is

$$y_k = \sigma_0 * v_k \tag{3.15}$$

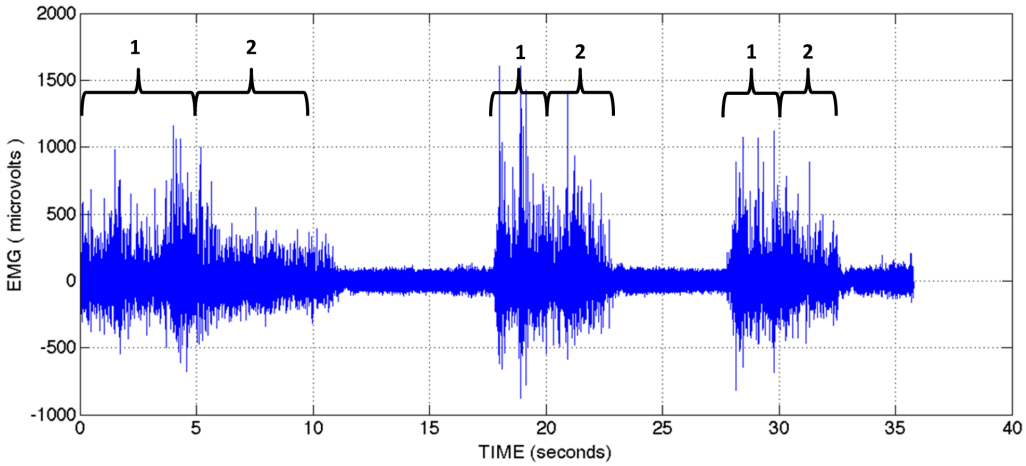

Figure 3.4: Original EMG data from the wrist of a participant where 1: Wrist Flexion and 2: Wrist Extension.

3.4 Experimental Results

3.4.1 Feature Extraction

3.4.1.1 Feature Set-I: Time Frequency Features

Fig.3.4 shows a set of measured EMG data and Fig.3.5 displays the different features for '*Feature Set-I*. This feature set is computed on data from the elbow and the wrist movements and not that of hand opening and grasping. The EMG data has been sub-divided into time segments of 250ms and 500ms (with a 250ms moving window) and all the calculations have been made individually in each time window. The RMS value of the data for each time segment is also shown among the features as it gives an indication of the energy of the signal. Here, the wrist is under flexion and extension with a stationary time of approximately 5 seconds between movements. The analysis of remaining data sets too gives similar feature vectors.

A total of 12 features for each channel of EMG data for both the time segments are extracted. Thus, a 24-dimensional feature vector consisting of

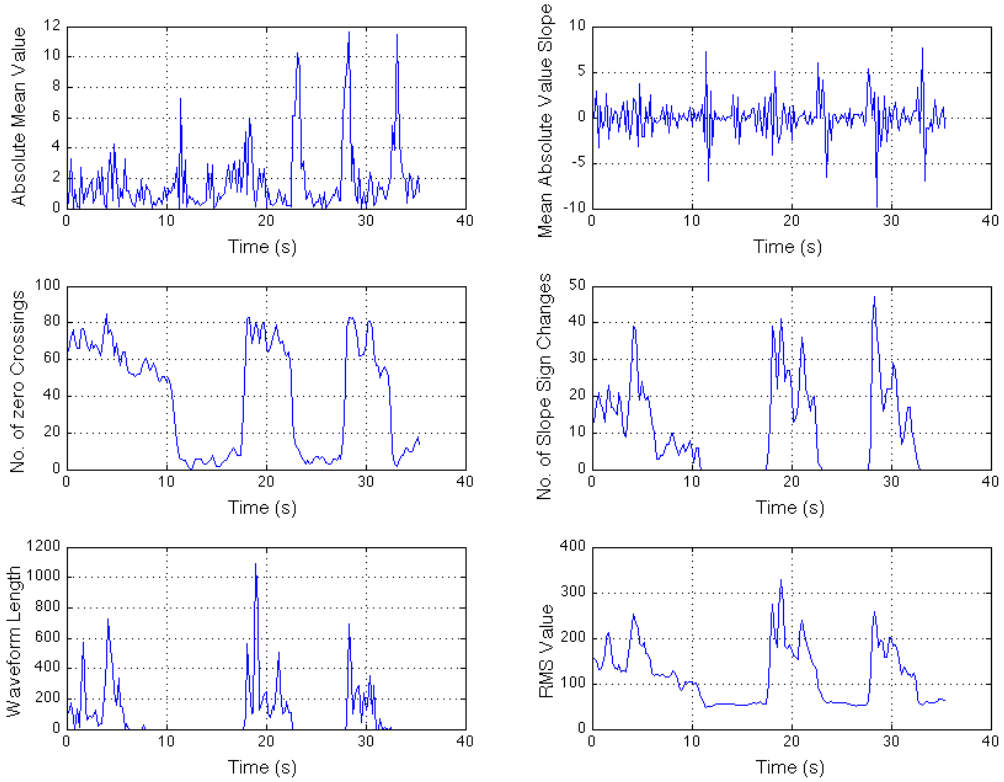

Figure 3.5: Feature set I for the EMG data in Fig.3.4.

the feature sets of each channel is formed and provided to a classifier.

- **OBSERVATIONS**

  - The temporal evolution of the Mean Absolute Value (MAV) of the signal is consistent with the signal. It is difficult to identify different hand movements based only on the MAV.

  - The mean absolute value slope is a better feature in separating the isometric component of the signal from the dynamic component of the signal. It can be observed that during the initiation of the movement(s) the mean absolute value slope increases sharply as compared to during no movement or during isometric contraction.

  - The number of ZC and SSC provide a boundary envelope for the signal movements. These features can be used to restrict the processing during specific time epochs when there is movement.

  - The waveform length not only provides a boundary envelope for the signal movements but it also varies according to the signal strength. It is a good indicator of the amplitude and the frequency of the signal.

  - The temporal evolution of the RMS similarly varies according to the signal strength. It is not only an indicator of the energy of the signal but also of the noise present in the signal. It can be observed that the signal has considerable noise and if either the signal strength drops or the noise increases, it would become difficult to distinguish between energy of the signal and the noise.

3.4.1.2 Feature Set-II: Wavelet Features

Another set of features, *Feature Set-II*, is computed for the EMG data that contain samples of hand opening and grasping as well. Fig.3.6. displays the different wavelet sub-patterns for *Feature Set II* for the same data in Fig.3.4. The value of J specifying the level of decomposition is chosen as '5' while the wavelet used is a Daubechies family wavelet '*db3*' as to work with discrete systems. *D1, D2, D3, D4, D5* show the high frequency or the detailed sub-space at each level of decomposition while *A5* gives the low frequency or the approximate subspace and the final level of decomposition i.e. 5. The wavelet decomposition divides the EMG signal into different frequency bands. The different frequency bands for these components, at a sampling frequency of 960 Hz, are shown in Table 3.3. Fig.3.7 shows the wavelet entropy of all the sub-patterns of the data in each time analysis window. This feature vector also includes measured data of hand opening and grasping movements.

Table 3.3: Frequency Bands for different wavelet sub-patterns

Wavelet Sub-Pattern	Frequency Band
A5	0 - 15 Hz
D5	15 - 30 Hz
D4	30 - 60 Hz
D3	60 - 120 Hz
D2	120 - 240 Hz
D1	240 - 480 Hz

The six wavelet entropy values form the second feature set. The EMG data is sub-divided into time segments of 250 ms and 500 ms (with a 250 ms moving window) and all the calculations are made individually in each time window; hence, we have 12 features for each channel of EMG. Thus, a 24-dimensional feature vector consisting of the feature sets of each channel is formed as Feature Set II and provided to a classifier.

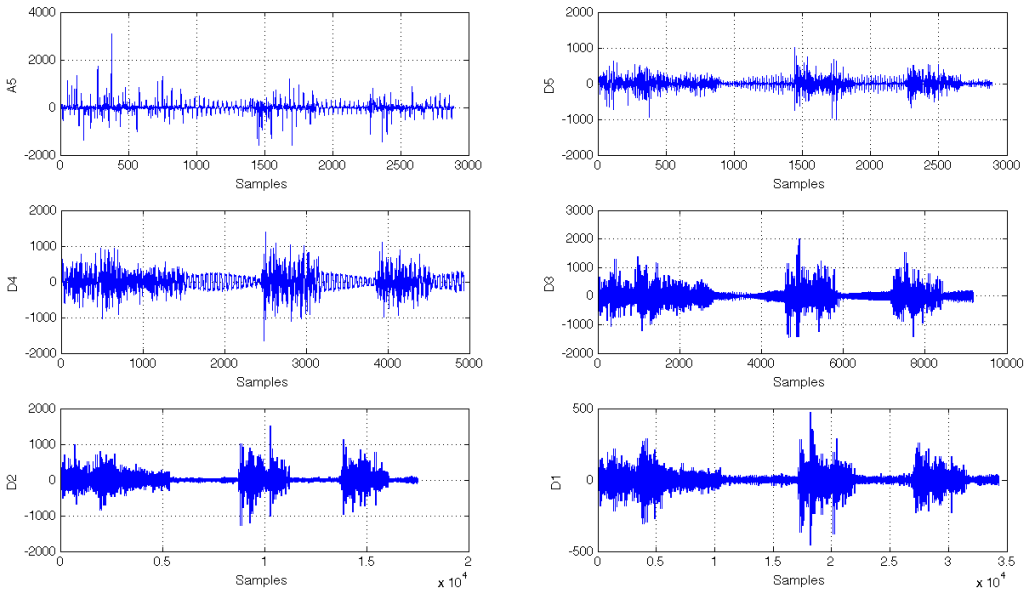

Figure 3.6: Wavelet Sub-Patterns for the signal in Fig.3.4

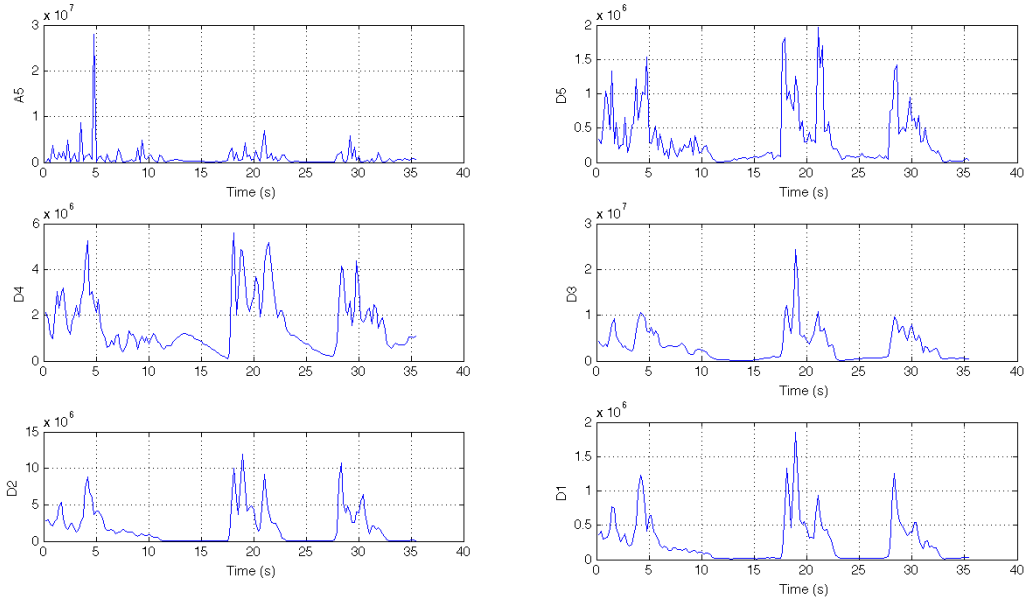

Figure 3.7: Feature Set II consisting of Wavelet Entropies for each of the wavelet sub-patterns of Fig.3.6

- **OBSERVATIONS**
  - It can be observed from Fig. 3.6, and Table 3.3 that the detail components 'D1-D3' are representative of the signal in each of the frequency bands.
  - The noise present in the signal is not present in the wavelet sub-patterns 'D4','D5' and 'A5' that are representative of the lower frequency bands of the signal.
  - The wavelet entropies in Fig. 3.7 of all the wavelet sub-patterns not only provide a boundary envelope for the signal movements but also vary according to the variations in each of them.
  - Wavelet entropies of wavelet sub-patterns 'D1-D5' can be used to distinguish not only the dynamic and the isometric components of the signal but also the different wrist movements.

3.4.2 k-Nearest Neighbor

The k-nearest neighbor algorithm is initially used to classify the feature set I. The two channels of the EMG signals were analysed separately. The data set was divided into thirty training and thirty test sets for each of the elbow and wrist movements. The value of 'k' for classification is taken as '3'. The classifier assigns one of the training set class to the test sample. The confusion matrix for the Classified Motion vs the Actual Motion for the test set is as shown in Table 3.4.

- **OBSERVATIONS**
  - It can be observed from Table 3.4 that the elbow flexion was classified accurately for all the test samples while elbow extension,

wrist flexion and wrist extension had success rates of 83.3%, 80% and 93.3% respectively.

– The elbow movements were not wrongly classified as wrist movements and vice versa as the data from the two channels of EMG were processed separately. The analysis was separate as the EMG signals from the two channels were mutually exclusive.

The k-nearest neighbor algorithm is computationally intensive as it computes the minimum Euclidean distance between the test feature and each of the training features. For the current training data of thirty sets, the threshold of 300 ms, before the user perceives a delay in the initiation of the action, is overshot. For a larger training set, the computational time would be even larger. Thus, implementing the k-nearest neighbor classifier for real-time application of myoelectric control is not feasible.

Table 3.4: Cofusion Matrix for k-Nearest neighbor Classifier (k=3)

Actual Motion	Classified Motion			
	EF	EE	WF	WE
Elbow Flexion (EF)	30	0	0	0
Elbow Extension (EE)	5	25	0	0
Wrist Flexion (WF)	0	0	24	6
Wrist Extension (WE)	0	0	2	28

3.4.3 Linear Discriminant Classifier

The linear discriminant classifier is used to classify the Feature Set-I. The two channels of the EMG signals were analysed separately by two different linear classifiers, namely, one for wrist flexion and extension and the other for elbow flexion and extension. This reduces the 4-class problem to two 2-class classification problems. The data set was divided into thirty training and

thirty test sets for each of the wrist and elbow movements. The classifier is trained using the training set and the thresholds for the classifier are determined.

The four control outputs of the linear classifier, two corresponding to elbow movements and two to wrist movements, are as follows:

1. Elbow Control Signal
   (a) 1 : Elbow Flexion (EF)
   (b) -1: Elbow Extension(EE)
2. Wrist Control Signal
   (a) 1 : Wrist Flexion (EF)
   (b) -1: Elbow Extension(EE)

The confusion matrix for the Classified Motion vs. the Actual Motion for the test set is shown in Table 3.5.

Table 3.5: Confusion Matrix for Linear Discriminant Classifier

Actual Motion	Classified Motion			
	EF	EE	WF	WE
Elbow Flexion (EF)	29	1	0	0
Elbow Extension (EE)	2	28	0	0
Wrist Flexion (WF)	0	0	26	4
Wrist Extension (WE)	0	0	2	28

Ideally, these control outputs are connected to the corresponding servo motors for wrist and elbow movement on the robotic manipulator such that,

- Elbow Flexion and Wrist Flexion: Clockwise rotation of the respective motor and

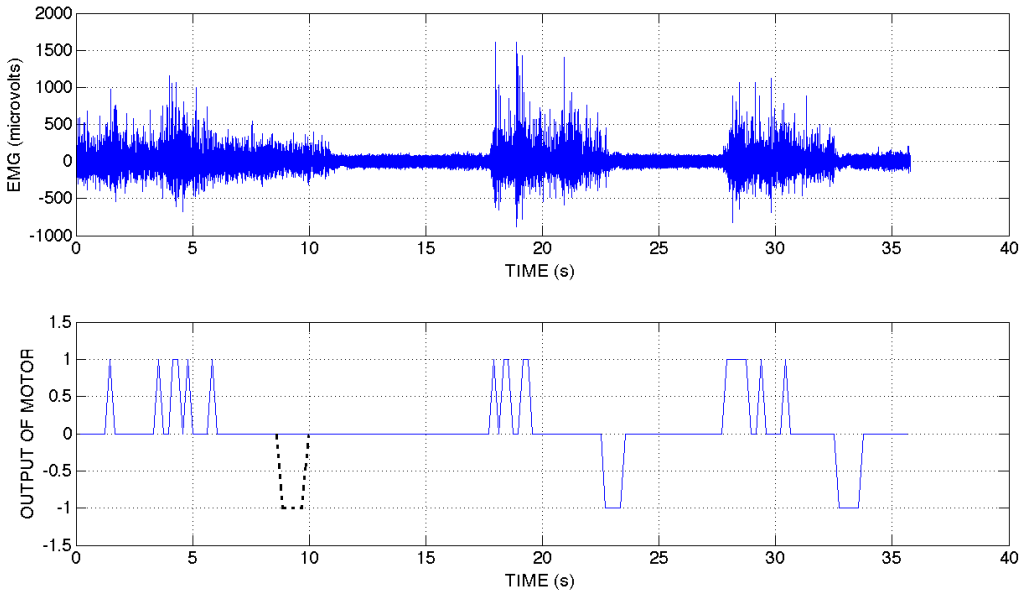

Figure 3.8: Wrist Control Output of the Linear Discriminant classifier to the Manipulator

- Elbow Extension and Wrist Extension: Anti-clockwise rotation of the respective motors.

The control outputs to the manipulator for the EMG data of the wrist and the elbow are shown in Fig.3.8 and Fig.3.9 respectively.

- **OBSERVATIONS**
  - It can be observed from Table 3.5 that the elbow flexion was classified with an accuracy of 96.67% while elbow extension, wrist flexion and wrist extension had success rates of 93.3%, 86.6% and 93.3% respectively.
  - The elbow movements were not wrongly classified as wrist movements and vice versa as different linear discriminant classifiers were used to process the data from the two channels of EMG separately. The analysis was separate as the EMG signals from the two channels were mutually exclusive.

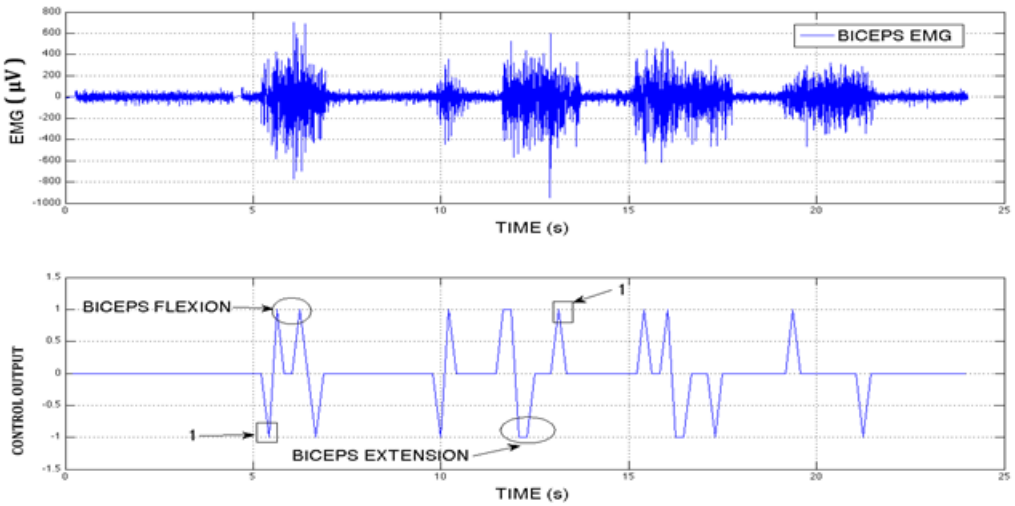

Figure 3.9: Elbow Control Output of the Linear Discriminant classifier to the Manipulator

- As seen in Fig.3.8 , the linear classifier is unable to classify one of the wrist extension movements as shown by the black dotted lines. Similarly, the classified motions '1' in Fig.3.9 have been wrongly classified.
- Each time the output goes to either 1 or -1, the servomotor stays in that position until the linear classifier gives an opposing control output.
- The processing time required by the linear classifiers to generate the control signal is well within 300 ms (the threshold of for the user to perceive a delay in the initiation of the action).

3.4.4 Multilayer Perceptron Classifier

The MLP classifier is used to classify the feature set II. The data set also consisted of hand opening and grasping apart from the wrist and elbow movements. The data set was divided into thirty training and thirty test sets for each of the wrist and elbow movements and fifteen training and fifteen

test sets for the hand opening and grasping movements. Thus, a total of six hand movements are classified using 2 channels of EMG data. The output layer neurons of the MLP classifier each corresponds to one of the following hand movements:

1. Elbow Control Signal
   (a) 1 : Elbow Flexion (EF)
   (b) -1: Elbow Extension(EE)
2. Wrist Control Signal
   (a) 1 : Wrist Flexion (EF)
   (b) -1: Elbow Extension(EE)
3. Hand Control Signal
   (a) 1 : Hand Grasping(HG)
   (b) -1: Hand Opening (HO)

The confusion matrix for the Classified Motion vs the Actual Motion for the test set is given in Table 3.6. The control outputs to the manipulator for the EMG data of the hand opening and grasping is as shown in Fig 3.10. The output for the wrist and elbow movements mirror that of the linear discriminant classifier.

- **OBSERVATIONS**
  - It can be observed from Table 3.6 that the elbow flexion was classified accurately for all the test samples while elbow extension, wrist flexion and wrist extension had success rates of 93.3%, 93.3% and 93.3% respectively. The hand grasping and hand opening movements had success rates of 73.3% and 66.67% respectively.

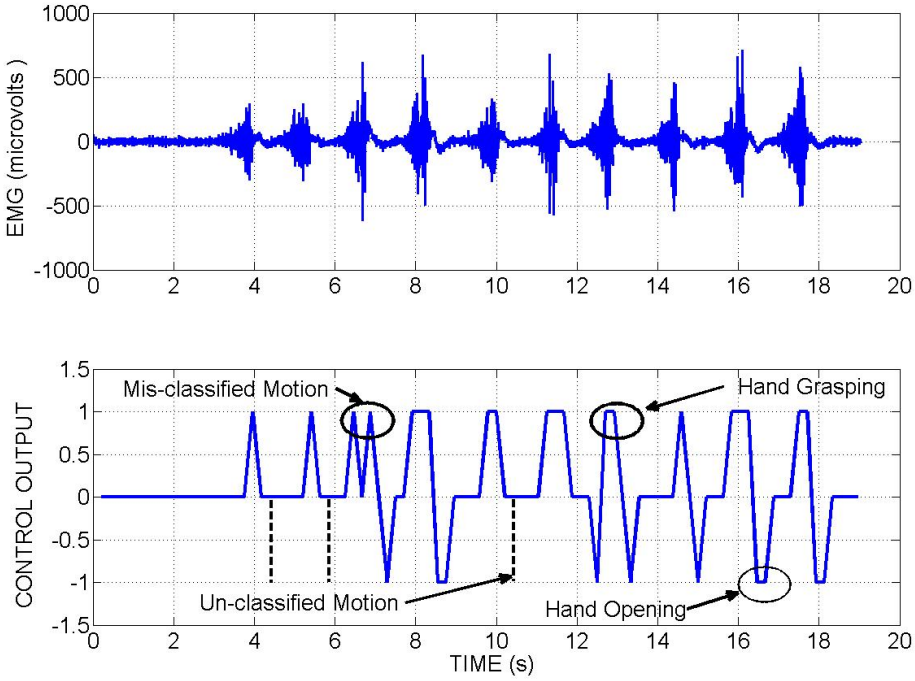

Figure 3.10: Hand Control Output of the MLP classifier to the Manipulator

Table 3.6: Confusion Matrix for Multilayer Perceptron Classifier

Actual Motion	Classified Motion					
	EF	EE	WF	WE	HG	HO
Elbow Flexion (EF)	30	0	0	0	0	0
Elbow Extension (EE)	2	28	0	0	0	0
Wrist Flexion (WF)	0	0	28	2	0	0
Wrist Extension (WE)	0	0	2	28	0	0
Hand Grasping (HG)	0	0	3	1	11	0
Hand Opening (HO)	0	0	0	5	0	10

- The elbow movements were not wrongly classified as wrist movements or hand movements as the data from the two channels of EMG were processed separately. The analysis was separate as the EMG signals from the two channels were mutually exclusive.
- As seen in Fig.3.10, the MLP classifier is unable to classify some of the hand opening movements as shown by the dotted lines.
- As seen in Fig.3.10, the MLP classifier is wrongly classifying some of the hand closing and opening.

It can be seen from the confusion matrix for the MLP classifier that the elbow and wrist movement classification rates are similar to that of the linear discriminant classifier. The MLP classifier is able to classify all but the hand opening and grasping movements quite accurately. The success rate for hand grasping and hand opening is quite low as they are wrongly classified as wrist flexion or extension.

3.5 Myoelectric Glove

An attempt is made to implement the above results on a myoelectric glove designed in the laboratory. The outline of the control system of the myoelectric glove is shown in Fig. 3.11. The basic components of the system are a microcontroller, the myoelectric glove, and a differential amplifier for measuring the surface EMG signals.

3.5.1 Hardware

The input signal is amplified by a differential amplifier with an isolated input and with a gain of 100-dB. To ensure a faithful signal, the input impedance

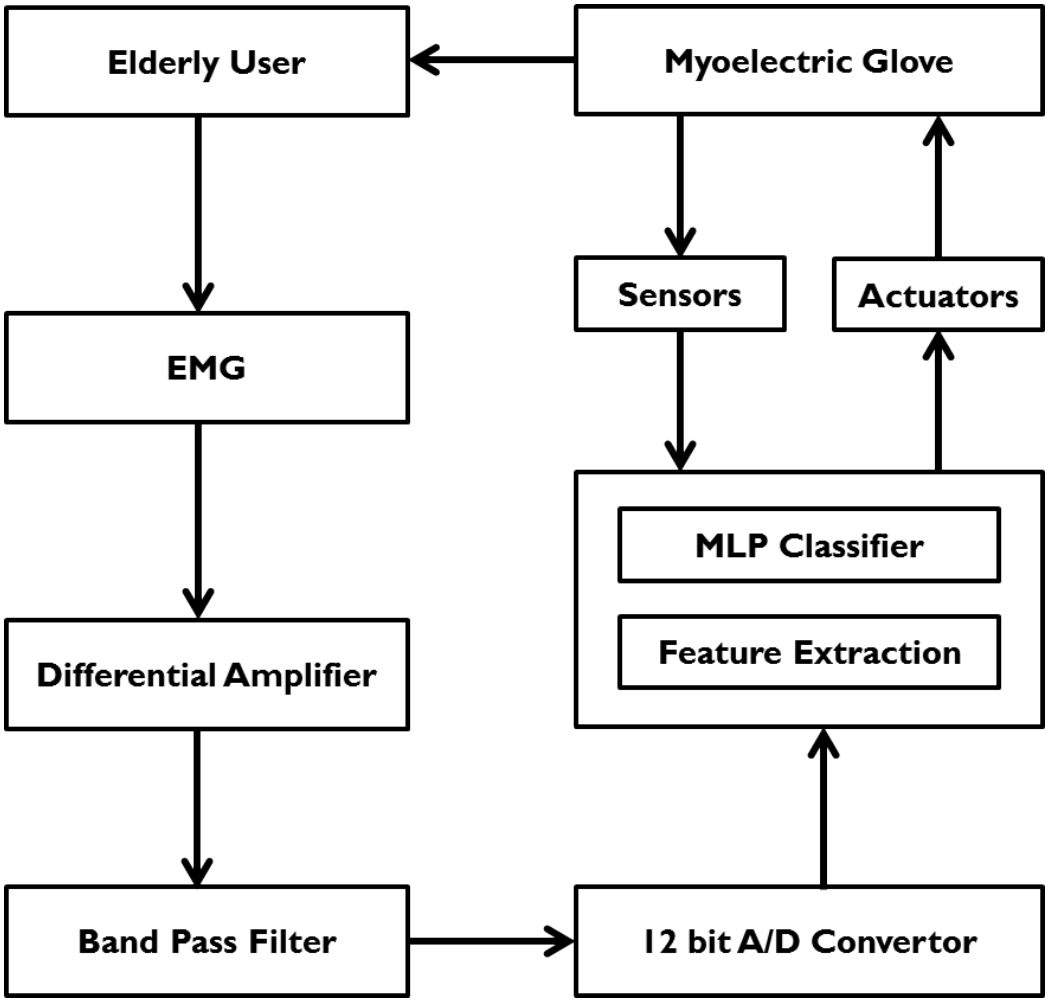

Figure 3.11: Outline of the control system of the Myoelectric Glove

of the amplifier should be of the order of 100 MΩ. The dominant energy spectrum of the EMG signal generally lies between 20 to 350 Hz. Hence, an analog 2^{nd} order Butterworth band pass filter with cut-off frequencies of 10 Hz and 350 Hz is designed to filter out any other unwanted frequencies present in the signal. As per Nyquist criterion, the sampling frequency should be more than twice the maximum frequency present in the signal i.e. it should be greater than 700 Hz. The amplified EMG signal is over-sampled at a rate of 1500 Hz using a 12-bit analog to digital converter available as a microcontroller peripheral. The microcontroller analyses the digitised EMG signal and generates control signals to actuate the servo motors to move the glove.

The effect of crosstalk in EMG has been discussed before. It can lead to a sudden increase in the amplitude and frequency of the sampled EMG signal which may lead to random and unwanted motion of the actuators. Thus sensors are used on the glove that give a feedback of the real-time actual position and velocity of the glove. This enables the micro-controller to take corrective action to prevent these random motions in the event of crosstalk or a sudden change in the EMG amplitude or frequency.

3.5.2 Microcontroller System

The microcontroller is used to process the digitized EMG signals, implement the classifier, generate control signals for the servo motors and receive position information from the sensors. A PIC microcontroller (Microchip PIC 24HJ128) with a crystal frequency of 10MHz and memory of 128 kilobyte, sufficient enough for the myoelectric glove, is at the heart of the system. It is programmed in C in the IAR embedded workbench software and uses standard C libraries.

3.5.3 Myoelectric Exoskeleton

The myoelectric exoskeleton consists of two units, one at the elbow and the other at the wrist. Each unit consists of a fixed part and a moving part with the elbow unit consisting of a plastic exoskeleton with the fixed part strapped to the hand at the *biceps* and the moving part to the forearm. The wrist unit's fixed part is strapped to the hand at the wrist and the moving part to the dorsum of the hand.

The human wrist has a flexion and extension range of about 160° and the wrist unit uses a Hitec servo HS-755HB as the actuator. The elbow has a flexion and extension range of about 120° and the elbow unit uses a Hitec servo HS-805BB. The different servos are used as higher torque is required for elbow movement as compared to wrist movement.

Sensors are required to give feedback on the actual position and velocity of the glove. A potentiometer is used along with the servo motor of the wrist unit to monitor the position of the wrist.

3.5.4 Control System

The microcontroller implements the multilayer perceptron classifier to generate the control signals for the actuators. The control output for each of the four hand motions are as follows:

1. Elbow Motor
   (a) 1 : Elbow Flexion (EF)
   (b) -1: Elbow Extension(EE)
2. Wrist Motor
   (a) 1 : Wrist Flexion (EF)

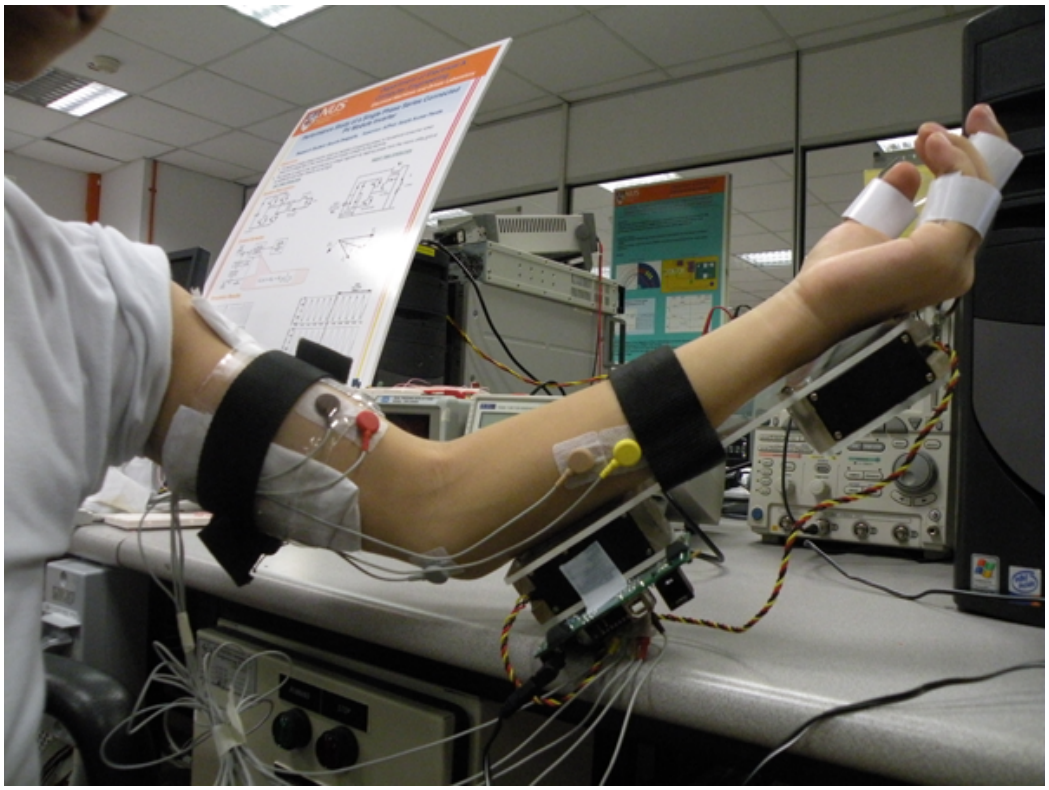

Figure 3.12: Myoelectric Glove Prototype

(b) -1: Elbow Extension(EE)

The activation of the elbow motor results in the servo motor rotating by an angle of 7.5° in either direction while the activation of the wrist motor results in the servo motor rotating an angle of *15*° in either direction. The human wrist has a flexion and extension range of about 160° while the elbow has a flexion and extension range of about 120°. The rotation of the actuator is proportional to the muscle electrical activity. The system checks the sensor information for the current position of the actuator and compares it with the boundary conditions and then regulates the speed of the actuator accordingly. Thus, if the patient's wrist or elbow is already at its maximum flexion and extension positions, then the system doesn't allow any further actuations. Fig.3.12 shows the myoelectric glove in operation.

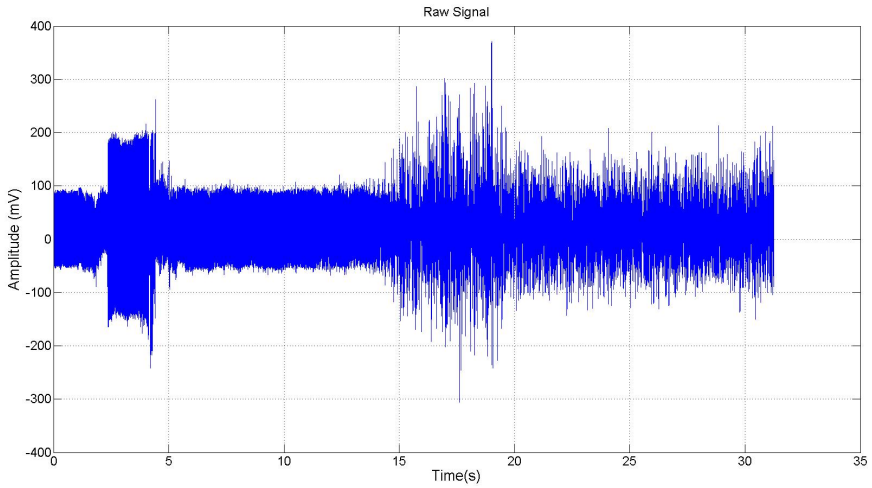

Figure 3.13: Raw *biceps* EMG measured using the hardware setup

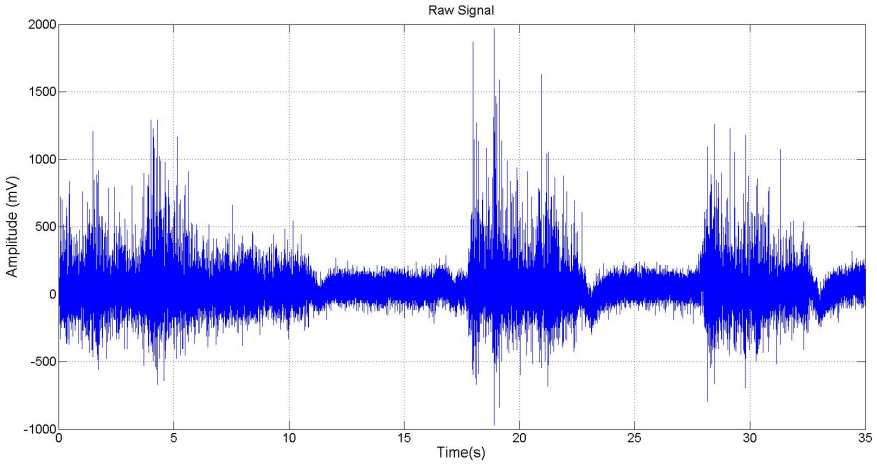

Figure 3.14: Raw Wrist EMG measured using the hardware setup

3.5.5 Results

3.5.5.1 Measured EMG signals for the Elbow and the Wrist Muscle Groups

It can be inferred from Fig.3.13 and Fig.3.14 that the EMG raw signals have a large amount of noise. The signal strength is very low and it is difficult to identify the signal from the raw signal. It becomes clear from Fig.3.15 and Fig.3.16 that the noise is predominantly the power line interference. The

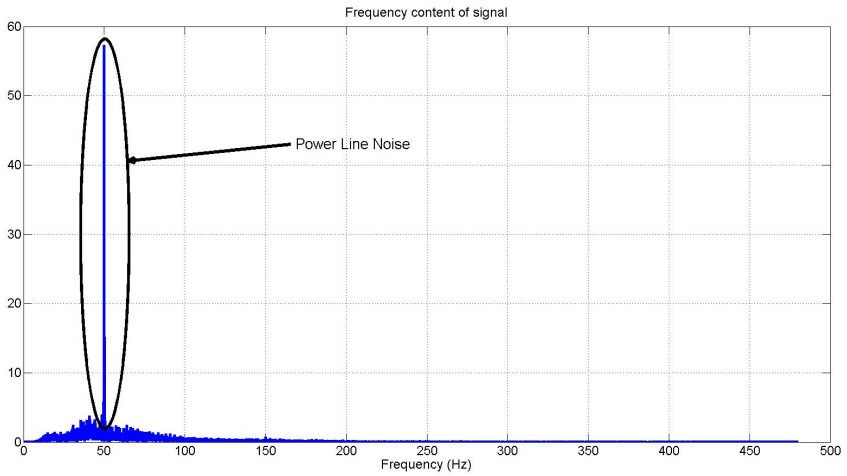

Figure 3.15: FFT for the *biceps* EMG in Fig.3.13

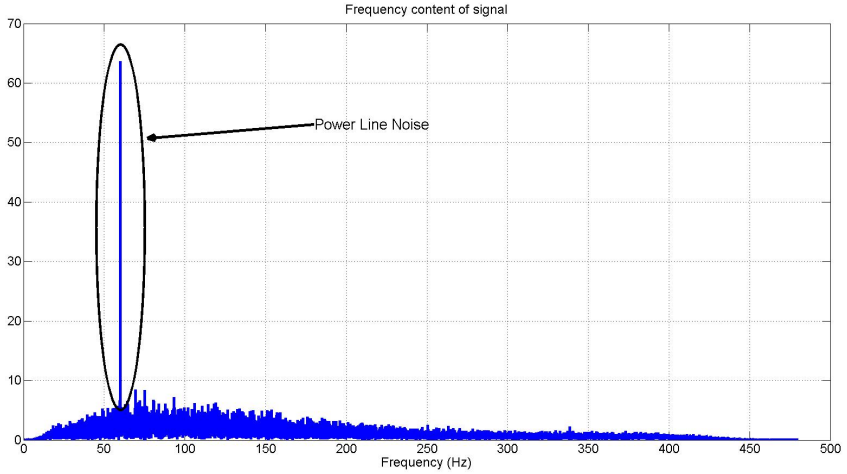

Figure 3.16: FFT for the Wrist EMG in Fig.3.14

magnitude of the power line interference is very high compared to the actual signal strength of the EMG.

3.5.5.2 Classification Results for the MLP hardware Classifier

The confusion matrix for the Classified Motion vs. the Actual Motion for the hardware implementation is shown in Table 3.7.

Table 3.7: Confusion Matrix for the Hardware MLP Classifier

Actual Motion	Classified Motion			
	EF	EE	WF	WE
Elbow Flexion (EF)	12	6	0	0
Elbow Extension (EE)	8	14	0	0
Wrist Flexion (WF)	0	0	16	9
Wrist Extension (WE)	0	0	4	11

It can be clearly seen from the confusion matrix in Table 3.7 that the classifier misclassifies the motions with a high percentage.

- **OBSERVATIONS**
  - It can be observed from Table 3.7 that the elbow flexion was classified with a low accuracy of 66.67% while elbow extension, wrist flexion and wrist extension had success rates of 70%, 80% and 55% respectively.
  - The elbow test samples were not wrongly classified as wrist movements and vice versa by the MLP classifier as they were mutually independent of each other.
  - The hardware based MLP classifier uses the same decision window of 250 ms with an analysis window of 500 ms for classification of the hand movements which is maintained well within 300 ms,

the threshold beyond which the user may perceive a delay in the initiation of the action.

3.6 Discussion

An attempt is made to classify the basic six elbow and wrist motions using two channels of EMG data. A pattern recognition method is used for the classification of the EMG signals based on different movements of the upper limb and includes feature identification and selection and different classifiers are used to distinguish between different movements of the upper limb using the identified features. Three classifiers were studied and it is found that the Multilayer Perceptron (MLP) works best for classifying different movements of the upper limb as compared to the the linear classifier or the k-nearest neighbor classifier.

While the off-line implementation of the control algorithms worked with good accuracies, the hardware implementation of the myoelectric glove based on the outputs resulted in much poorer results. The EMG signal acquisition had very low signal to noise ration and the resulting implementation did not give a high success rate. Removing power line noise from the EMG signal is challenging because of the overlapping bandwidths of the two signals. Modern biomedical amplifiers have a very high common mode rejection ratio. Nevertheless, recordings are still contaminated by residual power-line interference. The power line interference is not fixed at 50 Hz and has been found to vary between 49 Hz to 51 Hz as shown in Fig. 3.15 and Fig. 3.16. Hence, a fixed notch filter of 50 Hz would lead to ineffective filtering if there is a deviation of frequency in the power line interference. Moreover, there will be signal components at the power line frequencies and using a notch filter

would eliminate the useful signal along with the power line noise.

Classification of the hand movements at the larger joints such as the elbow joint is a challenge to implement in a pattern classification based system. Though the system is able to classify the movements correctly, it is not able to predict the initial and final states of the hand positions from the EMG data as shown in Fig.3.9. This is fine for the smaller joint movements like the hand open and close where joint torque information is not as critical as the elbow joint as shown in Fig.3.10. Thus, a relation needs to be established between the larger joint torques and the EMG signal for the continuous movement of the actuator.

It can also be inferred from the results that more the number of EMG electrodes, better the classification rates for a pattern recognition based signal processing system. The problem with such an approach as outlined earlier is the reluctance of the elderly person to attach and detach multiple electrodes for rehabilitation. However, using only one set of EMG electrodes would prove detrimental to the rehabilitation process itself. Thus, there is a need to establish a multimodal system of sensors that are embedded into the rehabilitation device itself with minimum hindrance to the elderly user.

To circumvent the above mentioned problems the following approaches are outlined in the succeeding chapters:

- Adaptive filtering approach to remove the power line interference from the EMG signal.
- Dividing the signal acquisition system into two complimenting sensor systems.
- Use of EMG sensors to build an EMG-Joint Torque model for estimation of elbow torque.

- Use of MMG sensors to design a pattern recognition based system to differentiate the different movements of the hand and the wrist.

3.7 Summary

This chapter details the preliminary results for the signal processing of the EMG signal for application in elderly rehabilitation. Feature extraction based on basic time frequency parameters and wavelet parameters was initially described. The subsequent sections describes the classification of the EMG signals based on different movements of the upper limb and include feature identification and selection, and different classifiers used to distinguish between different movements of the upper limb using the identified features. It is found that the Multilayer Perceptron (MLP) works best for classifying different movements of the upper limb as compared to the the linear classifier or the k-nearest neighbor classifier.

Next to that, hardware implementation of the myoelectric glove based on the outputs from Section 3.3 along with the experimental results and classification accuracies for the hardware MLP classifier is detailed.

Finally, the problems associated with the above approach are outlined and alternative solutions are provided for implementation in the succeeding chapters.

4

A Modified Hilbert-Huang Algorithm based Adaptive Filter for Elimination of Power line Interference from Surface Electromyography

It was observed in Chapter 3 that the EMG raw signals have a large amount of noise. The signal strength is very low and it is difficult to identify the signal from the raw signal. It was also clear that the noise is predominantly the power line interference. The magnitude of the power line interference is very high compared to the actual signal strength of the EMG. This is also augmented by the fact that the signal strength for the elderly's EMG is much lesser as compared to a young healthy person.

This chapter details the study for the removal of Power Line Interference (PLI) from EMG. Section 4.1 and 4.2 details the methods for estimating the power line frequency in the EMG signal as well as the theoretical basis for adaptive filtering of the EMG signal. Section 4.3 describes the simulations results for the designed filter and the corresponding discussions while Section 4.4 and 4.5 outlines the experimental results and discussion for the designed filter for removing power line noise from EMG signal.

The EMG adaptive signal processing problem can be described as follows:

- Estimate the frequency of Power Line Interference (PLI) in the measured signal in real time.
- Design an adaptive filter that reacts to the change in frequencies in real time and accordingly removes just the noise and not the EMG data signal.

An adaptive filter requires a reference input that is correlated with the Power Line Interference (PLI) that needs to be removed [106]. This reference input is constructed mathematically using the estimated instantaneous frequency of the power line interference with Hilbert-Huang Transform (HHT) and subsequently applied to the adaptive filter structure. *Zhidong et.al.* in [107] use a similar method to estimate the PLI in ECG signals using Empirical Mode Decomposition (EMD). The advantage the authors had in designing the algorithm was that the noise signal bandwidth and the ECG signal bandwidth don't interfere with each other hence, removal of the noise is much easier. *Bourdraa et.al.* [30] proposed a signal filtering method based on EMD, by removing the noisy Intrinsic Mode Function (IMF) to filter the signal. The authors focus on the removal of high frequency noise from standard test signals and not on signals with overlapping bandwidths. But filtering the PLI from EMG is challenging as, the bandwidths of the EMG signal and the PLI overlap. Since HHT can be used to determine the instantaneous frequency of non-linear and non-stationary signals, it would be apt to use it in real-time to estimate the instantaneous frequency of the PLI and accordingly eliminate it.

In this section an adaptive Variable Least Mean Square filter is proposed to eliminate the PLI from the EMG signal. This notch filter can decrease the numbers of mathematical operations significantly and is suitable for practical implementation. The characteristics of adaptive LMS filter makes it more stable than many other Infinite Impulse Response (IIR) filters. In

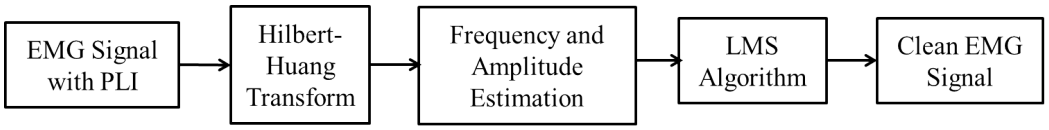

Figure 4.1: Overview of the HHT-LMS adaptive filter

this study, recording of the the reference signals (i.e. 50/60 Hz PLI signal) for an adaptive structure is not required as a synthetic signal is generated that emulates the PLI in the EMG signal. This reduces the complexity of hardware and eliminates the need for supplementary electrodes that collect the noise reference.

The surface EMG signals are measured from the *biceps brachii*, which measures the MES activity during the flexion and extension of the elbow. Data was acquired from normally-limbed individuals who were instructed to perform dynamic elbow extension and flexion with 1 kg of weight in their hand and sampled at a frequency of 960 Hz.

The overview of the HHT-LMS adaptive filter is shown in Fig. 4.1. The different blocks are described in the subsequent sections.

4.1 Hilbert-Huang Transform (HHT)

The Hilbert-Huang Transform (HHT) [108] is an empirically based data-analysis method. Its basis of expansion is adaptive, so that it can produce physically meaningful representations of data from nonlinear and non-stationary processes. The HHT consists of two parts: Empirical Mode Decomposition (EMD) and Hilbert Spectral Analysis (HSA) as explained below:

4.1.1 Empirical Mode Decomposition (Sifting Process)

The EMD method is necessary to deal with data from non-stationary and nonlinear processes and is represented by different Intrinsic Mode Function (IMF) with the following definition:

A. in the whole dataset, the number of extrema and the number of zero-crossings must either equal or differ at most by one and

B. at any point, the mean value of the envelope defined by the local maxima and the envelope defined by the local minima is zero.

The signal is decomposed into its constituent IMF(s) based on the above definition as follows:

(a) Find the local extrema in the data *x(t)* including all the maxima and minima.

(b) Connect the maxima and minima separately using smooth cubic splines, to get the upper envelope $e_{max}(t)$ and the lower envelope $e_{min}(t)$ respectively.

(c) Calculate the mean of the upper and the lower envelopes. Thus,

$$m(t) = \frac{(e_{max}(t) + e_{min}(t))}{2} \tag{4.1}$$

(d) Since the IMF needs to have a local zero mean, subtract *m(t)* from the original signal *x(t)* to get $x_1(t)$. Thus,

$$x_1(t) = x(t) - m(t) \tag{4.2}$$

(e) Verify that the normalized squared distance between two successful sifting

is small. The value of SD chosen for this algorithm is 0.1.

$$SD_k = \frac{\sum_{t=0}^{T} |x_{k-1}(t) - x_k(t)|^2}{\sum_{t=0}^{T} x_{k-1}^2(t)} \tag{4.3}$$

(f) Check if $x_1(t)$ fulfills the definition of an IMF.

(g) If yes, terminate the process, else continue with steps (a) to (f) till $x_1(t)$ is an IMF or results in a residual term $c(t)$ that is less than a predetermined small number or becomes monotonic.

For a given signal $x(t)$, the EMD ends up with a representation of the form:

$$x(t) = c(t) + \sum_{n=1}^{k} x_n(t) \tag{4.4}$$

where, $c(t)$ denotes the residual term and $x_n(t)$ denotes the different IMF of the signal $x(t)$.

4.1.2 Hilbert Spectral Analysis (HSA)

After obtaining the IMF(s) components, the Hilbert transform is applied to each IMF component, and then the instantaneous frequency is computed. After performing Hilbert transform on each IMF component, the original signal can be represented by the real part of the following equation:

$$x(t) = Real\left\{\sum_{j=1}^{n} a_j(t) exp\left[i \int \omega_j(t) dt\right]\right\} \tag{4.5}$$

where, n is the total number of IMF(s), a_j is the instantaneous amplitude and ω_j is the instantaneous phase of the j_{th} IMF.

The EMD decomposes the non-stationary signal into narrow-band components with decreasing frequency. The decomposition is complete, local and

adaptive. The basis formed by the IMF(s) directly comes from the signal which guarantees the inherent characteristic of signal and avoids the diffusion and leakage of signal energy. The sifting process eliminates riding waves, so each IMF is more symmetrical and is a zero mean signal. By construction, the number of extrema is decreased when going from one residual to the next thus ensuring that there are a finite number of steps for the complete decomposition.

4.1.3 Estimation of Power Line Frequency

The following algorithm is used for estimating the instantaneous frequency of the PLI present in the signal:

1. The signal is divided into N time windows each of length 500 ms. A moving window scheme is applied with a processing window of 250 ms and a 250 ms moving window.

2. The signal is decomposed into its constituent IMF(s) using the EMD method in each of the time windows.

3. The Hilbert Transform is applied to each IMF component to estimate the instantaneous amplitude and frequency of the signal. Hilbert energy spectrum of the different IMF(s) is also calculated.

4. The IMF(s) that contain the power line noise are isolated and are sorted according to decreasing values of the Hilbert energy spectrum.

5. The powerline instantaneous frequency is calculated as a weighted sum of the individual instantaneous frequencies as follows [109]:

$$IF_n(x(t)) = \frac{\sum_{j=1}^{3} a_j^2(t) v_j(t)}{\sum_{j=1}^{3} a_j^2(t)} \tag{4.6}$$

Here, the number of IMF(s) for calculation of the powerline instantaneous frequency is chosen as three, isolating the IMF(s) with the maximum Hilbert spectrum with respect to the powerline frequency.

6. Since the power line frequency can vary between ± 2% of the nominal frequency, lower limit and upper limit of 49 Hz and 51 Hz respectively are fixed for a nominal frequency of 50 Hz.

7. The average amplitude of the power line noise (A_n) is calculated using the instantaneous amplitudes of the above isolated IMF(s).

8. Frequencies between 48 HZ and 52Hz are evaluated in each time window. If the amplitude is within ±10% of A_n, the corresponding frequency $f_n(x(t))$ is noted as noise and the time of its occurrence recorded.

9. The list of frequencies and the time of their occurrence along with their respective amplitudes in each time window is given as an input to the adaptive filter block for eliminating the power line interference from EMG.

4.2 Least Mean Squares (LMS) Algorithm

The Least Mean Squares (LMS) algorithm is an approximation of the steepest descent algorithm, which uses an instantaneous estimate of the gradient vector of a cost function. The estimate of the gradient is based on sample values of the input vector and an error signal. The algorithm iterates over each coefficient in the filter, moving it in the direction of the approximated gradient. For the LMS algorithm, it is necessary to have a reference signal $d(t)$ representing the desired filter output. The difference between the reference signal and the actual output of the transversal filter is the error signal.

Applying this scheme to the problem of filtering a noisy EMG signal, the primary input *x(t)* of the system corresponds to the clean EMG signal *s(t)* corrupted by power line noise *p(t)*. The reference input *r(t)* is a sinusoidal signal with frequency *'f'* and zero phase and is defined as

$$r(t) = A * Sin(2\pi ft) \tag{4.7}$$

The output *y(t)* of the filter, is estimated to match the noise *p(t)* in the primary input. If the M-dimensional filter coefficient vector is defined as *w(t)* $= [w_0(t)\ w_1(t)\ ...\ w_{M-1}(t)]^T$, then the equations that describe the adaptation of the system based on the LMS algorithm with fixed step-size are given by

$$y(t) = w^T(t)r(t) \tag{4.8}$$

$$e(t) = d(t) - y(t) \tag{4.9}$$

$$w(t+1) = w(t) + \mu e(t)r(t) \tag{4.10}$$

Let *d(t)* denote the desired signal, which in this case is equivalent to the primary input *x(t)*. If the error signal *e(t)* is defined as the difference between the desired signal *d(t)* and the filters output signal $y(t) = \hat{p}(t)$, then

$$e(t) = x(t) - y(t) \tag{4.11}$$

$$e(t) = s(t) + p(t) - \hat{p}(t) \tag{4.12}$$

$$e(t) = \hat{s}(t) \tag{4.13}$$

It can be seen from Eqn.4.13 that $\hat{s}$(t) is an estimate of the noise-free EMG signal and the LMS algorithm is designed to minimize an instantaneous version of the Mean Squared Error (MSE) given by $E\{e(t)^2\}=E\{\hat{s}(t)^2\}$

For removal of PLI from the EMG signal, it is desired to have the smallest notch bandwidth; however, it is not possible to minimize this bandwidth by making μ arbitrarily small. Instead, the step-size parameter needs to be chosen in an optimal way at every iteration of the algorithm to ensure an optimal equilibrium between all the desired filter characteristics. Several variable step-size parameter algorithms have been proposed in the literature [25, 26, 29, 110, 111]. Most of the algorithms mentioned in [25, 26, 29, 110] are not suitable for the application of interest due to its complexity in implementing in real time.

The objective is to ensure large μ(t) when the algorithm is far from the optimum, and decrease μ(t) as we approach the optimum, hence, the need for decreasing the notch bandwidth and increasing noise attenuation. The step-size adjustment proposed in [111, 112] is controlled by the square of the prediction error. The simplicity of the algorithm and its sensitivity to changes in the error signal makes it a good candidate to implement it in the adaptive noise cancellation scheme. The algorithm for updating μ(t) is as follows:

$$\mu(t+1) = \alpha\mu(t) + \gamma e^2(t) \tag{4.14}$$

The constant, α is a forgetting factor and varies between 0 and 1 while γ is the step-size parameter for the adaptation of μ and is greater than zero. Substituting the variable step size in Eqn.4.10, the updated equation for the filter becomes:

$$w(t+1) = w(t) + \mu(t)e(t)r(t) \tag{4.15}$$

4.3 Simulation Results

4.3.1 Signal Model

The signal observation model is given by

$$x(t) = s(t) + p(t) \tag{4.16}$$

where *s(t)* is the EMG signal of interest and *p(t)* is an additive time-varying sinusoidal interference.

Several mathematical models have been developed to describe EMG signals. Some examples include AR models, matching pursuit method-based models, Kalman filters, and Gaussian shaping filters. In this study, a shaping filter is used to generate the surface EMG signal by passing white Gaussian noise through it. The transfer function of the shaping filter is as follows:

$$H_{EMG}(\omega) = \frac{jK\omega_h^2\omega}{(\omega_l + j\omega)(\omega_h + j\omega)^2} \tag{4.17}$$

In Eqn.4.17 ω_l and ω_h are the shape adjusting parameters of the EMG spectrum while K is the gain factor and is adjusted to normalize the power of the EMG signal to 1. Fig. 4.2 shows the simulated EMG signal generated using Eqn. 4.17 while Fig. 4.3 shows its corresponding frequency plot.

The power line interference is added to the EMG signal by generating a sinusoid with a given amplitude and frequency. The amplitude of the sinusoid is calculated based on the desired signal to noise ratio (SNR). For the simulations, SNR is varied between -20 dB and +20 dB in 5 dB increments. The frequency of the synthetic power line interference is varied between 49 Hz and 51 Hz at 0.25 Hz increments. Fig. 4.4 shows the FFT plot of the signal

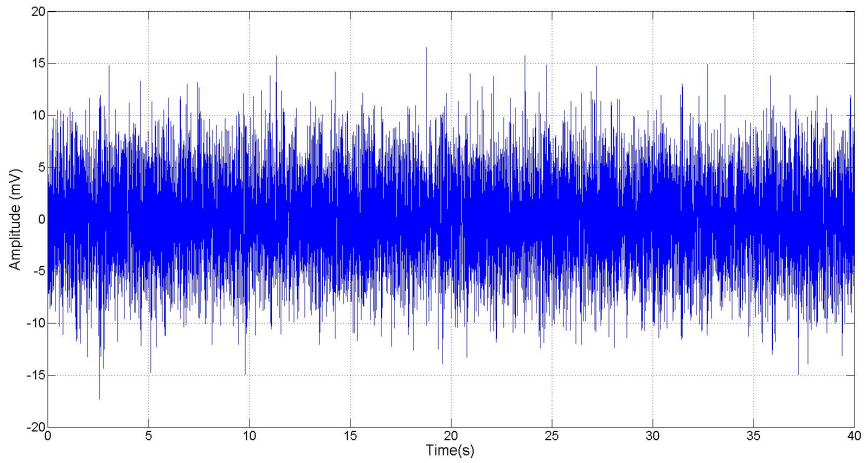

Figure 4.2: The simulated EMG signal generated using the spectral filter in Eqn.4.17

in Fig. 4.2 with added PLI at 50 Hz.

4.3.2 Simulation Results

4.3.2.1 Empirical Mode Decomposition of the EMG Signal

In this section, the EMG signal is decomposed into its constituent IMF(s). The EMG signal is processed as follows:

- Firstly, the dataset is processed offline
- The signal is divided into time epochs of 500 ms with a moving window of 250 ms to simulate real time processing conditions.

4.3.2.2 Hilbert Spectral Analysis and Frequency Estimation

The instantaneous frequency of the signal can be estimated by performing the Hilbert Spectral Analysis (HSA)of the above derived IMF(s). The frequency-time plot for the signal in Fig. 4.5 is shown in Fig 4.6 for the first four IMF(s).

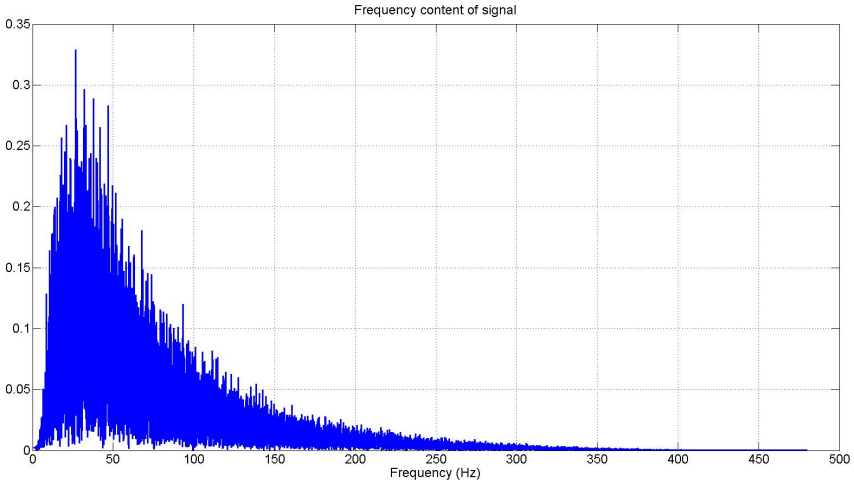

Figure 4.3: FFT of the signal in Fig.4.2

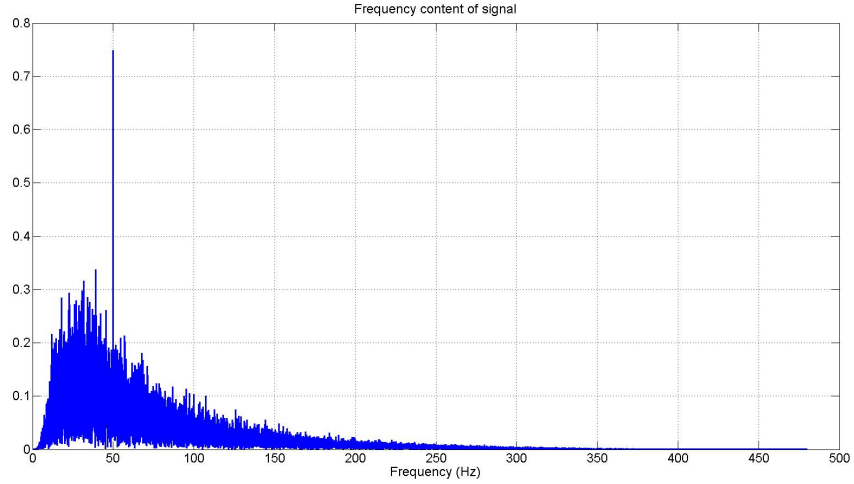

Figure 4.4: FFT of the signal in Fig.4.2 with added power line noise

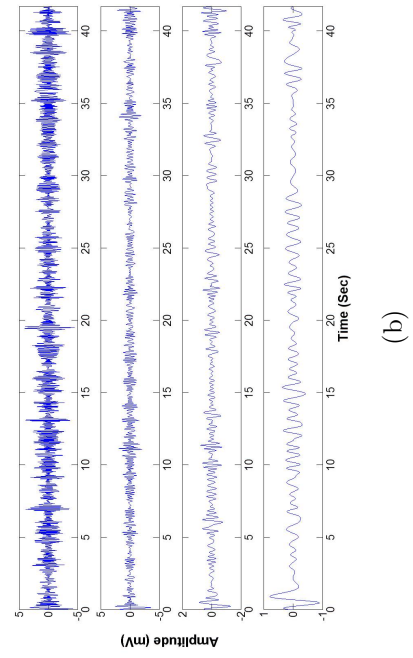

(b)

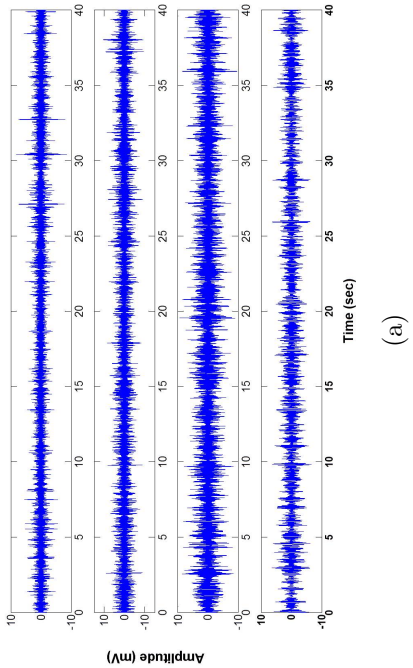

(a)

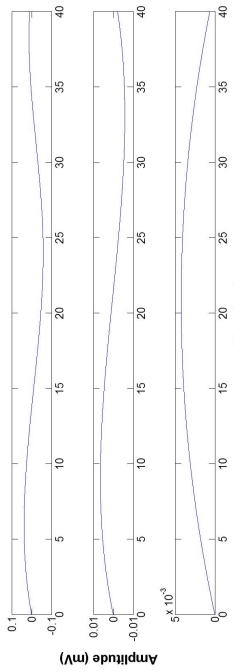

(d)

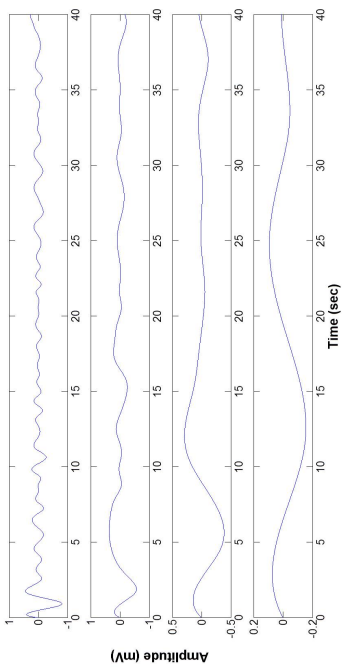

(c)

Figure 4.5: Intrinsic Mode Functions of the EMG Signal with added power line noise

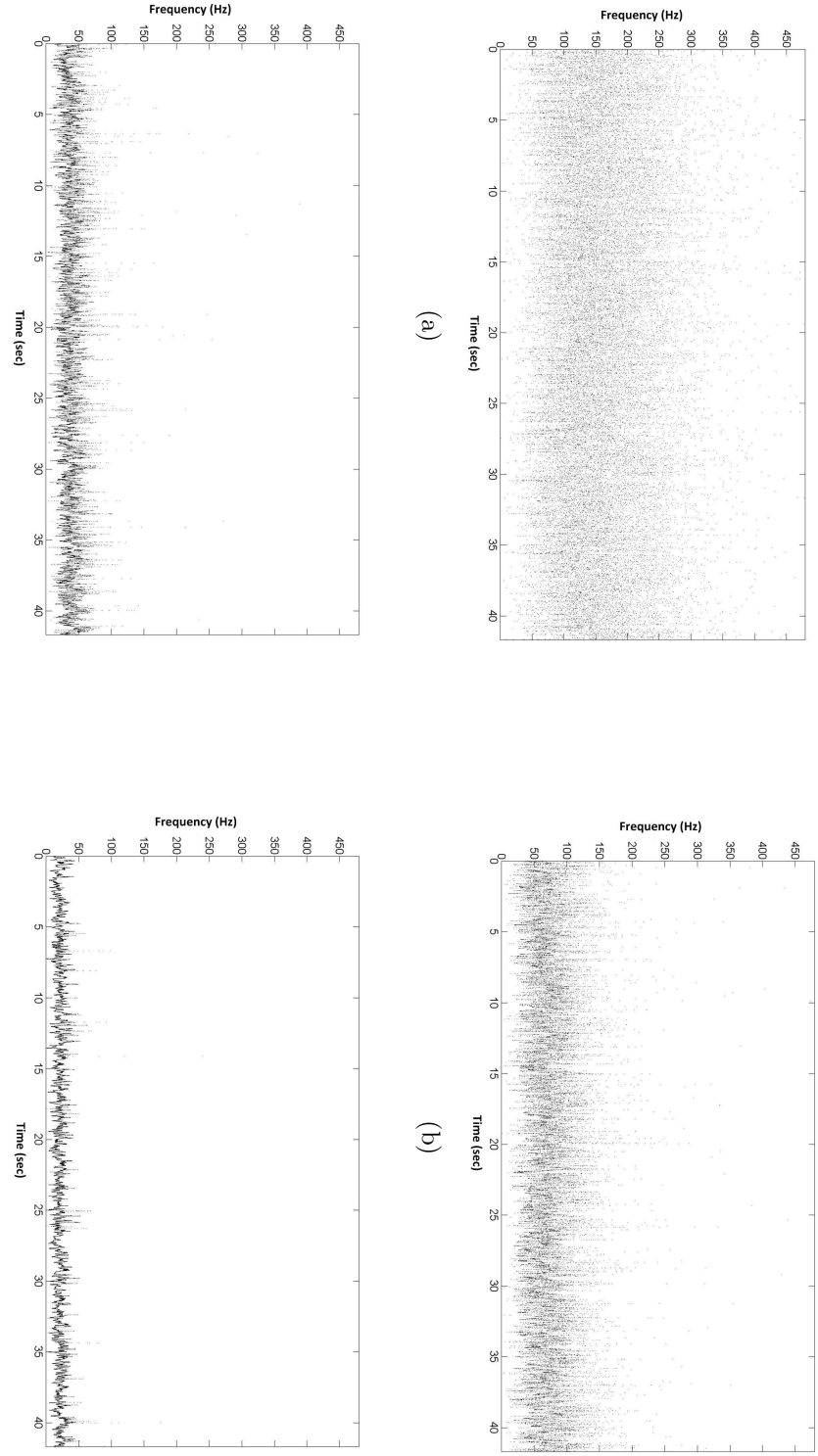

Figure 4.6: The Instantaneous Frequencies-time plots of the first four IMFs in Fig4.5

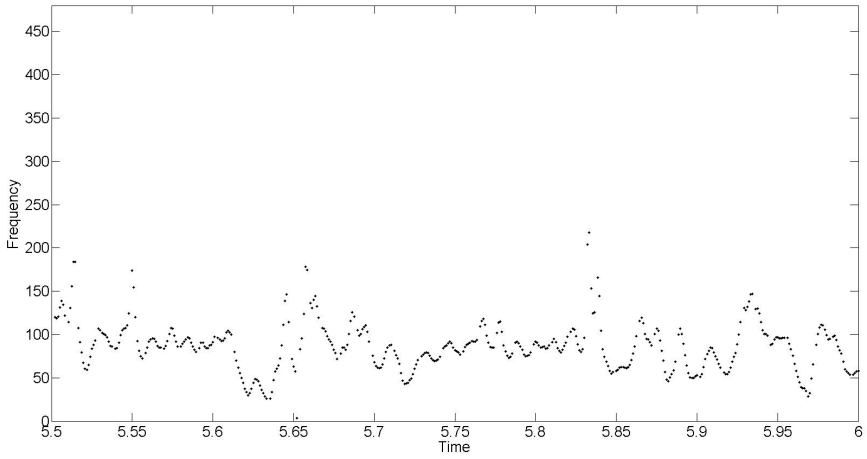

Figure 4.7: Instantaneous frequency-time plot for the second IMF in Fig4.5 for the time epoch of 0.5 sec.

It can be seen from Fig 4.6 that the power line noise is actually spread across different IMF(s). By using the power line frequency estimation algorithm, the power line noise is estimated and fed to the adaptive LMS filter. The instantaneous frequency-time plot for a half second EMG data for the second IMF is shown in Fig 4.7. It can be observed from the figure that, the instantaneous frequencies predicted lie in the range from 40 to 150 Hz with the dominant frequency being around 90 Hz.

The various power line frequencies estimated using Eqn.4.6 in the simulated EMG signal are shown in Table 4.1. These are the variations in the PLI for the EMG signal for different power line frequencies.

Table 4.1: Error in the Estimated Power Line Frequencies by the HHT-LMS algorithm

Power Line Frequency	Error in Estimation
49.50	0.12 Hz
49.75	0.10 Hz
50.00	0.03 Hz
50.25	0.06 Hz
50.50	0.10 Hz

4.3.2.3 Least-Mean Squares (LMS) Algorithm for Adaptive Filtering

The LMS algorithm is implemented to eliminate the power line noise in the EMG signal. The power line frequency is estimated from the Hilbert-Huang transform and input to the LMS algorithm for its removal.

Simulation 1:

The noisy signal is generated by mixing the simulated EMG signal with a power line noise of fixed frequency and amplitude. The simulation results of the HHT-LMS algorithm are shown in Fig. 4.9 and 4.11 while, the noisy signal's FFT plot and Power Spectral Density (PSD) plot is shown in Fig. 4.8 and 4.10 respectively. The PSD plot is important in gauging the spectral distortion of the cleaned signal w.r.t to the measured signal. This is to ensure that filtering doesn't remove EMG components.

- **OBSERVATIONS**
  - Fig. 4.8 shows the FFT plot of the noisy simulated signal while Fig. 4.9 shows the FFT plot of the signal after it has passed through the adaptive filter.
  - Fig. 4.10 shows the Power Spectral Density (PSD) plot of the noisy simulated signal while Fig. 4.11 shows the PSD plot of the signal after it has passed through the adaptive filter.
  - It can be inferred from the Fig. 4.8 and Fig. 4.9 that the HHT-LMS adaptive filter faithfully removes the power line noise from the simulated EMG signal.
  - This is further proved by examining the PSD plots of the clean and noisy EMG signals. The PSD plot of the cleaned EMG signal

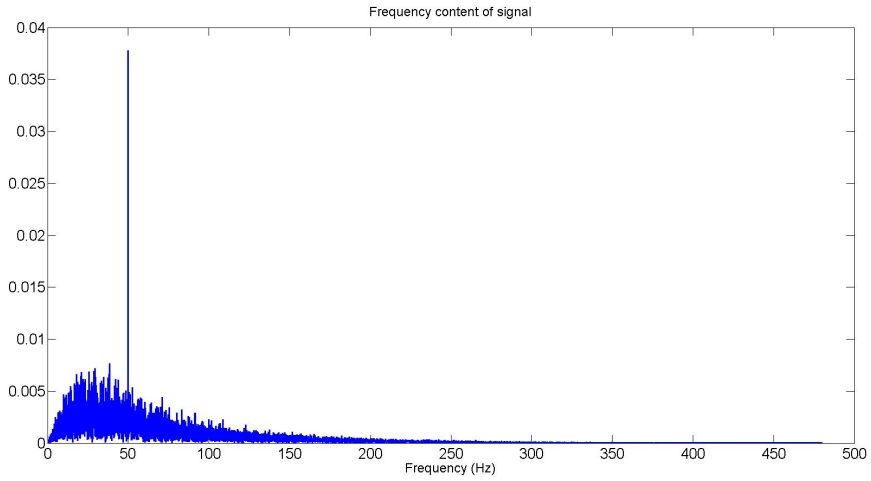

Figure 4.8: FFT plot for the noisy signal in simulation for a fixed power line noise

shows no distortion in its spectral content while there is a noticeable bump in the PSD spectrum of the the noisy EMG signal.

Simulation 2:

To validate the above algorithm, another condition is simulated with variable amplitude of the power line noise. In the first case the power line noise is scaled to ten times to that of the signal amplitude corresponding to a Signal to Noise Ratio (SNR) of -20dB. In the second case the power line noise is scaled to one-tenths of the signal amplitude corresponding to a SNR of +20dB. The powerline component in noisy signals with SNR higher than 20 dB doesn't contribute to the distortion of the spectral content of the EMG signal. Each of the power line signals is then added to the simulated EMG signal to generate the noisy signal. The simulation results for the HHT-LMS algorithm, variable step LMS algorithm and for LMS algorithm are shown below.

- **OBSERVATIONS**
  - Fig. 4.12 shows the PSD plot of the noisy simulated signal for

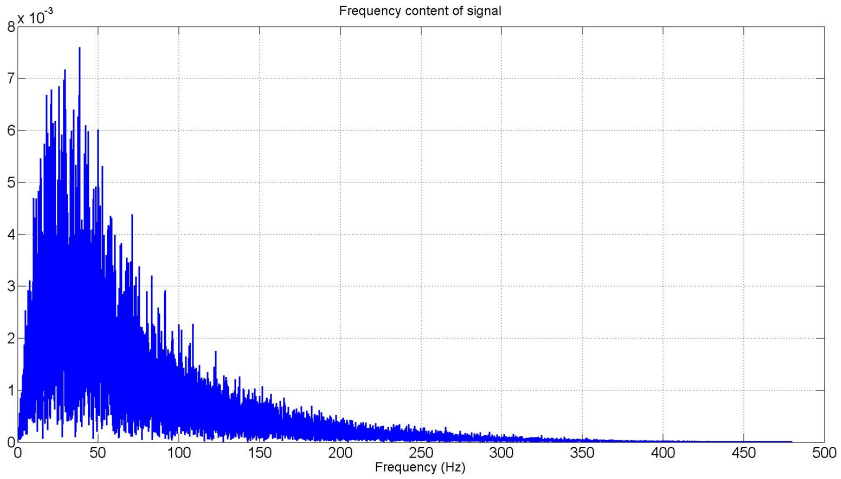

Figure 4.9: FFT plot for the cleaned signal in simulation for a fixed power line noise

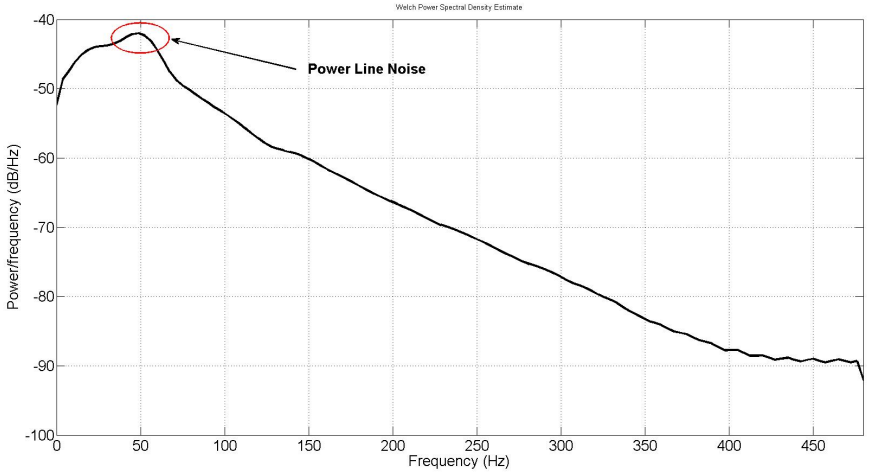

Figure 4.10: Welch Power Spectral Density (PSD) plot for the noisy signal in simulation for a fixed power line noise

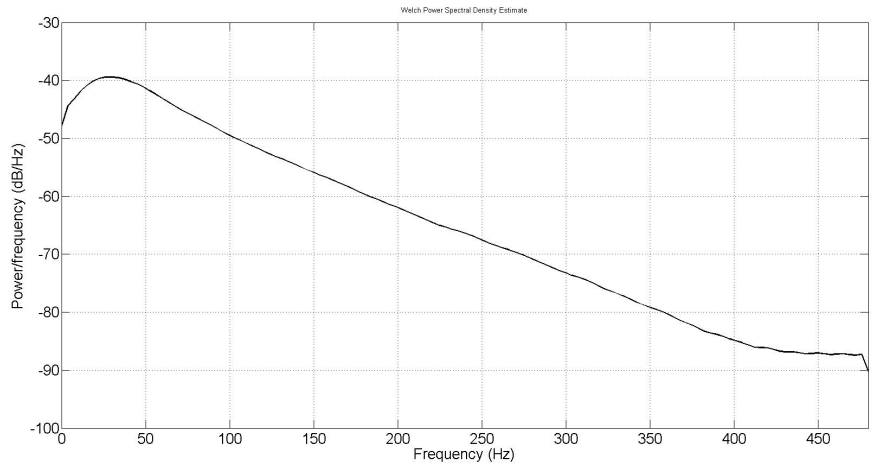

Figure 4.11: Welch PSD plot for the cleaned signal in simulation for a fixed power line noise

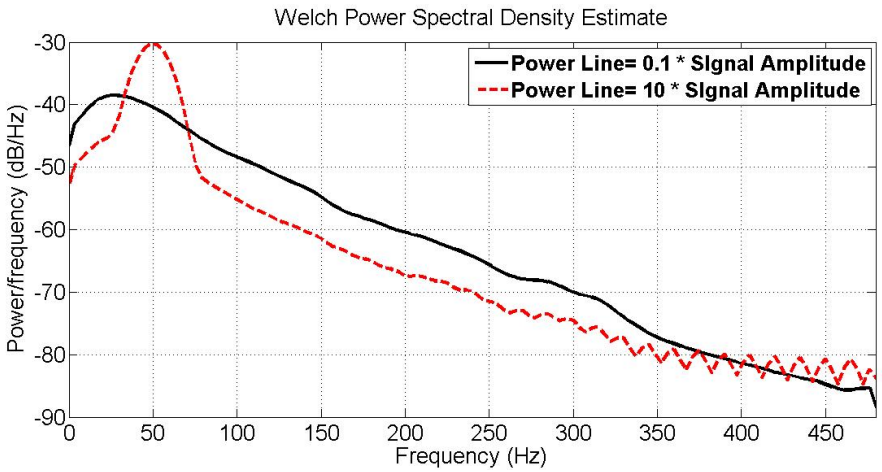

Figure 4.12: Welch Power Spectral Density plot for the noisy signal for power line noise amplitudes scaled to ten times and one-tenth of the signal amplitude

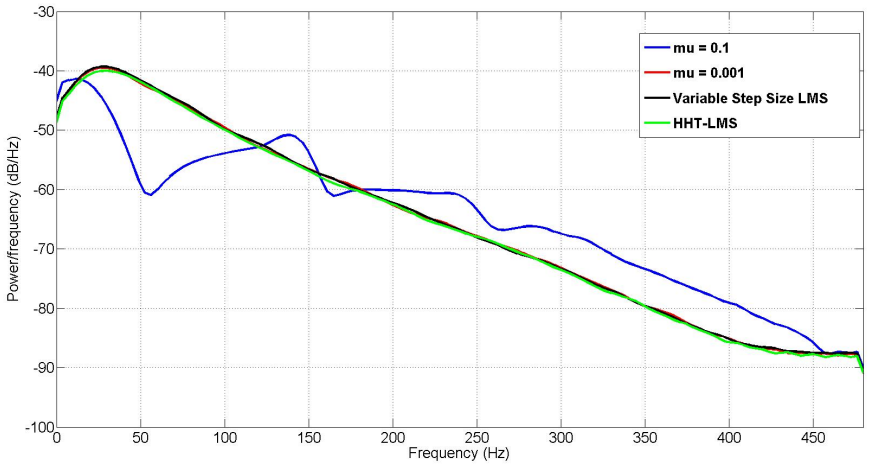

Figure 4.13: Welch Power Spectral Density plot for the cleaned signal for different adaptive filters in simulation for an power line noise amplitude scaled down to one-tenth of the signal amplitude

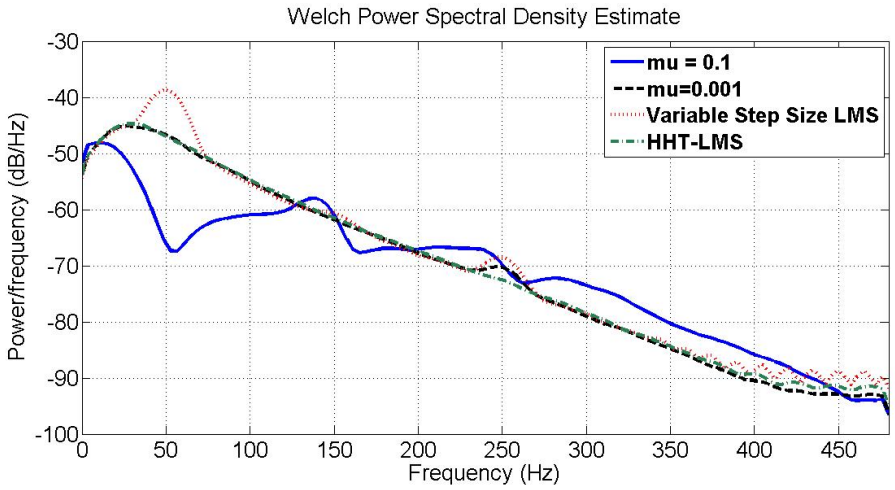

Figure 4.14: Welch Power Spectral Density plot for the cleaned signal for different adaptive filters in simulation for an power line noise amplitude scaled up to ten times of the signal amplitude

power line noise amplitudes scaled to ten times and one-tenth of the signal amplitude. Fig.4.13 shows the PSD plot for the cleaned signal for different adaptive filters in simulation for a power line noise amplitude scaled up to ten times of the signal amplitude while Fig.4.14 shows the PSD plot for the cleaned signal for different adaptive filters in simulation for a PLI amplitude scaled down to one tenth of the signal amplitude.

- It can be inferred from the Fig.4.13 and Fig.4.14 that there is no spectral distortion in the cleaned EMG signal for the HHT-LMS adaptive filter.
- For a fixed step size of $\mu = 0.1$ the LMS filter does not perform well for both the cases as there are large spectral distortion in the cleaned signals in Figs. 4.13 and 4.14.
- For a fixed step size of $\mu = 0.001$ the LMS filter performs similar to the HHT-LMS filter for both the cases. But the number of iterations required by the algorithm for this step size is well above the threshold of 300 ms set for this study.
- The variable step size LMS filter does perform similar to the HHT-LMS filter when the PLI is small but an increase in the amplitude of the power line results in the filter not being able to eliminate the power line noise completely.

4.4 Experimental Results

The HHT-LMS algorithm is applied to an actual EMG signal measured from the *biceps* of a participant. The measurement methodology for measuring the EMG signal is described in Chapter 2.

4.4.1 Empirical Mode Decomposition of the EMG Signal

In this section the EMG signal is decomposed into its constituent IMF(s). Similar to the simulations, firstly, the signal is processed offline as a whole dataset and then the signal is divided into time windows of half a second each to simulate real time processing conditions.Fig 4.15 shows the *biceps* EMG signal and Fig. 4.16 the FFT plot for the same signal.

It can be observed from Fig 4.15 that the EMG signal is not noise free and in fact it is really difficult to discern between the actual EMG signal and the noise levels apart from certain points in the data. Moreover, from Fig. 4.16 it can also be observed that a constant DC offset is present in the signal. Looking at the raw signal, it is possible to gauge the starting and ending of the movement but it is not possible to distinguish between the noise and the constant torque portion of the movement.

As evident from the Fig. 4.17 the initial iteration of the sifting algorithm consists of the higher frequencies in the signal. Following the procedure described earlier to calculate the IMF(s), the number of maxima and minima reduces in subsequent IMF(s). Hence, these IMF(s) consists of the lower frequencies in the signal spectrum. It ties in with the conclusion by *Flandrin et.al.* in [113] that, EMD acts essentially as a dyadic filter bank.

4.4.2 Hilbert Spectral Analysis and Frequency Estimation

The instantaneous frequency of the signal can be estimated by doing the Hilbert spectral analysis of the above derived intrinsic mode functions. The frequency-time plot for the signal in Fig. 4.15 is shown in Fig. 4.19. The

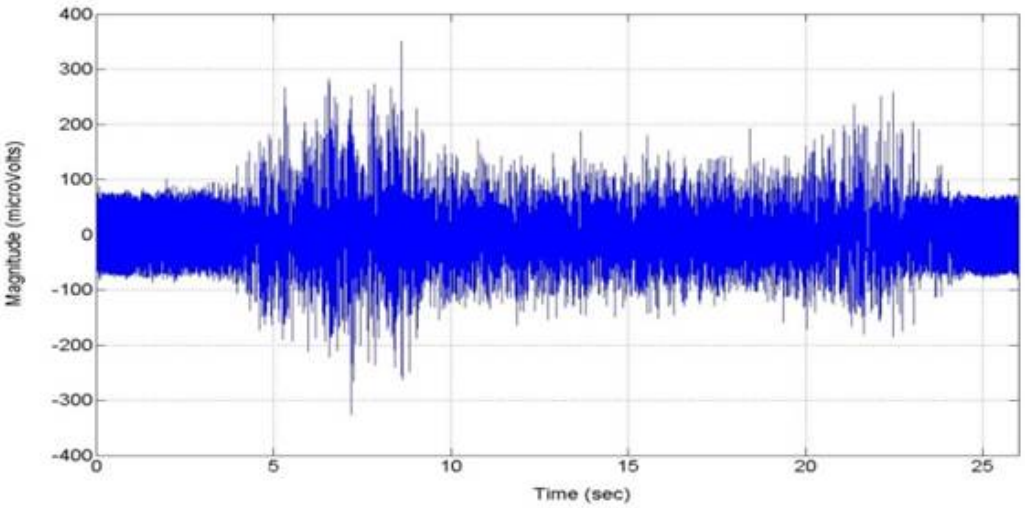

Figure 4.15: *biceps* EMG Signal for one elbow flexion-extension motion

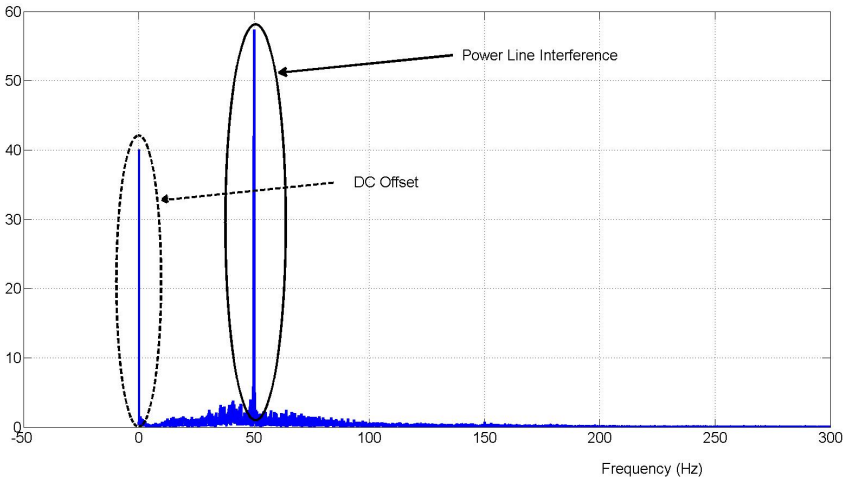

Figure 4.16: FFT plot for the raw signal in Fig. 4.15

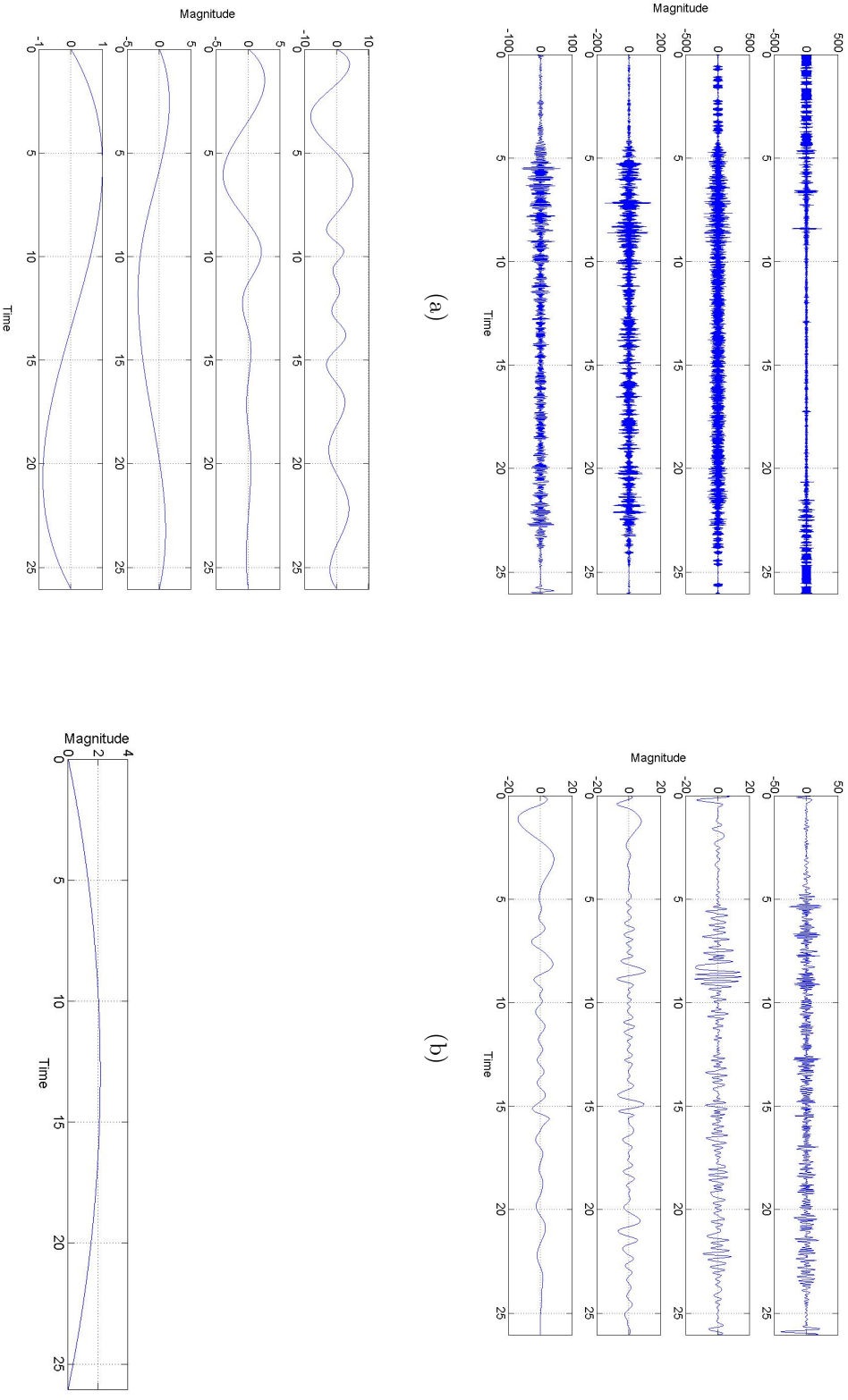

Figure 4.17: The Intrinsic Mode Functions of the EMG Signal in Fig4.15

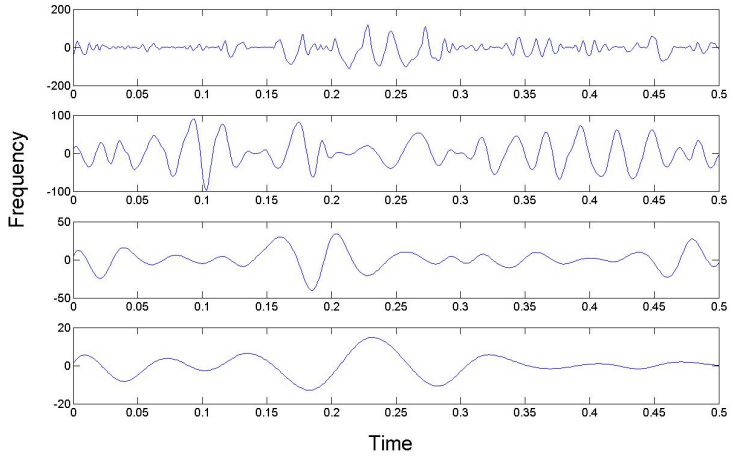

(a)

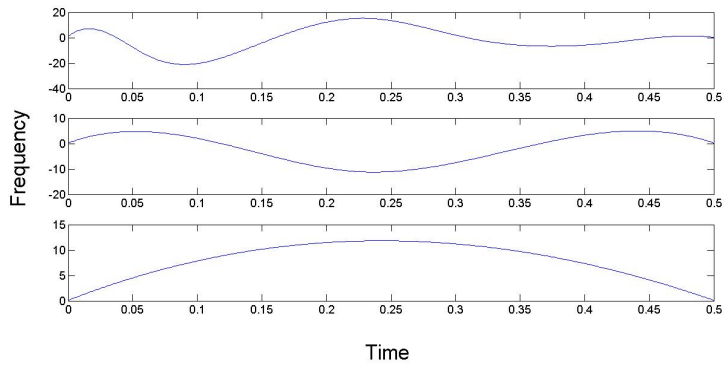

(b)

Figure 4.18: The Intrinsic Mode Functions of the EMG Signal in Fig4.15 for 0.5 seconds

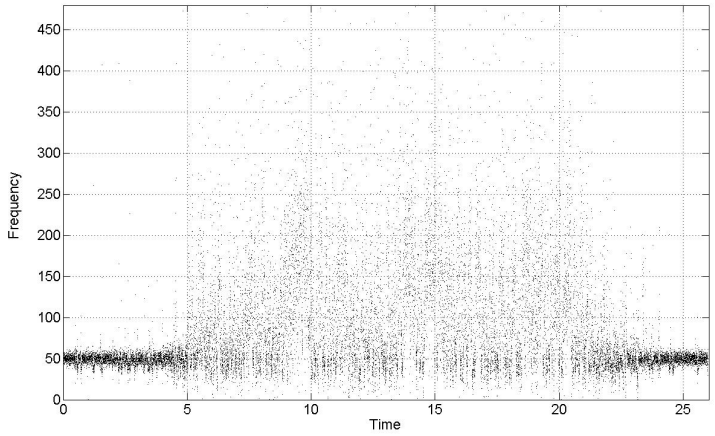

(a)

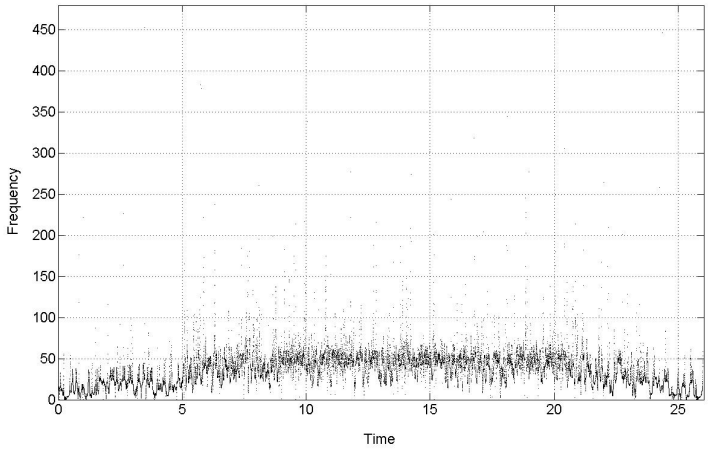

(b)

Figure 4.19: The Instantaneous Frequencies-time plots of the first two IMFs in Fig4.18

EMD spectrum for half a second of the data set taken randomly is shown in Fig. 4.20.

- **OBSERVATIONS**
  - As can be seen from Fig.4.19(a), the EMG signal for the first '5' seconds and for time greater than '22' seconds mainly consists of noise as there is no elbow movement during this period of operation.
  - It can be seen from Fig.4.19(a) that the value of the instantaneous

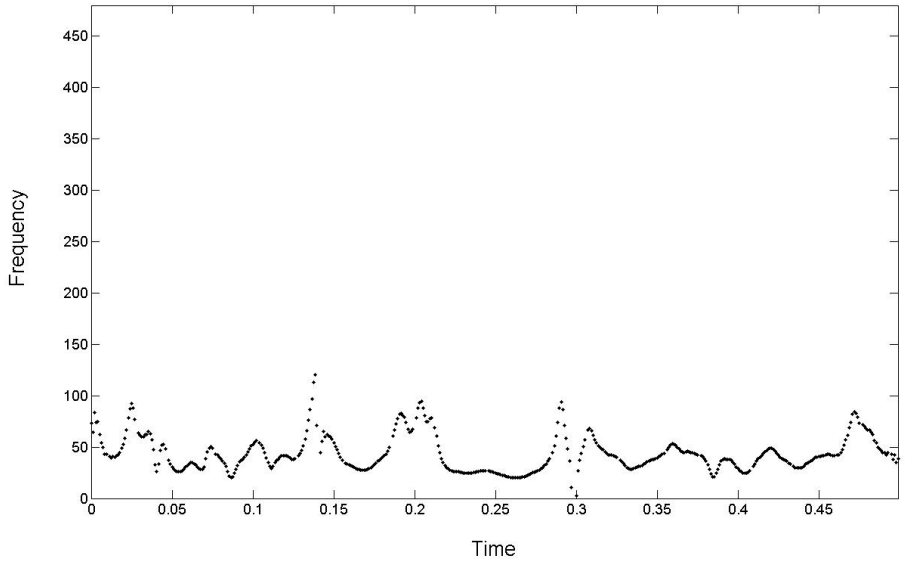

Figure 4.20: Instantaneous frequency-time plot for the EMG signal in Fig4.15

frequency during the time period before '5' seconds is around 50Hz or near to it.

– Similar results can be verified for a processing window of 500 ms as shown by the instantaneous frequency-time plot for the half second EMG data shown in Fig4.20.

The various power line frequencies measured in the raw EMG signal are shown in Table 4.2. These are the estimates of the variations in the PLI for the EMG signal in Fig. 4.15.

Table 4.2: List of Frequencies identified as power line frequencies by the HHT-LMS algorithm

49.965	49.99	50.015	50.039	50.088

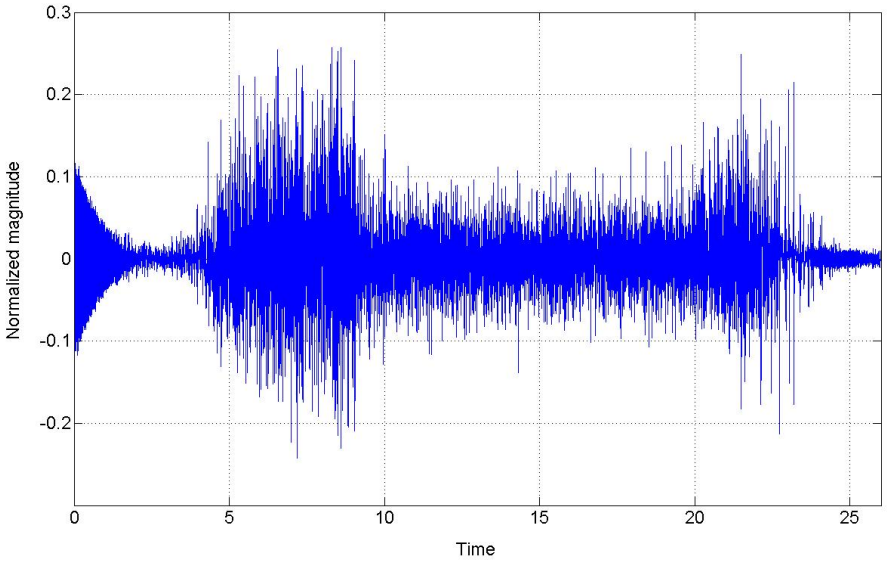

Figure 4.21: LMS-HHT filter Output of the for the raw signal in Fig. 4.15

4.4.3 Least-Mean Squares (LMS) Algorithm for Adaptive Filtering

The LMS algorithm is implemented to eliminate the power line noise and the fixed white Gaussian noise in the EMG signal. The power line frequency is estimated from the Hilbert-Huang transform and input to the LMS algorithm for its removal. Fig. 4.16 shows the FFT plot for the EMG signal in Fig.4.15. It can be inferred from Fig. 4.16 that the magnitude of the power line interference in the signal is significantly much higher than the frequencies in the EMG spectrum.

Applying the HHT-LMS algorithm to the raw EMG signal in Fig.4.15, we get the output as shown in Fig. 4.21.

- **OBSERVATIONS**
  - It can be seen from Fig.4.22 that the frequency at which the maximum magnitude of the EMG signal is measured is close to

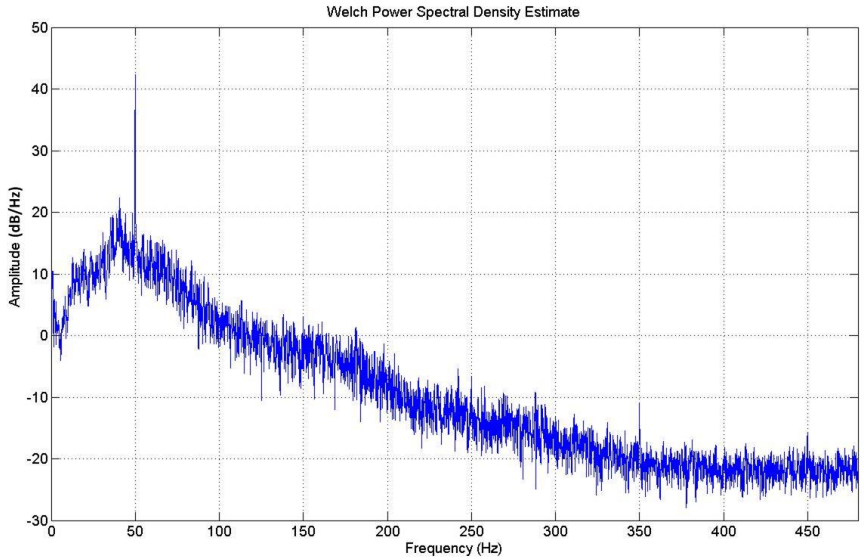

Figure 4.22: Welch Power Density Plot for the raw signal in Fig. 4.15

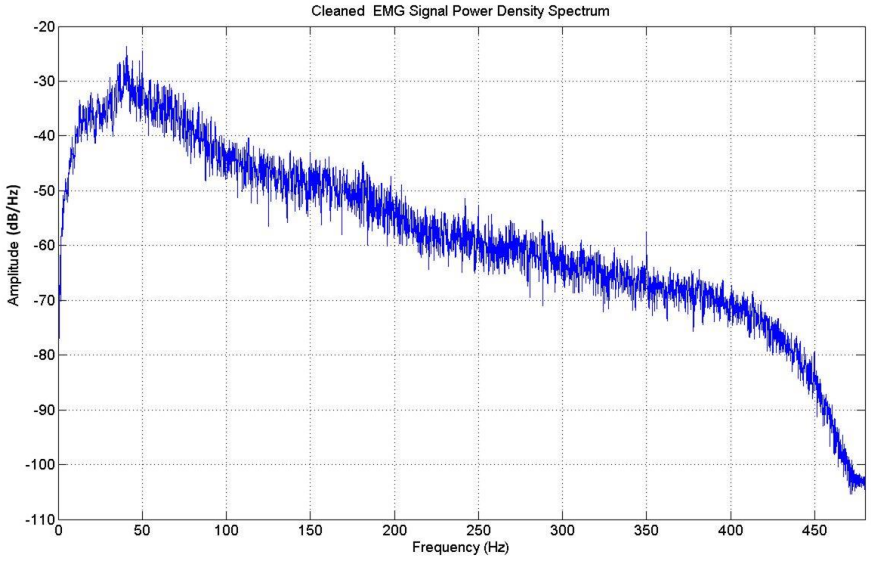

Figure 4.23: Welch Power Density Plot for the cleaned signal in Fig. 4.21

the power line interference.

- It is seen from Fig.4.23 that the HHT-LMS adaptive filter can remove the power line interference from the raw EMG signal without affecting the spectral content of the biceps EMG signal.
- The HHT-LMS adaptive filter operates in the time constraint of the 300 ms threshold for a real time assistive rehabilitation system as the processing window for the signal is taken as 250 ms.

4.5 Discussion

The HHT is an attractive solution for the estimation of power line interference in a spectrum of overlapping frequencies . It eliminates the need for a priori defined functional basis, as is generally required for the traditional signal analysis techniques (e.g., the Fourier transform expresses a signal in terms of global harmonic basis functions, and the wavelet transform in terms of local basis functions). Being purely data-driven, the HHT precisely determines the most appropriate empirical adaptive basis. This ability to adapt is crucial, given the individualistic nature of nonlinear systems. Another key feature of the method is that, by utilizing the Hilbert transform, it operates at the scale of one oscillation and is, thus, truly able to track local changes in signals.

The frequency estimator using modified Hilbert-Huang transform calculated the changes in the power line frequency faithfully in the time period of '5' to '22' seconds as is evident from Table 4.2 . However, the instantaneous frequency plots for time periods prior to '5' seconds and for time periods after '22' seconds show that there are many estimates along the power line frequency. This can be explained by the inherent nature of the Hilbert-Huang transform to create noisy IMF(s) from the signal [109, 114, 115]. This problem

is reduced in the current study by rounding off the frequency estimates to two decimal places.

The EMD decomposes the non-stationary signal into narrow-band components with decreasing frequency. The decomposition is complete, local and adaptive. The basis formed by the IMF directly comes from the signal which guarantees the inherent characteristic of signal and avoids the diffusion and leakage of signal energy.

The LMS algorithm adapts well to the changes in frequency of the power line interference at different time instants except at the beginning of the signal as seen from Fig.4.21. This can be explained as the time required for the LMS filter to adjust its weights to adapt it to the noisy signal from its initial state.

4.6 Summary

This chapter describes the adaptive filtering of EMG signal using a modified Hilbert-Huang based LMS adaptive filter (HHT-LMS). The estimation of the frequency of the power line interference is done using the HHT. The estimated power line frequencies and amplitudes are provided to a variable step LMS filter for their removal.

The simulation results for the designed filter and the corresponding observations are described next. Different conditions were simulated to ensure that the designed HHT-LMS filter performed satisfactorily under all conditions and a comparison was made to a LMS adaptive filter and a variable step size adaptive filter. The HHT-LMS filter is shown to remove power line noise from the EMG signal while maintaining the structure of the relevant EMG data for all simulated data.

Experimental results and discussion for the designed filter for removing

power line noise from EMG signal are presented. The algorithm was designed while keeping in mind the real time constraints for an assistive rehabilitation system. The HHT-LMS filter is shown to remove power line noise from the EMG signal while maintaining the structure of the relevant EMG data for measured EMG data as well.There was no spectral distortion while using the HHT-LMS filter for both simulated and experimental data.

5

Parameter Estimation of a Hybrid Muscle Model using an Iterative Learning Predictor for the Estimation of Joint Torque

The feature identification and classification alone is not a robust way for generating control signals for the assistive system as seen in Chapter 3. The generation of the control signal for such a case doesn't have any correlation to the torque that needs to be produced by the actuator. This system is acceptable if the torque required for the movement is not substantial. In other words, smaller joints like the wrists and hand can be actuated using a control system shown in Chapter 3. But the torque required for the actuation of the joints such as the elbow joint is high and it would be detrimental to use a pattern recognition based system for classifying such motions. The amount of time required to complete a movement is not fixed, and varies from person to person and a pattern recognition based system is unable to predict the *'in-between'* states between the initial and final motions. These transient states need to be programmed into the actuator accordingly and there is no surety that it mimics the elderly user's intention.

The EMG signal too is a direct indicator of the torque required for joint actuation. If a direct relationship can be established between the measured

EMG and the actual joint torque or force, it would be beneficial for the myoelectric control of prosthetics or orthotics, especially for the larger joints like the elbow and the knee. Research in this area is divided into following three major methods:

- The first methodology is to build the physiological muscle model of the human muscle and then predict the joint torque as a function of the neural activation derived from the EMG signal [42–44, 46–53, 65, 116, 117]. The obvious disadvantage of this method is the need to model complicated muscle dynamics to get an accurate joint torque estimate while the advantage is that once the model is tuned it predicts the joint torque quite accurately as it is a function of the neural activation.

- The second method is to model the EMG-Torque function using some known function [118, 119]. The same method also involves optimizing the said function to best fit the EMG-Torque dataset.

- The final method is to model the EMG-Torque function using a neural network [62, 63, 67–70]. The advantage of this method is that the governing equations or the characteristics of the system need not be known for modeling the data.

To assuage the above problems of EMG-Torque modelling, a new hybrid model is proposed for estimation of the joint torque. The advantages of the EMG hybrid model are:

- In the proposed model, only two channels of EMG data is used to predict the joint torque at the elbow. The two muscle groups studied are the *biceps* and the *triceps* muscle groups. An agonist-antagonist model modification of the Hill's muscle model, proposed by *Winters*

et.al. in [120] is used. This augurs well with the primary aim of this study: i.e., to keep the number of electrodes to the minimum.

- The joint torque for the two channel EMG data is predicted using the physiological model of the muscle.
- To ensure faster estimation of the unknown parameters of the physiological muscle model, an Iterative Learning Predictor (ILP) is implemented in the physiological model.
- This predicted torque is correlated to the actual torque output using a neural network.

5.1 Methodology

The EMG measurement protocols have been discussed in detail in Chapter 2. The following sections describe the subjects participated and the specific tasks performed by them for this study. Data was collected from two muscle sites represented in this study as shown in Table 5.1.

Table 5.1: Electromyography Electrode Notation and Muscle Sites

Muscle Site	Notation
biceps brachii	E1
triceps brachii	E2

5.1.1 Subjects

Data was acquired from six able-bodied individuals, aged 23 $\pm$ 6 years. All subjects were healthy and reported no physical or mental disorders. Each subject had access to the full range of forearm motions with no previous history of musculoskeletal illness.

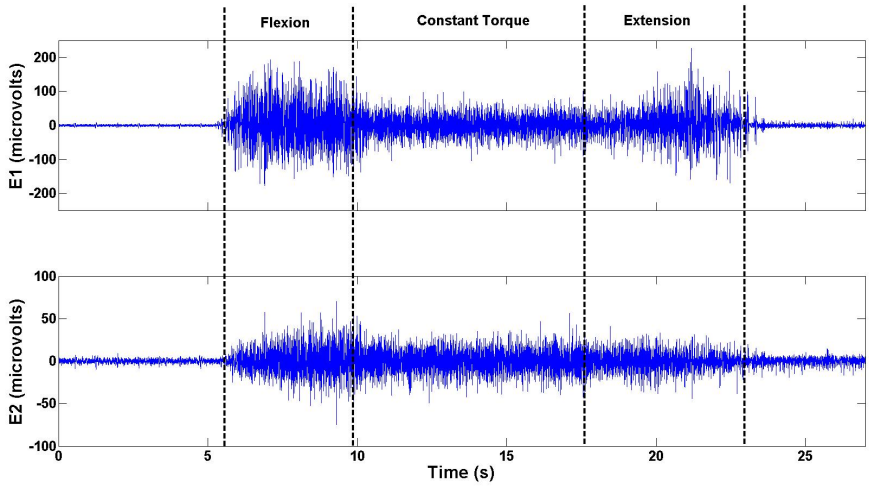

Figure 5.1: The EMG signal at the two muscle sites for the elbow flexion and elbow extension movements.

5.1.2 Experimental protocol

All subjects were instructed not to perform fatiguing upper limb exercise one day prior to the sessions. The CleaveMed BioCapture system was used to start data acquisition and the participants were visually cued by the operator of the BioCapture System to perform the elbow flexion and elbow extension movements. A numerical index is used for each class of the hand motion for identification during pattern recognition as shown in Table 5.2. The raw EMG signals at the two muscle sites *biceps brachii* and *triceps brachii* for the elbow flexion and elbow extension are shown in Fig. 5.1.

Table 5.2: Index for different hand motions for classification

Elbow Motion	Index
Elbow Flexion	I
Elbow Extension	II

Subjects performed twenty repetitions of each of the above motions. Each motion was comprised of the full range of motion from the resting position to the final position, followed by the limb being held in the final position for

5-10 seconds. The first motion performed was '*elbow flexion*' while the next motion was *'elbow extension'*. This sequence was then repeated for the rest of the session. The data was collected on multiple sessions, each session lasting not more than 2 minutes to avoid muscle fatigue. To ensure that the data measured was representative of the elderly population, all measurements were taken with a Maximum Voluntary Contraction (MVC) under 20%.

5.1.3 Signal Pre-processing

The measured and filtered surface EMG signals were stored and analysed on a PC using MATLAB software. Each channel of the EMG data was processed and analysed separately. The DC offset was removed by filtering the mean value in the EMG data while the 2nd order Butterworth high pass and low pass filters, with cut-off frequencies of 10 Hz and 350 Hz respectively, were applied to filter out the noise and motion artifacts including changes in forearm joint angles. It can be observed from Fig. 5.1 that the Power Line Interference (PLI) present in the noise is very large. This PLI is removed from the signal using the HHT-LMS adaptive filter method as discussed in Chapter 4.

The preprocessed signal is then rectified and passed through a low pass filter of 5 Hz to generate the signal envelope of the EMG signal [47, 48]. This EMG signal is used to estimate the level of the Neural Activation (NA) for each muscle under study. The NA is a normalized signal which indicates a state of maximal voluntary activation and represents no muscle activation. Commonly, the NA level is estimated by using the envelope of the rectified and normalized EMG signal. A nonlinear scaling [119], defines the degree of nonlinearity of the neural activation where A is a non-linear factor, *u(t)* is the rectified EMG signal and *a(t)* is the Neural Activation (NA).

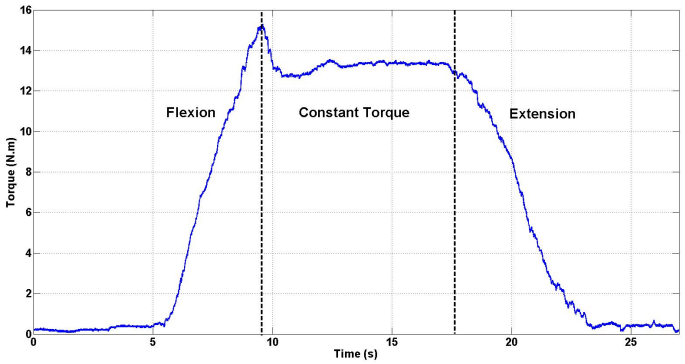

(a) Joint Torque for the Elbow

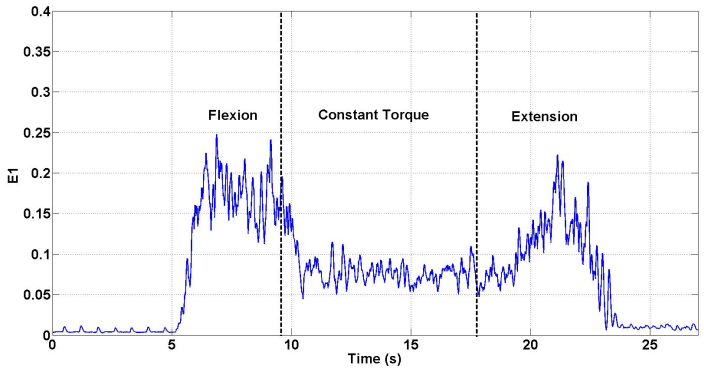

(b) Normalized Neural Activation for the *biceps brachii*

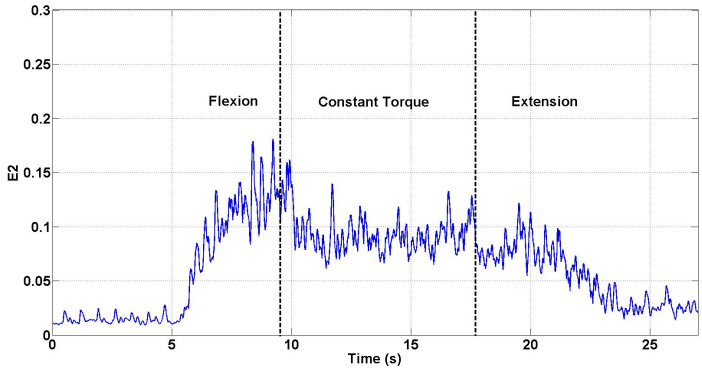

(c) Normalized Neural Activation for the *triceps brachii*

Figure 5.2: Nomalized Neural Activation calculated for the *biceps brachii* (Fig. 5.2(b)) and triceps *brachii* (Fig. 5.2(c)) for the joint torque at the elbow (Fig. 5.2(a))

$$a(t) = \frac{A^{u(t)} - 1}{A - 1} \tag{5.1}$$

This normalized NA derived from the EMG signal for the two muscle sites for the elbow flexion and elbow extension movements are shown in Fig. 5.2.

5.1.4 Muscle Length and Moment Arm Calculation

In order to obtain the muscle lengths and the corresponding muscle moment arms, the angular positions of each joint spanned by the muscle, as well as anatomical information about the arm, are used. Several estimations of length and moment arms for the upper limb muscles are available [121–124]. However, data are available only for a selected number of muscles and they are expressed as average values or as polynomial interpolations with respect to individual joint angles. Garner et.al. in [122, 125, 126] have developed models describing the complex path of muscle from origin to insertion points. These models facilitate the evaluation of muscle lengths and moment arms across the elbow joint and hence are chosen for this study.

The joint angle measured at the elbow joint is shown in Fig.5.3(a). Fig. 5.3(b) and Fig. 5.3(c) show the calculated muscle lengths from the joint angle data in Fig. 5.3(a).

- **OBSERVATIONS**
  - The muscle lengths of the *biceps* and *triceps* in Fig. 5.3 indicate that the *biceps* muscle groups are the agonist muscles for the flexion movement while the *triceps* muscle groups are the antagonist muscle groups for the same.
  - For the elbow extension, the *biceps* muscle groups are the antagonist muscles while the *triceps* muscle groups are the agonist muscles.

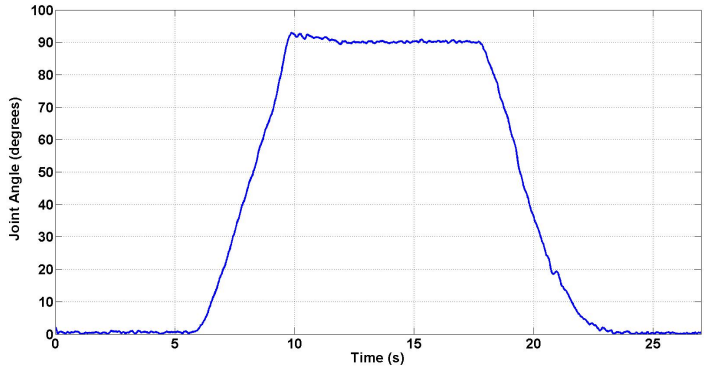

(a) Joint Angle measured at the Elbow

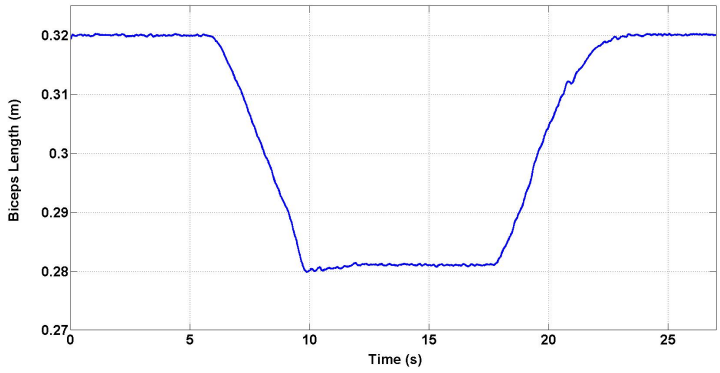

(b) Muscle length calculated for the changes in the *biceps brachii*

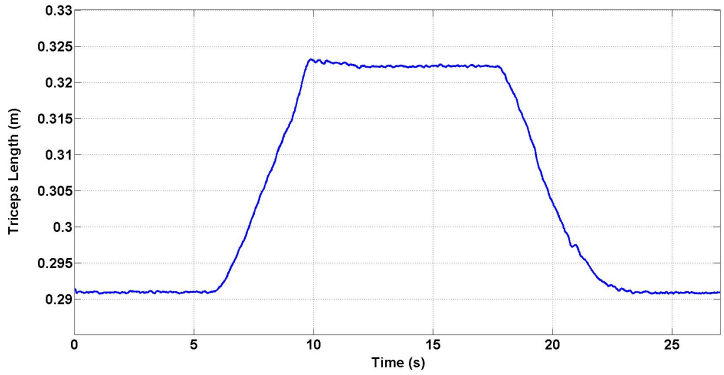

(c) Muscle length calculated for the changes in the *triceps brachii*

Figure 5.3: Muscle length calculated for the *biceps brachii*(Fig. 5.3(b)) and *triceps brachii* (Fig. 5.3(c)) for the joint angle measured at the elbow (Fig. 5.3(a))

5.2 Preliminary Tests

Preliminary tests were carried out with the measured data for predicting the joint torque using the fixed function and neural network models.

5.2.1 EMG-Torque Relation as a Fixed Function Model

Here the EMG-Torque relation is modeled using the following equation [57]:

$$y(t) = x(t)^a * exp(b - c * x(t)) \tag{5.2}$$

where,

y(t) = Output Torque of the Elbow Joint;

x(t) = Normalized *triceps* Neural Activation signal

a,b,c = Constants to be determined

The normalized *triceps* EMG signal and torque output shown in Fig. 5.2(c) and Fig. 5.2(a) respectively are used to tune the above equation.

A Genetic Algorithm (GA)[57, 68] is used to tune Eqn. 5.2 with the above values of EMG and Torque. The values of *a, b*, and *c* found out by the optimization algorithm are given in Table 5.3. These values are the mean of 1000 iterations of the GA algorithm.

Table 5.3: Values of the constants a, b and c calculated using GA

a	*b*	*c*
1.109	1.992	0.155

Substituting these values into Eqn. 5.2 and then calculating the output torque one can get to Fig.5.4. Comparing Fig.5.4 with Fig.5.2(a), it can be noticed that the error in the calculated torque is large. The calculated torque

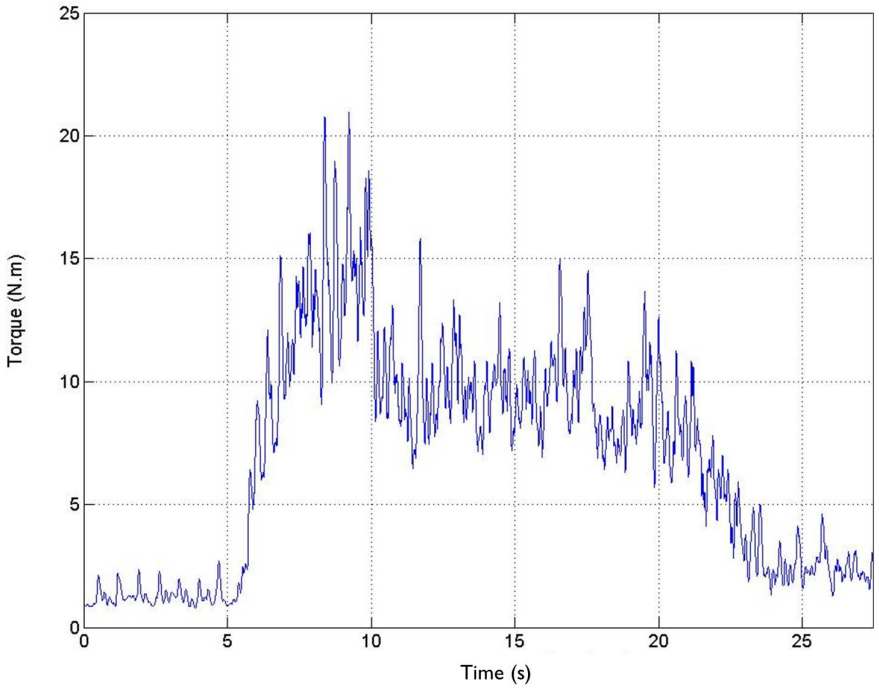

Figure 5.4: The calculated output torque using Eqn.5.2 for the data in Fig. 5.2

envelope does not follow the structure of the measured torque and there are lots of transients that were not present in the measurements.

As is evident from Fig.5.2(c), the variable nature of the EMG during dynamic contractions makes it difficult to model it with respect to any pre-known function. A more stringent filtering may smoothen the EMG envelope further more to give better results but that would result in a higher error in the actual torque produced by the function as data is being smoothened by adding information not present in the measured data.

5.2.2 EMG-Torque Relation using Neural Network

Many authors have tried to establish the relationship between the EMG and the joint torque using the black box model for the relation between the joint torque and the EMG [60–63, 127, 128]. *Wang et.al.* in [64] have combined

the neural network approach to the physiological approach by using a neural network to predict the neural activation and then using the predicted neural activation in the Hill muscle model to obtain the joint torque.

In this section, two neural networks are analysed. The data used for the network is shown in Fig.5.2. Firstly, a single input neural network with single channel normalized neural activation of the *triceps* EMG as the input and the other neural network model has the normalized EMG as well as the joint angle as inputs to the neural network.

Both the neural networks have one hidden layer with 20 neurons to enable comparison between the performances of the two networks. The input EMG signal and the output torque signal is the same as in Fig. 5.2(c) while the corresponding torque output is shown in Fig. 5.2(a).

Neural Network 1:

Table 5.4: Parameters for Neural Network 1

Inputs	1(Normalized Neural Activation of the *triceps*)
Neurons in the Hidden Layer	20
Output	1 (Elbow Joint Torque)

Fig. 5.5. shows the output of the trained network with one channel input.

- **OBSERVATIONS**
  - It can be seen from Fig. 5.5 that with only one input to the neural network, the algorithm has trouble adjusting to the variations or changes in torque but it is quite stable for constant torque regions of the EMG data.
  - It can be interpreted that the torque predicted by the neural network in Fig. 5.5 does not follow the measured torque Fig. 5.2(a) smoothly.

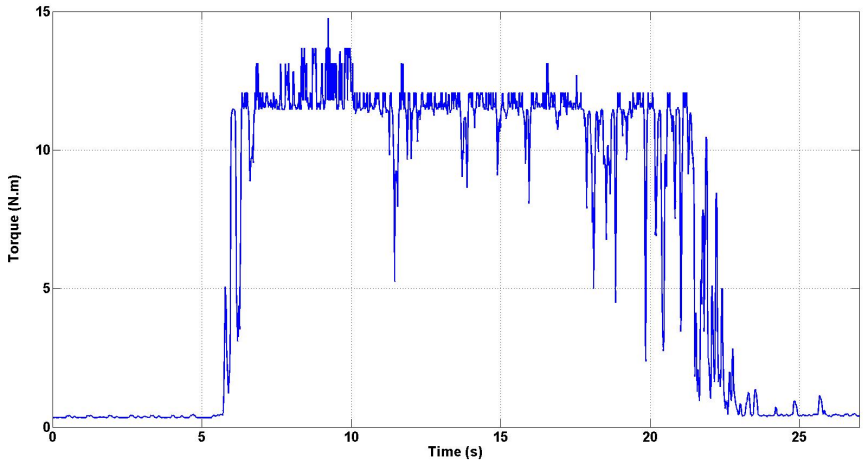

Figure 5.5: Output Torque of the *neural network 1* using the training data set

– But it is evident that only one input won't help in bettering the accuracy of the algorithm. Though the one input neuron approach is better than the constant function EMG-Torque relation, it is still not safe and accurate for implementation for orthotic or prosthetic control.

Neural Network 2:

Table 5.5: Parameters for Neural Network 2

Inputs	2 (Normalized Neural Activation of the *triceps* and Elbow Joint Angle)
Neurons in the Hidden Layer	20
Output	1 (Elbow Joint Torque)

The input EMG signal and the output torque signal is the same as in Fig. 5.2(c) while the corresponding torque output is shown in Fig. 5.2(a). The second input in the neural network is the joint angle shown in Fig. 5.3(a). The output of the trained network is shown in Fig. 5.6.

- **OBSERVATIONS**

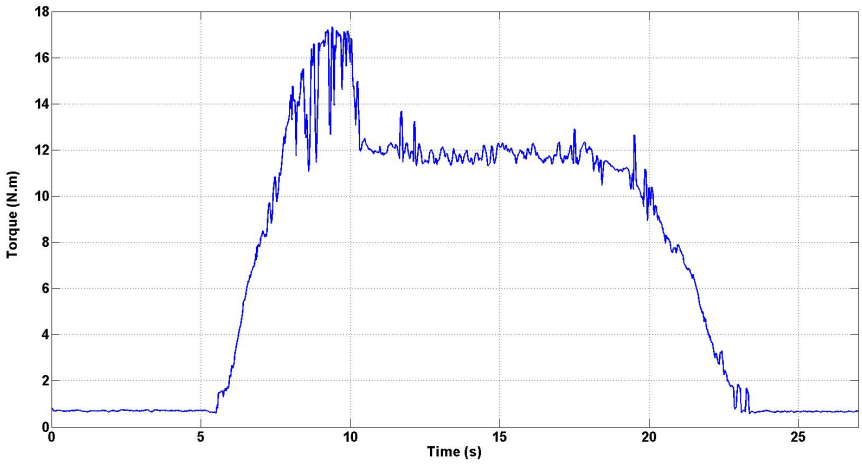

Figure 5.6: Output Torque of the *neural network 2* using the training data set

– It can be seen from Fig.5.6 that with two inputs to the neural network, the algorithm has easily reduced the mean square error and doesn't have any trouble adjusting to the variations or changes in torque. It is relatively stable for constant torque regions of the EMG data compared to the single input neural network.

– From Fig.5.2(a) and Fig.5.6, it can be interpreted that the output torque calculated through the neural network for the test data follows the measured torque quite closely though it varies in the constant torque region of the EMG signal.

– The problem with using angular data as a neural network input neuron is that the neural network ignores the changes in EMG in the constant torque region of the data. This is because the joint angle is maintained constant and, hence, the neural network maintains the torque constant. But changes in the EMG due to fatigue or minor movements of the hand are not considered in this scheme.

It is evident that only one input won't help in improving the accuracy of the predicted joint torque. Though the one input neuron approach is better than the constant function EMG-Torque relation, it is still not safe and accurate for implementation for orthotic or prosthetic control. The use of joint angle as an input in the neural network is feasible only for isometric contractions to stabilise the output torque but is not realistic to use the same for dynamic contractions.

5.3 Hybrid Muscle Model

5.3.1 Physiological Model of the Muscle

One of the earliest and most classic muscle models is Hill's model developed by A.V. Hill in 1938 [42]. The key finding of Hill's model is the observation that a sudden change in force (or length) would result in nearly instantaneous change in length (or force) for a given sustained level of neural activation. This suggests the relationship of a spring:

$$k = \frac{\Delta f}{\Delta l} \tag{5.3}$$

where k is called the spring constant for the muscle. The classic Hill's model of human muscle is shown in Fig. 5.7, with lightly-damped spring-like elements both in series (SE) and in parallel (PE) with Contractile Element (CE) [42].

The contractile element is freely extendable when at rest, but shortens when an electrical stimulus is activated. It represents the muscle fibre, that is connected to an elastic serial element.

The series elastic component accounts for the muscle elasticity during isometric (constant muscle length) force condition that is due in a large part

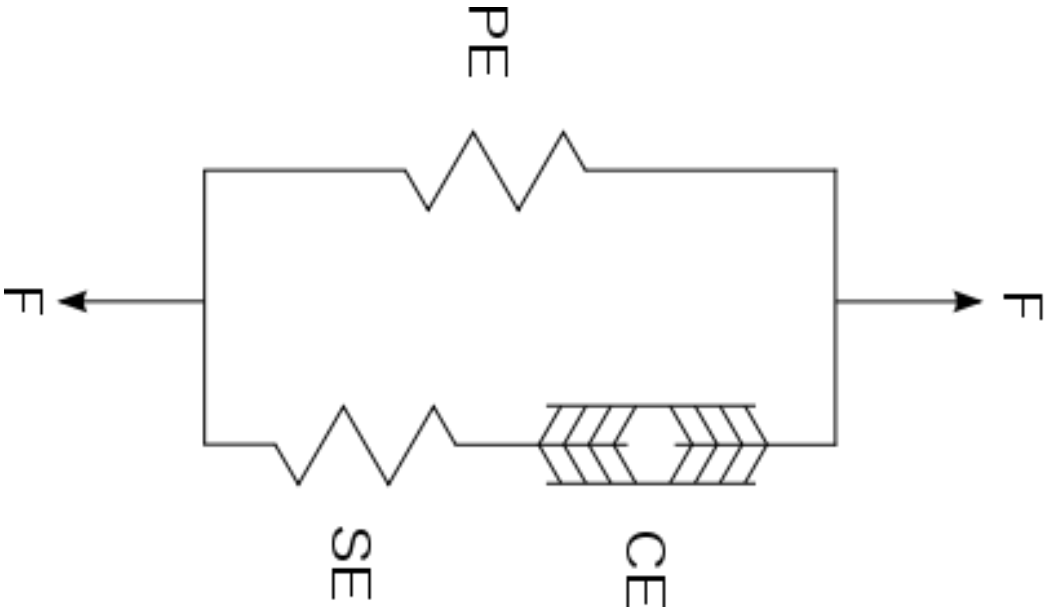

Figure 5.7: Hill's classical elastic muscle model

to the elasticity of the cross-bridges in the muscle. This element is equivalent to the tendon muscle.

Parallel elastic component accounts for the inter-muscular connective tissue surrounding the muscle fibres. It is physically represented by the muscle membrane.

Active tension is modeled by the contractile component, while passive tension is modeled by the series and parallel elastic components. The contractile tissue consists of the groups of muscle fibres which produce the active tension. It has two unique features, length-tension relationship and force-velocity relationship.

The output force of the model can be written as a function of the forces generated in the SE, PE and the CE. Given the mechanical arrangement of the PE, SE, and CE components, the two parallel branches of the model share the same displacement. In addition, the two elements in series on the same branch share the same force. Finally, the total force generated by the muscle is the sum of the forces developed by each branch. These relations are given

below:

$$L_{PE} = L_{SE} + L_{CE} \tag{5.4}$$

$$F_{CE} = F_{SE} \tag{5.5}$$

$$F_{tot} = F_{SE} + F_{PE} = F_{CE} + F_{PE} \tag{5.6}$$

where F is the force and L is the length of the segment as shown in Fig.5.7.

Given the passive nature of the PE and SE elements, the force generated by these two elements as a function of the displacement can be expressed by the same equation (Eqn.5.7) provided that different internal parameters (S, F_{max}, ΔL_{max}) are used.

$$F = \left[\frac{F_{max}}{e^S - 1}\right]\left[e^{\left(\frac{S}{\triangle L_{max}}\triangle L\right)} - 1\right] \tag{5.7}$$

where, F is the passive force generated by the PE or the SE element, ΔL is the change in length of the element with respect to the slack length, S is a shape parameter (related to the stiffness of the element) and F_{max} is the maximal force exerted by the element for the maximum change in length ΔL_{max}.

The only unknown parameter in Eqn.5.7 is the change in length ΔL for the length of each element. The change in length of the PE element is the same as the total change in the muscle length. Hence, by determining the change in total muscle length for the corresponding elbow movement, the passive force generated by the PE element can be determined. The change in total muscle length is a function of the joint angle at the elbow. The change in the muscle length is modeled according to the work by [122, 125, 126] where the change in the muscle length is made a function of the joint angle.

5.3.2 Numerical Implementation of Hill's Muscle Model

The force generated by the CE element, F_{CE} is a function of neural activation a, of the normalized force-length function f_l, of the normalized force-velocity function f_v, and of a fixed parameter defining the maximal force the element can generate, i.e. F_{CEmax} have been simplified and quantified by different authors. Here, the simplification presented in [43, 44] is used to define these different parameters as follows:

$$F_{CE} = a * f_l * f_v * F_{CEmax} \tag{5.8}$$

$$f_l = exp\left(-0.5\left(\frac{\frac{\Delta L_{CE}}{L_{CE0}} - \phi_m}{\phi_v}\right)^2\right) \tag{5.9}$$

$$f_v = \frac{0.1433}{0.1074 + exp\left(-1.3sinh\left(2.8\frac{V_{CE}}{V_{CE0}} + 1.64\right)\right)} \tag{5.10}$$

$$V_{CE0} = 0.5 * (a + 1) * V_{CEmax} \tag{5.11}$$

The function f_l is modeled as a Gaussian function where L_{CE} is the length change for the CE element and L_{CE0} is the optimal fiber length; m and v are parameters affecting the mean value and variance of the Gaussian. The force-velocity equation is defined by Eqn. 5.10 where V_{CE} is the CE velocity and V_{CE0} is the maximal CE velocity when $F_{CE} = 0$. V_{CE0}, as shown in Eqn.5.12, can be expressed as a function of neural activation and V_{CEmax}, i.e., V_{CE0} when the activation is maximum (a = 1). Moreover, the following relations represent some of the parameters in the previous equations:

$$V_{CEmax} = 2 * L_{CE0} + 8 * L_{CE0} * \alpha \tag{5.12}$$

$$F_{PEmax} = 0.5 * F_{CEmax} \tag{5.13}$$

$$\Delta PE_{max} = L_{max} - (L_{CE0} + L_{TS}) \tag{5.14}$$

$$F_{SEmax} = 1.3 * F_{CEmax} \tag{5.15}$$

$$\Delta SE_{max} = 0.03 * L_{TS} \tag{5.16}$$

where, α is the percentage of fast fibers in a muscle, L_{TS} is the tendon slack length.

Substituting Eqn.5.10 in Eqn.5.8 and expressing all the terms with respect to $\Delta L_{CE}[n]$ we get

$$F_{CE}\left(\Delta L_{CE}\left[n\right]\right) = \frac{0.1433 * a * f_l * (\Delta L_{CE[n]}) * F_{CEmax}}{0.1074 + exp\left(-1.3sinh\left(2.8\frac{V_{CE}}{V_{CE0}} + 1.64\right)\right)} \tag{5.17}$$

where, $\Delta L_{CE}[n]$ is the change in length of the L_CE element at time *'n'*. From Eqns. 5.4, 5.5 and 5.17

$$\begin{aligned} &\left[\frac{F_{SEmax}}{e^{S_{SE}}-1}\right]\left[e^{\left(\frac{S_{SE}}{\triangle L_{SEmax}}\triangle(L_{PE}[n]-L_{CE}[n])\right)}-1\right] \\ &= \frac{0.1433 * a * f_l * (\Delta L_{CE[n]}) * F_{CEmax}}{0.1074 + exp\left(-1.3sinh\left(2.8\frac{V_{CE}}{V_{CE0}} + 1.64\right)\right)} \end{aligned} \tag{5.18}$$

The numerical muscle model described in Eqn.5.18 can be rewritten as a function of ΔL_{CE} and V_{CE}.

$$\Delta L_{PE} = f(\Delta L_{CE}, V_{CE}) \tag{5.19}$$

The CE velocity can be represented as a finite difference equation as given in [67],

$$V_{CE}[n] = \frac{\Delta L_{CE}[n] - \Delta L_{CE}[n-1]}{\Delta t} \tag{5.20}$$

where, Δt is the time difference between the changes in CE length at time n and *n-1*.

The unknown parameter in Eqn. 5.19 is the change in the contractile length element, ΔL_{CE}. Since the other parameters are known, the above equality can be used to find out the change in the contractile element. The other parameter that changes with time is the muscle length. The change in the length of the contractile element is modelled with respect to the change in muscle length.

The change in the CE length depends on the changes in muscle length which is a function of the joint angle. The joint angle is fixed for isometric contractions but varies with respect to the hand movements for dynamic contractions. Thus, it is not possible to describe 5.19 as a static system for use with simple parameter estimation methods such as GA or Particle Swarm Optimization (PSO).

Optimization techniques such as GA, PSO, [67–70] have been used to estimate different parameters of the hill muscle model. The parameters estimated in such studies were either constants or the values changed minimally during dynamic contractions. Since a changing parameter is to be estimated, which is a function of the muscle activation as well as the muscle length under consideration, optimization techniques would be complicated and a huge burden on computing power.

In general, the method used depends on the behavior of the target function. Based on the function, the problem of identification of parameters for a highly nonlinear system can also be solved as a root finding problem when the number of input and output is the same. To estimate the change in the CE element of the muscle model, a root finding technique needs to be utilized in this context.

Cavallaro et. al. in [67] have used the bisection method for solving Eqn.5.18. The authors have also mentioned that this method is not suitable if the muscle activation is nil or not detected as, then the root of Eqn.5.18 would approach infinity.

In this study, an Iterative Learning Predictor (ILP) is proposed that is a simple and effective solution to the parameter identification problems of the muscle model which is highly nonlinear and multi-dimensional. The ILP method can guarantee the learning process convergence even if the plant model is partially unknown or difficult to analyze.

The concept of iterative learning was first introduced in control to deal with a repeated control task without requiring the perfect knowledge such as the plant model or parameters [129, 130]. It is a tracking control method for systems that work in a repetitive mode. The present control action could be updated by using information obtained from previous control action and previous error signal, even though the control plant is highly nonlinear.

The rehabilitation task requires repetition of the same elbow movements for retraining the brain. The elderly user keeps on repeating the same set of exercises for a fixed interval of time. This feature is exploited in predicting unknown parameters in Hill's muscle model by the ILP.

A pointwise Iterative Learning Predictor (ILP) is implemented where the data points in the signal are iterated one-by-one till the desired output is the same as the actual system output. Table 5.6 lists the different parameters and the ILP equation for the muscle model parameter estimator.

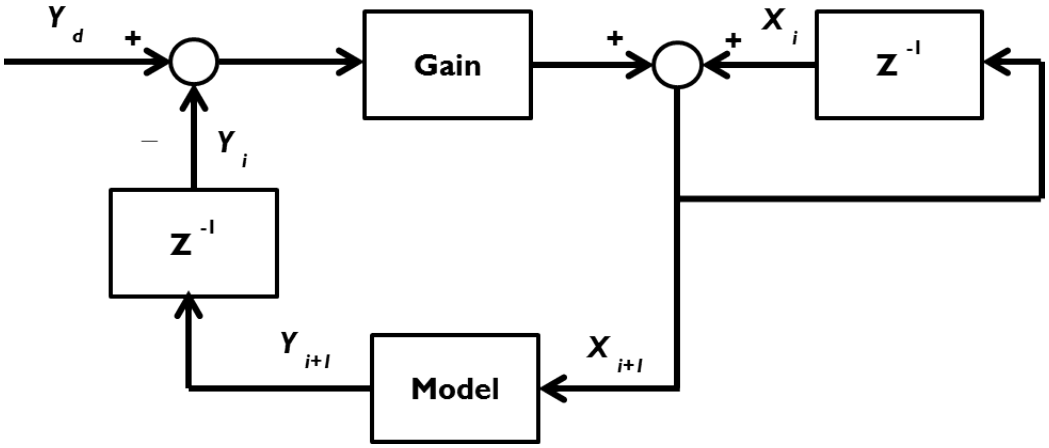

Figure 5.8: Iterative Learning Predictor for Parameter Identification

5.3.3 Design of the Iterative Learning Control Predictor

Considering the relationship between parameters and muscle force described by the mapping:

$$y = f(x) \tag{5.21}$$

where x and y indicate the unknown parameters and the change in muscle length in the model respectively. The process gradient is defined as:

$$F(x) = \frac{\delta f(x)}{\delta x} \tag{5.22}$$

The learning objective is to find suitable parameters x such that, the muscle length *'y'* can reach a given region around the desired value of y_d .

The principal idea of Iterative Learning Control (ILC) is to construct a convergent equation:

$$y_d - y_{i+1} = A(y_d - y_i) \tag{5.23}$$

where the norm of A is strictly less than one, so that learning process could

be convergent after i^{th} iteration or learning trial. To achieve the convergent equation 5.23, the relevant repetitive learning law is:

$$x_{i+1} = x_i + g_i(y_d - y_i) \tag{5.24}$$

where, g_i is the learning gain.

It can be seen that the learning law updates parameters from the previously tuned parameters, x_i and the previous performance error (y_d-y_i). The schematic of the ILC process for parameters identification is shown in Fig. 5.8, where x_i is the input of this system and y_{i+1} is the output response of the muscle model. The performance error can also be represented as

$$\begin{aligned} y_d - y_{i+1} &= y_d - y_{i+1} \\ &= y_d - f(x_{i+1}) \\ &= y_d - f(x_i) + f(x_i) - f(x_{i+1}) \\ &= y_d - y_i + \frac{\delta F}{\delta x}(x_i - x_{i+1}) \end{aligned} \tag{5.25}$$

Substituting x_{i+1} from Eqn.5.24 in Eqn.5.25,

$$\begin{aligned} y_d - y_{i+1} &= y_d - y_i + \frac{\delta F}{\delta x}\left(-g_i e(i)\right) \\ &= y_d - y_i - \frac{\delta F}{\delta x}\left(g_i(y_d - y_i)\right) \\ &= \left(1 - g_i\frac{\delta F}{\delta x}\right)(y_d - y_i) \end{aligned} \tag{5.26}$$

Comparing Eqn.5.17 and Eqn.5.26, the magnitude of A is

$$|A| = \left|1 - g_i\frac{\delta F}{\delta x}\right| < 1 \tag{5.27}$$

$$g_i < \frac{2}{\frac{\delta F}{\delta x}} \tag{5.28}$$

Table 5.6: Parameters for the Iterative Learning Predictor

y_d	ΔL_{PE}
x_i	ΔL_{CE}
ILP Equation	$L_{PE}=f(L_{CE})$

Once the parameters are estimated for the *biceps* and *triceps* muscle groups, the force and the torque generated are calculated using the Hill's muscle model for the same.

5.3.4 Design of the Hybrid Muscle Model

The disadvantage of using the Hill muscle model is that all the muscle forces corresponding to a particular joint need to be known for predicting the torque at that joint. For example, the elbow joint has thirteen muscle groups associated with its movement. This would require the use of thirteen pairs of electrodes for measuring the EMG for predicting the joint torque which would not be fruitful for the rehabilitation process. Here, the muscle torques calculated from the two biggest muscle groups (in this case the *biceps brachii* and the *triceps brachii*) are used as inputs to a neural network model for predicting the overall joint torque at the elbow. The neural network parameters are given in Table 5.7.

Table 5.7: Parameters for the Neural Network for the Hybrid Muscle Model

Inputs	2 (Calculated Joint Torques of the *biceps brachii* and *triceps brachii*)
Neurons in the Hidden Layer	20
Output	1 (Elbow Joint Torque)

The data set was divided into 15 training and 5 test sets for the elbow

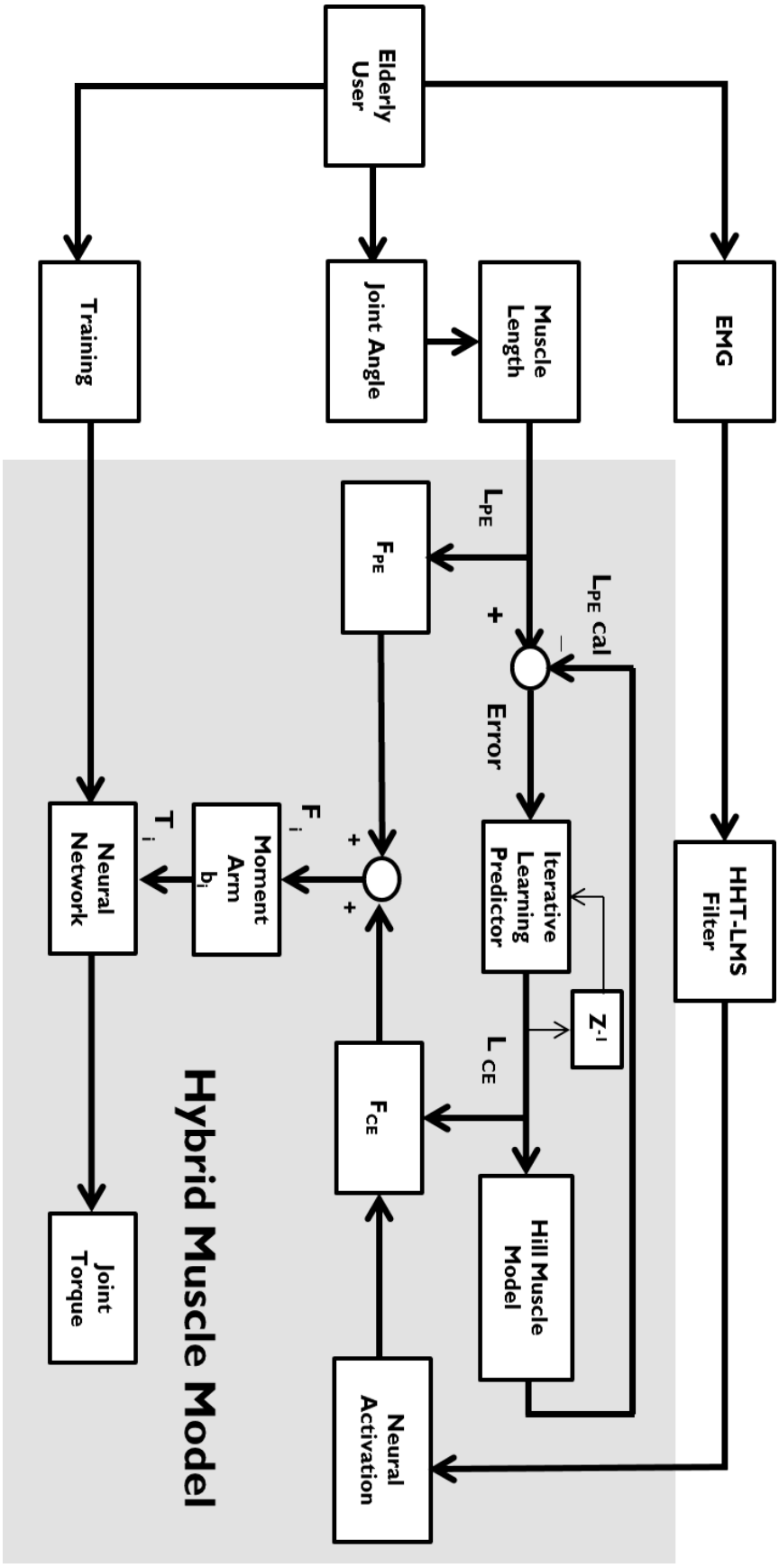

Figure 5.9: Overview of the Hybrid Muscle Model

flexion and elbow extension movements for each subject. The overview of the Hybrid Muscle Model is shown in Fig. 5.9.

5.4 Experimental Results

5.4.1 Estimation of the Joint Torque

Fig. 5.9 outlines the algorithm for the calculation of the *biceps* force, *triceps* force, *biceps* torque and *triceps* torque. The changes in the joint angle during elbow flexion and extension are measured using the accelerometer. As described in Section 5.1.4, the variation in the muscle length is proportional to this change in the joint angle. The variation in the muscle length (L_m)is taken as the desired input to this system. The ILP predicts the changes in the Contractile Element (CE) length (L_{CE}) according to the changes in the muscle length. L_{CE} is input to modified Hill's model to numerically compute the changes in the muscle length *($L_{m,cal}$)*. This calculated value for the muscle length acts as a feedback to the system and is compared with the measured value of the same. The error between *($L_{m,cal}$)* and L_m is fed into to the ILP to tune its parameters. This process is iterated till the error is minimal.

The predicted value of L_{CE} for each muscle is used to calculate their respective contractile element force using Eqn. 5.12. The measured change in length for each muscle, which is also representative of L_{PE} is used to calculate the respective parallel element force using Eqn. 5.7. The two forces for each muscle, F_{PE} and F_{CE}, are summed up together to generate the total force F_{tot} generated by each muscle as shown in Fig.5.10(a) and Fig.5.10(b). The moment arm calculated for each muscle is used in conjugation with F_{tot} to generate the joint torque component of that muscle (Fig.5.10(c) and Fig.5.10(d)). The total joint torque is then computed by summing up each

muscle's joint torque component as shown in Fig. 5.11(a).

- **OBSERVATIONS**
  - The *biceps* and the *triceps* forces in Fig.5.10(a) and Fig.5.10(b) respectively, are dependent on the respective *biceps* and *triceps* EMG signals and, hence, the muscle activations. These forces closely follow the structure of the neural activation of the respective EMG signals.
  - The joint torques generated by the *biceps* and the *triceps* muscle groups, shown in Fig.5.10(c) and Fig.5.10(c)is directly proportional to the respective *biceps* and *triceps* forces,
  - It can be observed from 5.2(a) and 5.10(c) that during the elbow flexion, there is a sharp rise in the torque generated by the *biceps* muscle groups. The *biceps* torque generated then drops down during the 'no movement' stage and then rises again closer to the flexion peak during the elbow extension initiation.
  - It can be observed from 5.2(a) and 5.10(d) that during the elbow flexion the rise in the *triceps* torque follows that of the *biceps* torque, though the drop during the 'no movement' stage is gradual compared to the *biceps* muscle group. There is no rise in the *triceps* torque during the elbow extension initiation.
  - It can be seen from Fig. 5.11(b) that with two input muscle model to the neural network, the algorithm has reduced the mean square error and doesn't have any trouble adjusting to the variations or changes in torque. It is relatively stable for constant torque regions of the EMG data compared to the previous results.

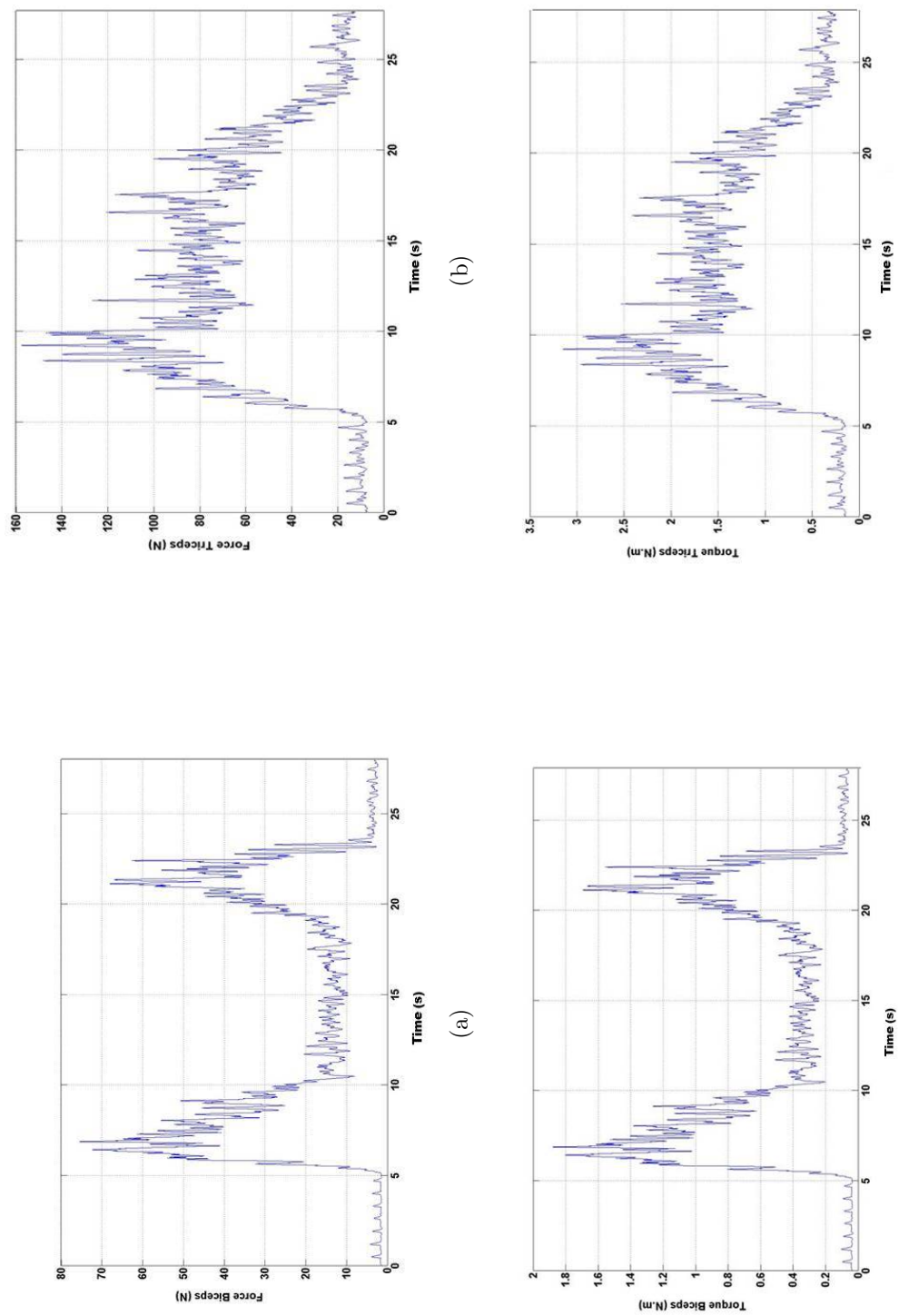

Figure 5.10: *Biceps* Force (Fig. 5.10(a))and the *Triceps* Force (Fig. 5.10(b)) calculated from the Muscle Model along with the torque generated by the *biceps* Force (Fig. 5.10(c)) and the *triceps* Force (Fig. 5.10(d)).

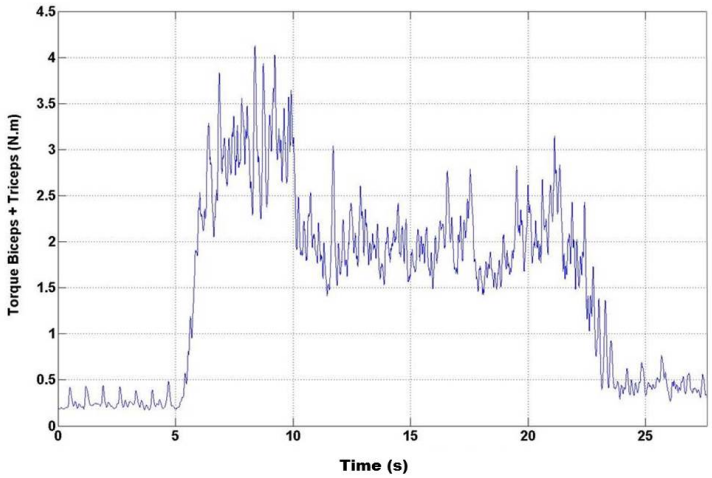

(a)

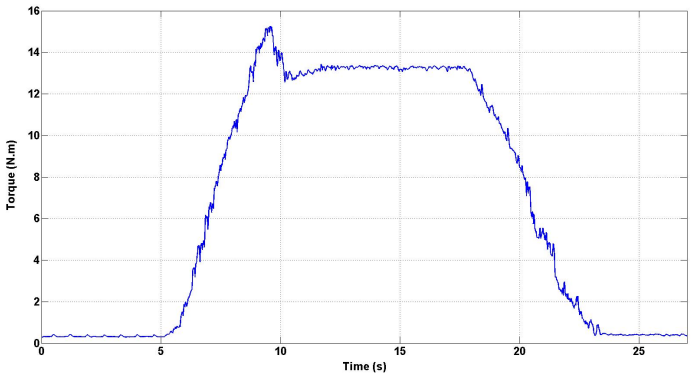

(b)

Figure 5.11: The Joint Torque generated by the *triceps* and the *biceps* muscle groups (Fig. 5.11(a)) and the output of the neural network of the hybrid model for EMG-Joint Torque Relation (Fig. 5.11(b)) for the joint torque at the elbow Fig. 5.2(a)

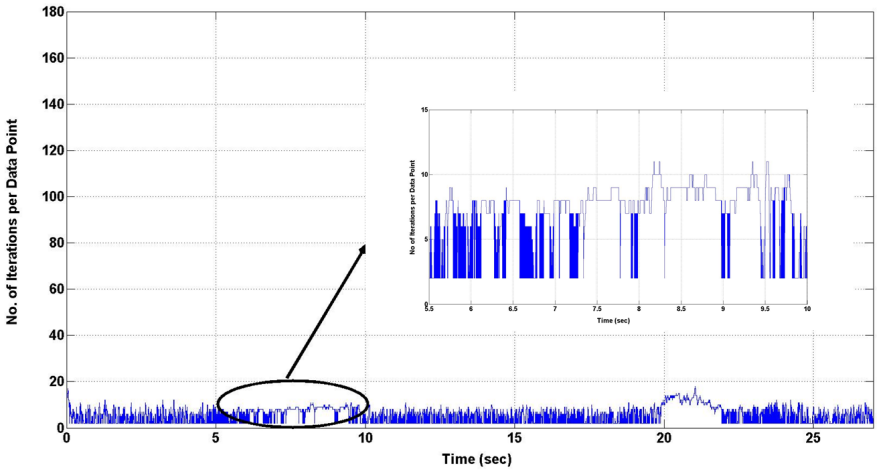

Figure 5.12: Number of iterations for each data point in the Iterative Learning Predictor (ILP)

- From Fig. 5.11(b) and Fig. 5.2(a), it can be interpreted that the test data follows the measured torque quite closely.

- Fig. 5.12 shows the number of iterations required for processing each data point in the ILP algorithm. The number of iterations is less than 10 for most of the data points except when there is a change in the muscle length.

- The maximum number of iterations for processing each data point for calculation of the contractile element length is less than 20 as shown in Fig.5.12. On a hardware platform, it is possible to implement this ILP with real time constraints.

5.4.2 Mean Squared Error

The Mean Squared Error (MSE)for the different models is calculated as follows:

$$MSE = \frac{1}{N}\left[\sum_{i=1}^{N}\left(\hat{T}_i - T_i\right)^2\right] \tag{5.29}$$

When we compare the MSE of the different models in Table 5.8, it is evident that the hybrid model performs the best for a two channel agonist-antagonist model to map the joint torque to the EMG.

Table 5.8: Mean Squared Error in the Estimated Joint Torque

Muscle Model	Mean Squared Error (MSE)
Hybrid Model	0.07
Fixed Function Model	6.73
Neural Network 1	4.59
Neural Network 2	1.58

5.5 Discussion

Iterative Learning Predictor (ILP) is a simple and effective solution to the parameter identification problems of the muscle model which is highly nonlinear and multi-dimensional. ILC method can guarantee the learning process convergence even if the muscle model is partially unknown or difficult to analyze. The use of the ILP ensures that (i) the model doesn't predict unreasonable values for the parameter and (ii) the time required for processing the data is minimized. This is due to the repetitive nature of rehabilitation exercises and the dependency of the predicted output on the previously predicted value and the error calculated. A pointwise ILP is implemented where the data points in the signal are iterated one-by-one till the desired output reaches the same as the actual system output.

The dependency of the muscle physiological model on the muscle activation of all the muscle groups involved in the joint movement makes for complex and tedious calculations for prediction of the joint torque. The neural network model is a black box model for predicting the joint torque. Solving such models using single or two channel data results in gross inaccuracies that are

not tolerated in rehabilitation. It also requires multiple muscle activation data for good prediction.

A hybrid model is proposed that combines the muscle physiological model and the neural network to predict the joint torque of the elbow. The advantage of this method over neural network black box models in [131] is the predicted results follow the actual joint torque faithfully and the Mean Squared Error (MSE) is minimum of all the models. Moreover, the time required for executing the hybrid model is directly proportional to the number of iterations required per data point and the constant time required by the neural network for predicting the joint torque. The accuracy of the predicted output is neither just a function of the black box neural network nor it depends on multiple muscle activation data.

5.6 Summary

A brief description of the methodology used for data collection for EMG-Torque modelling including the experimental protocol for EMG measurement and the signal pre-processing is given in the initial section. Preliminary tests were carried out for estimating the joint torque of the elbow using the fixed function model and neural network models. The inability of these models led to the design of a hybrid muscle model for predicting the elbow joint torque. The physiological modelling of the muscle based on Hill's muscle model and its numerical implementation is derived. The design of an iterative learning predictor for estimating the missing parameters of the muscle model is outlined and a pointwise Iterative Learning Predictor (ILP) is proposed to ensure maximum tracking between the predicted muscle length and the measured muscle length. A hybrid muscle model is proposed that utilizes

the Hill's model to predict the joint torques for two channels of EMG data and this predicted torque is used to train a neural network for estimating the actual joint torque from the muscle activation.

The implementation of the ILP in this hybrid muscle model is presented and it is found that the error in the joint torque predicted by the hybrid model is less when compared to the fixed function and the neural network model.

6

Mechanomyography Feature Extraction and Classification of Forearm Movements using Empirical Mode Decomposition and Wavelet Transform

This chapter details the theoretical background and experimental results for feature extraction and pattern classification of different movements of the forearm and hand using Mechanomyography (MMG) as a control signal. Though Electromyography (EMG) is usually used to monitor the muscle activity, there is valuable information in the mechanical index of the muscle dynamics. Skeletal muscles, on contraction, emit low frequency vibrations that can be measured on the surface of the skin. These vibrations are generated as a resultant of the total lateral movement of the muscle at the start of a contraction, subsequent resonant frequency oscillations and physical changes in the active muscle fibers [84, 132–136]. The EMG is a direct function of the neural activation and, thus, is affected greatly by ageing and injury. MMG, being a function of the mechanical vibrations, is less likely to be affected by ageing and injury and, hence, can play an active role in designing a pattern recognition system for rehabilitation of the elderly [137] with input of comparative data from a younger age group of healthy individuals.

A description of MMG patterns is a critical step towards a better understanding of the mechanical activity of muscles during movement control. MMG can have applications in control of upper limb prosthesis or body-machine interfaces if unique patterns can be identified for different movements [81–83, 85]. This study focusses on isolating different patterns from the recorded MMG signals of the forearm muscle groups during hand and wrist movements, and classifying them for use in pattern recognition based assistive actuator systems. The features extracted are time-frequency domain features [75, 77, 85], wavelet features [78, 80, 134, 138] and features derived from the empirical mode decomposition of the signal [139].

6.1 Methodology

The MMG measurement protocols have been discussed in Chapter 2. The following sections describe the subjects participated and the specific tasks performed by them for this study. Data were collected from three muscle sites represented in this study as shown in Table 6.1.

Table 6.1: Accelerometer Notation and Muscle Sites

Muscle Site	Notation
flexor capri ulnaris	A1
brachioradialis supinator	A2
abductor pollicis longus	A3

6.1.1 Subjects

Data were acquired from six able-bodied individuals, aged 23 ± 6 years. All subjects were healthy and reported no physical or mental disorders. Each subject had access to the full range of forearm motions and no previous history of musculoskeletal illness.

6.1.2 Experimental protocol

All subjects were instructed not to perform fatiguing upper limb exercise one day prior to the sessions. A custom dSPACE graphical user interface (GUI) with a manual trigger was used to start data acquisition and visually cue participants to perform various classes of muscle activity corresponding to the following eight hand motions: hand open, hand close, wrist flexion, wrist extension, wrist pronation, wrist supination, wrist ulnar deviation and wrist radial deviation. A numerical index is used for each class of the hand motion for identification during pattern recognition as shown in Table 6.2. The raw MMG signals at the three muscle sites *flexor carpi ulnaris*, *brachioradialis supinator*, and *abductor pollicis longus* for all of the hand motions in the study are shown in Fig. 6.1.

It can be observed from Fig. 6.1 that, each accelerometer channel has some signal component present from different hand motions. This feature is exploited in designing the classifier system with lesser number of electrodes, as features identification here is focussed on extracting unique features that isolate each of the different hand movements from the same three sites.

Table 6.2: Index for different hand motions for classification

Hand and Wrist Motion	Index
Wrist Flexion	I
Wrist Extension	II
Hand Close	III
Hand Open	IV
Wrist Pronation	V
Wrist Supination	VI
Wrist Ulnar Deviation	VII
Wrist Radial Deviation	VIII

Subjects performed ten repetitions of each of the above motions. Each motion was comprised of the full range of motion from the resting position to

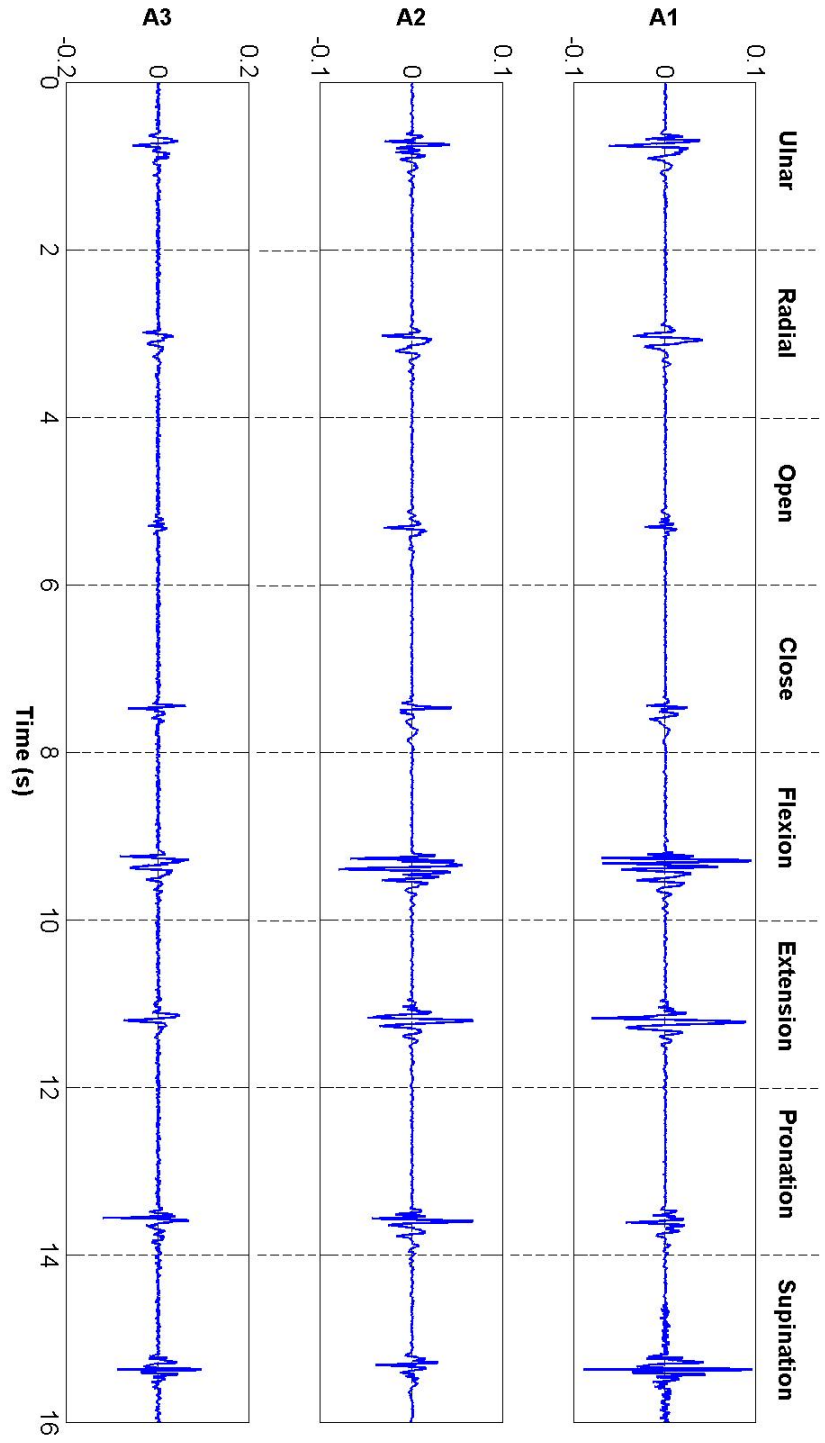

Figure 6.1: The MMG signal at the three muscle sites for all the hand motions in this study.

the final position, followed by 2 seconds of the hand being held in the final position. The different forearm motions are performed in pairs corresponding to their agonist and antagonist relations. For example, in Fig. 6.5 the first motion performed is the '*hand close'* while the next motion is the *'hand open'*. This sequence is then repeated for the rest of the session. The data were collected in multiple sessions, each session not exceeding more than 2 minutes to ensure that muscle fatigue doesn't adversely affect the readings.

6.1.3 Signal Pre-processing

The measured and filtered surface MMG signals were stored and analysed on a PC using MATLAB software. Each channel of the MMG data was processed and analysed separately. The DC offset was removed by filtering the mean value in the MMG data while the 2nd order Butterworth high pass and low pass filters, with cut-off frequencies of 5 Hz and 100 Hz respectively, were applied to filter out the noise and motion artifacts including changes in forearm joint angles.

6.1.4 Multilayer Perceptron Classifier

A multilayer perceptron classifier (MLP) is used for pattern classification for all the feature vectors. This network has an input layer, one hidden layer and an output layer. The detailed description is given in Section 3.3.3. The multilayer perceptron classifier layer structure for the pattern classification of MMG signals is shown in Fig. 6.2.

- Input Layer: The number of neurons in the input layer is equal to dimension of the feature vector which is described in Table 6.3
- Hidden Layer: A single hidden layer consisting of twenty (N_{hid}) neurons

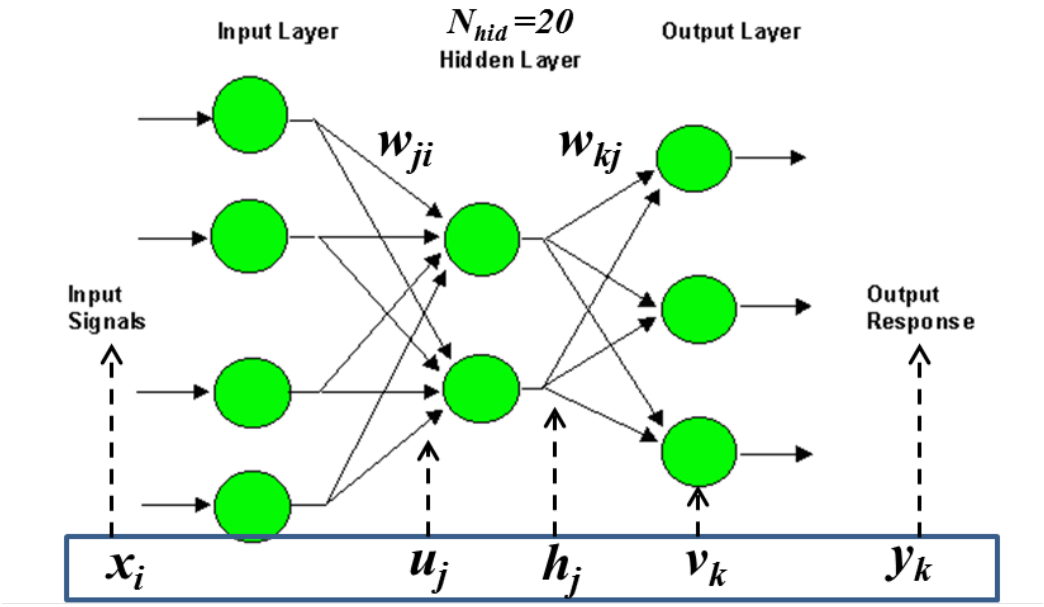

Figure 6.2: Layer structure of the Multilayer Perceptron classifier for the pattern classification of MMG signals

is used and a sigmoid function is chosen as the activation function for the hidden layer.

- Output Layer: The output layer has eight neurons corresponding to the eight motions to be classified and a linear function is used, as the activation function.

Table 6.3: Input Layer Size for Different Feature Extraction Methods

Feature Extraction Methods	Input Layer Size
Time-Frequency	18
Wavelet Transform	75
Empirical Mode Decomposition	150

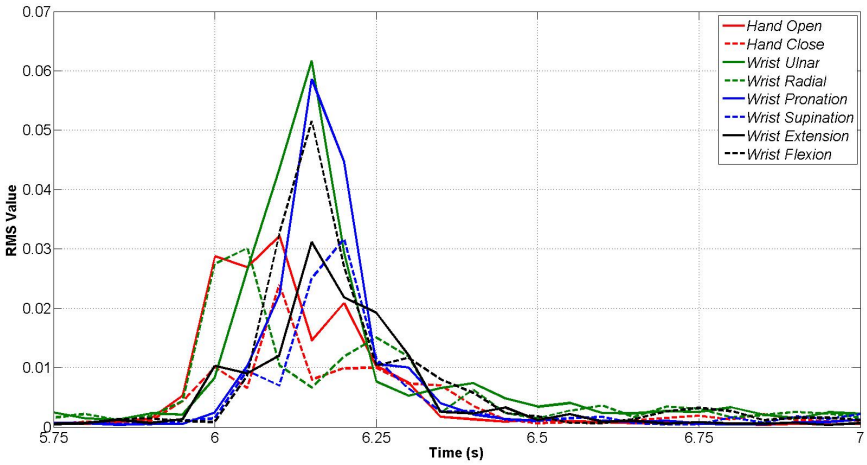

Figure 6.3: Temporal Evolution of the MMG Signal for different hand motions at the *flexor carpi ulnaris*

6.2 Time-Frequency Feature Extraction and Classification

6.2.1 Temporal Evolution of the muscle activity

To study the MMG signal's temporal evolution, the root mean square(RMS) value of the signal was evaluated over unique and consecutive 250 ms epochs for each hand/wrist movement at all the muscle sites. The RMS of the MMG signal is defines as :

$$A_{RMS} = \sqrt{\frac{1}{N}\sum_{i=1}^{N} x_i^2} \tag{6.1}$$

where x_i is the i_{th} sample of the measured MMG containing N number of samples.

Fig. 6.3 shows the typical time course of the MMG signals recorded at the *flexor carpi ulnaris* muscle site while Fig. 6.4 shows the temporal evolution of the MMG Signal for the *'Hand Close'* movement at the three muscle sites. From both these figures it can be observed that the RMS value increased

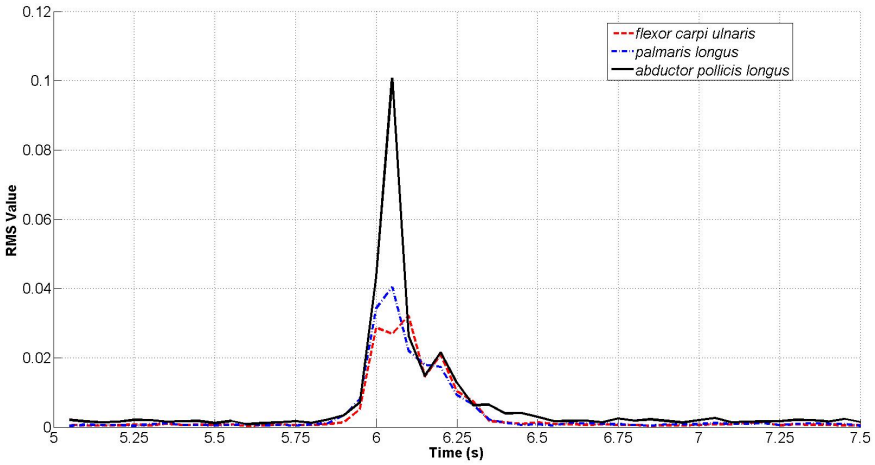

Figure 6.4: Temporal Evolution of the MMG Signal for the Hand Close Movement at the three muscle sites.

up to 250 ms from its resting value before the movement was detected by the accelerometer on the participant's hand. The RMS steadily increased, peaked between 250 to 500 ms after the initiation of movement, decayed, and stabilized after about 1250 ms. The time-to-peak and the steady-state RMS depended on the hand movement being performed. *Thus, it can be inferred that the minimum time needed for analysis of the MMG signal is 500 ms.*

It can also be observed from Fig. 6.3 that the hand motion directly associated with the corresponding muscle group had a peak RMS earlier and at a higher amplitude compared to other muscle groups.

For real time application, the minimum threshold for the response time of the system for the user to perceive a delay between the initiation of a hand movement and the generation of the control signal is 300 ms. Hence, a *decision window* of 250 ms is chosen. The MMG signal continuously changes during the progress of a contraction. The motion can be identified truly if the analysis window is at least 500 ms as inferred from the temporal analysis of the MMG signal. Thus, features are extracted with a decision window of 250 ms and an analysis window of 500 ms.

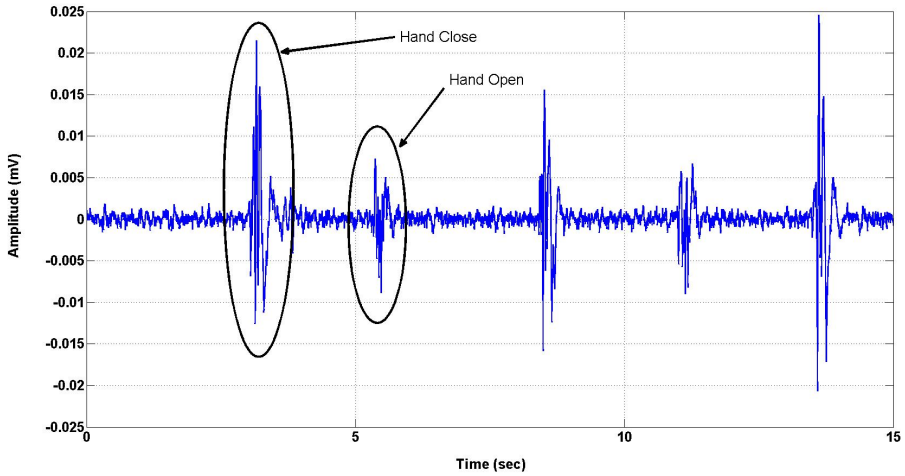

Figure 6.5: Raw MMG Signal at the *flexor carpi ulnaris* for hand open and close

6.2.2 Feature Extraction using Time-Frequency Features

The raw MMG signal at the *flexor carpi ulnaris* for hand open and close motions are shown in Fig. 6.5.

The following time domain features for the MMG signal are calculated for the decision windows of 250 ms. The features, defined earlier in Section 3.2.1, are extracted for all the different forearm motions mentioned in Table 6.2.

- Mean Absolute Value (MAV)
- Mean Absolute Value Slope
- Zero Crossings (ZC)
- Slope Sign Changes (SSC)
- Waveform Length
- Root Mean Square (RMS) Value

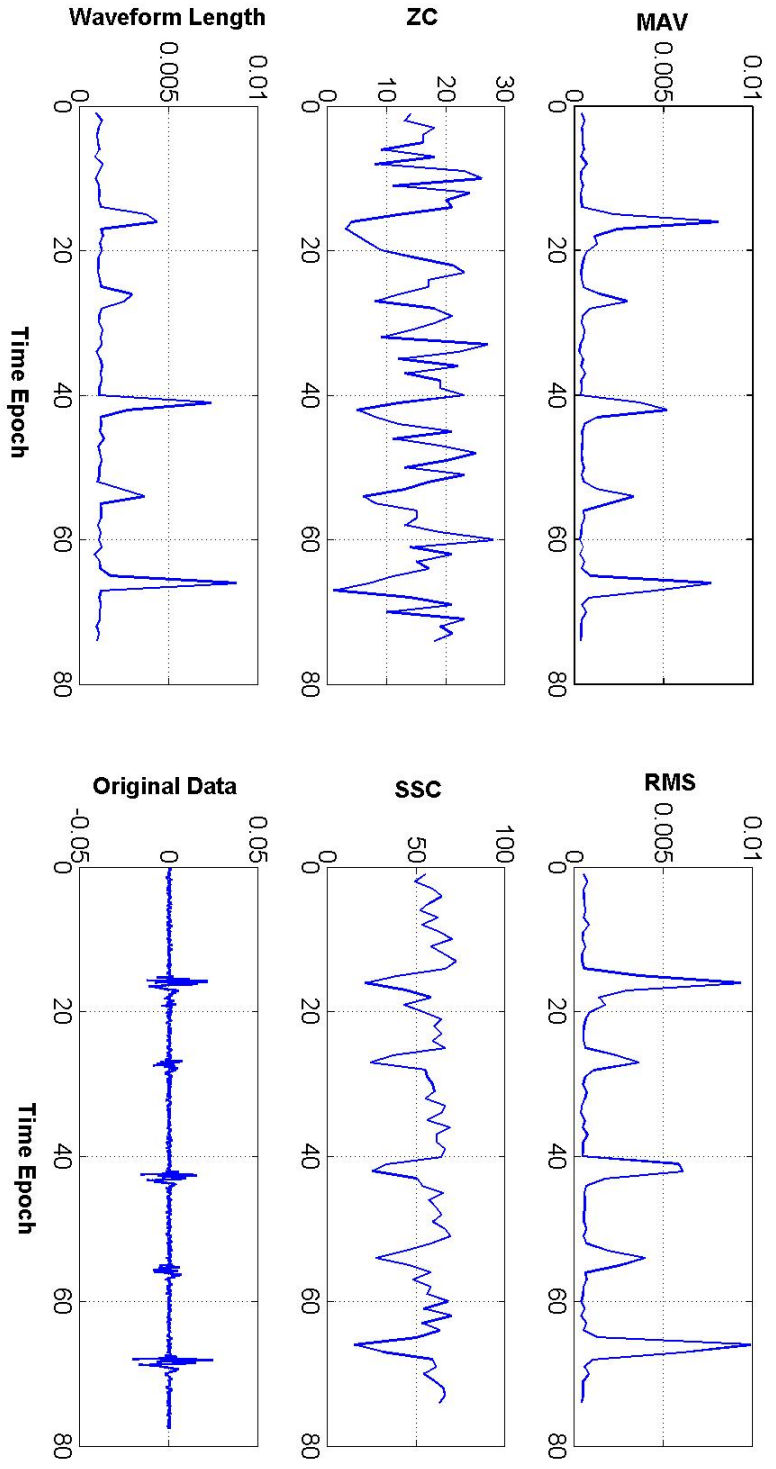

Figure 6.6: Time domain feature set for MMG Signal at the *flexor carpi ulnaris* for hand open and close

These features, extracted from the MMG signal constitute the feature set of six features per channel. Thus, the total number of time-frequency features extracted for each hand motion is eighteen for the three channels of MMG data.

Fig.6.6 displays the different time domain features for the *'hand open'* and *'hand close'* MMG signal in Fig. 6.5. This feature set is computed on data from the hand open and close movements. The MMG data has been sub-divided into time segment of 500ms (with a 250ms moving window) and all the calculations have been made individually in each time window. The RMS value of the data for each time segment is also shown among the features as it gives an indication of the energy of the signal. Here, the first noticeable motion is the hand opening and the next motion is that of the hand closing. The analysis of remaining data sets also give similar feature vectors.

- **OBSERVATIONS**
  - The temporal evolution of the Mean Absolute Value (MAV) of the signal is consistent with the signal. It is difficult to identify different hand movements based on only the MAV.
  - The drop in number of Slope Sign Changes (SSC) provides an indication of the initiation of the MMG signal. This feature can be used to identify the start of the motion and can be used to restrict the processing during specific time epochs when there is movement.
  - The drop in number of Zero Crossings (ZC) also provides an indication of the initiation of the MMG signal though not as clear as that of the number of SSC. Moreover, this feature is affected by other residual noise present in the signal.

- The waveform length not only provides a boundary envelope for the signal movements but it also varies according to the signal strength. It is a good indicator of the amplitude and the frequency of the signal.
- The temporal evolution of the RMS value of the signal varies according to the signal strength, similar to the MAV. It is not only an indicator of the energy of the signal but also of the noise present in the signal. The temporal evolution of the muscle activity is discussed in detail in the next section.

6.2.3 Classification of Time domain features using MLP Classifier

The confusion matrix of the time domain features for classification of the eight hand motions is given in Table 6.4

Table 6.4: Confusion Matrix for the MLP Classifier for the Time-Frequency features

Classified Motion	Actual Motion							
	I	II	III	IV	V	VI	VII	VII
Wrist Flexion (I)	31	0	0	0	5	0	4	3
Wrist Extension (II)	0	36	0	0	0	0	1	3
Hand Close (III)	0	0	37	0	3	0	0	0
Hand Open (IV)	1	0	0	48	3	0	1	0
Wrist Pronation (V)	0	0	1	0	26	0	0	0
Wrist Supination (VI)	0	0	0	0	0	38	0	0
Wrist Ulnar Deviation (VII)	4	0	2	1	2	0	27	5
Wrist Radial Deviation (VIII)	0	0	1	0	0	0	2	25

- **OBSERVATIONS**
  - It can be inferred from Table 6.5, that the overall classification rate for the MLP classifier for using time frequency features is 86.7

Table 6.5: Error in Classification for the MLP classifier using Time-Frequency features

Hand and Wrist Motion	Error
Wrist Flexion	0.139
Wrist Extension	0
Hand Close	0.075
Hand Open	0.040
Wrist Pronation	0.462
Wrist Supination	0
Wrist Ulnar Deviation	0.25
Wrist Radial Deviation	0.306
Total Error	0.133

%.

- The wrist pronation is the most poorly classified with an efficiency of 53.8% as seen from Tables 6.5 and 6.4.

- The next poorly classified motion is the wrist ulnar deviation that has a classification rate of 69.4% as seen from Tables 6.5 and 6.4.

- The wrist radial deviation is the next poorly classified motion with a classification rate of 75% as seen from Tables 6.5 and 6.4.

It can be concluded from the above observations that usage of only time frequency features does not give a good classification rate for the MMG signal. Though the overall classification rate is 86.7 %, the classification rates for wrist pronation, wrist ulnar deviation and wrist radial deviation are not acceptable for a pattern recognition based MMG classification system. The overall high classification rate is due to the MLP classifying the wrist supination, hand open and wrist extension motions with better accuracies.

6.3 Wavelet Transform Feature Extraction and Classification

6.3.1 Feature Extraction using Wavelet Transform

Different sets of features are extracted using wavelet transform for the analysis window of 500 ms with a moving window of 250 ms. A wavelet transform characterizes the signals locally in time domain in the analysis window and is useful for approximating non-stationary signals like MMG. The wavelet decomposition of a signal is detailed in Chapter 3.

The level of decomposition (J) is chosen as 4, while the wavelet used is a Daubechies family wavelet '*db4*'. The detailed sub-space or the high frequency sub-patterns at each level of decomposition are represented by *D1, D2, D3, D4, D5* while A5 is the low frequency sub-pattern or the approximate subspace, and is the final level of decomposition.

Using coefficients of the wavelets as features would be a computational disaster depending on the level of decomposition of the MMG signal. Hence, the following features were defined for each of the detailed and approximation wavelets. These features are extracted for all the different forearm motions mentioned in Table 6.2.

- Root Mean Square Value: Root mean square value of each wavelet in the time segment is defined as

$$W_{jk}^{RMS} = \sqrt{\frac{1}{N}\sum_{i=1}^{N} x_{ijk}^2} \tag{6.2}$$

  where x_{ijk} is the i_{th} sample of the j_{th} wavelet in the k_{th} time segment, containing N number of samples.

- Mean Absolute Value: The mean absolute value of the j_{th} wavelet in the k_{th} time segment is defined as

$$W_{jk}^{MAV} = \frac{1}{N}\sum_{i=1}^{N}|x_{ijk}| \tag{6.3}$$

- Shannon Entropy: The Shannon entropy of the j_{th} wavelet in the time segment k is

$$W_{jk}^{H} = -\sum_{i=1}^{N}P(x_{ijk})ln(P(x_{ijk})) \tag{6.4}$$

- Mean Frequency: The mean frequency component present in each wavelet is

$$W_{jk}^{MNF} = \frac{\sum x_{ijk}^2 f_{ijk}}{\sum x_{ijk}^2} \tag{6.5}$$

  where f_{ijk} is the i_{th} frequency component in the j_{th} wavelet in the k_{th} time segment and x_{ijk} is the corresponding amplitude component.

- Waveform Length: A feature which provides information on the wavelet amplitude, frequency and duration. It is the cumulative length of each wavelet over each analysis window.

$$W_{jk}^{WL_0} = \sum_{i=1}^{N}(x_{ijk} - x_{(i-1)jk}) \tag{6.6}$$

These features, extracted from the MMG signal constitute the feature set of five features per wavelet per channel. Thus, the total number of time-frequency features extracted for each hand motion is seventy-five for the three channels of MMG data and five wavelet coefficients.

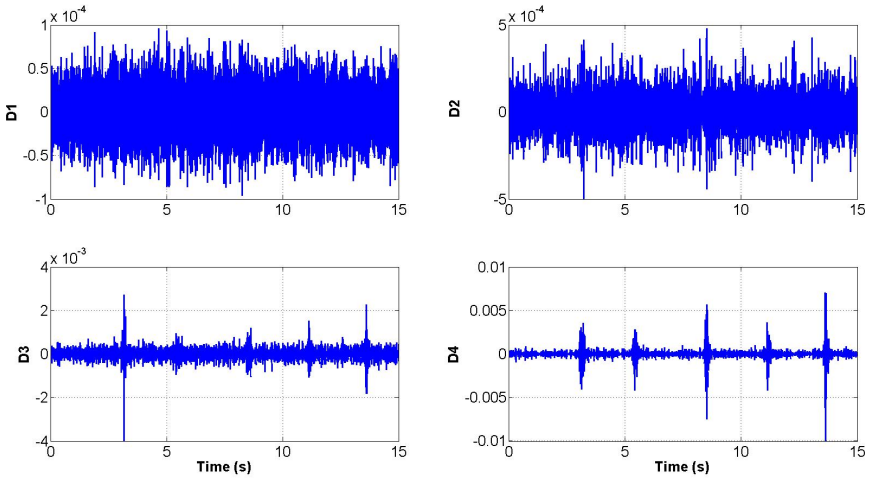

Figure 6.7: D1-D4 wavelet decomposition of the signal in Fig. 6.5

Fig. 6.7shows the high frequency sub-space or the *Detail* wavelet sub-patterns after the wavelet decomposition of the signal in Fig. 6.5. The approximation wavelet is isolated in Fig. 6.8 and a set of its time domain features are shown in Fig.6.9.

- **OBSERVATIONS**
  - It can be observed from Fig. 6.7 that the detail components 'D1' and 'D3' are representative of the noise present in the MMG signal in the higher frequency bands.
  - The detail component '*D4*' and the approximate component '*A4*' (Fig.6.8) are more representative of the actual MMG signal. The noise present in the signal is absent in these two wavelet sub-patterns as it is representative of the lower frequency band of the signal. Possible noise due to motion artifact has already been removed by the signal pre-processing detailed in Section 6.1.3
  - The detail component '*D2*' has both signal components and noise components present in the actual MMG signal. It is difficult to

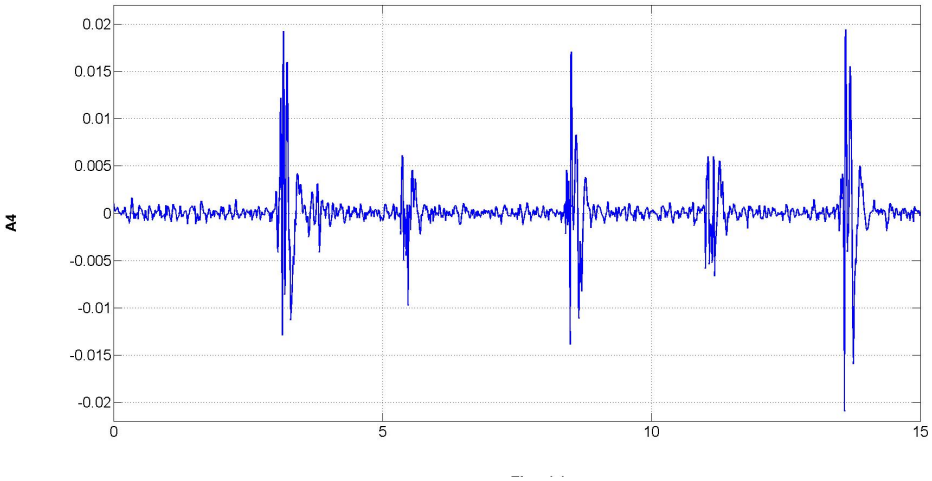

Figure 6.8: The A4 approximation of the wavelet decomposition of signal in Fig. 6.5

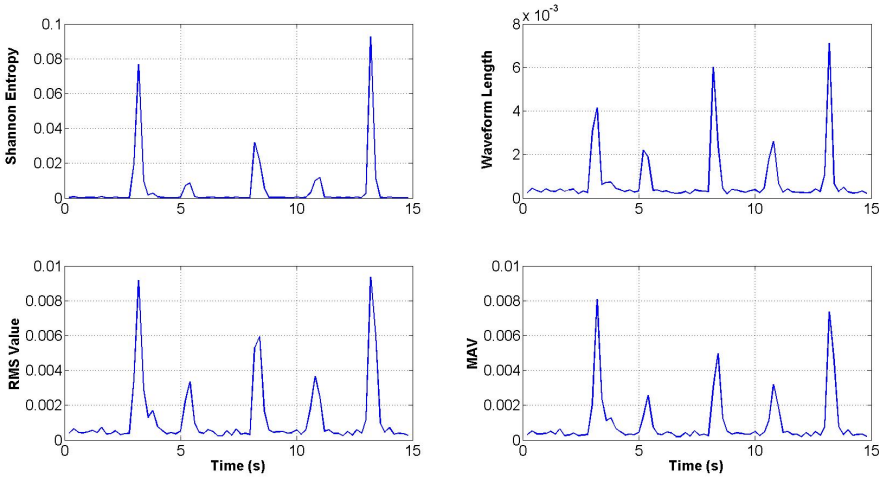

Figure 6.9: Time domain feature set for A4 wavelet MMG Signal at the flexor carpi ulnaris for hand open and close

distinguish between the hand motion and the noise in some cases.

– The Shannon wavelet entropies in Fig. 6.9 of all the wavelet sub-patterns not only provide a boundary envelope for the signal movements but also varies according to the variations in each of them.

– Waveform length, RMS value, and the MAV, look similar. These features along with the Shannon wavelet entropy can be used to distinguish not only the dynamic and the isometric components of the signal but also the different wrist movements.

6.3.2 Classification of Wavelet features using MLP Classifier

The confusion matrix of the wavelet features for classification of the eight hand motions is given in Table 6.6

Table 6.6: Confusion Matrix for the the MLP Classifier for the wavelet features

Classified Motion	Actual Motion							
	I	II	III	IV	V	VI	VII	VIII
Wrist Flexion (I)	35	0	0	0	1	0	1	0
Wrist Extension (II)	0	33	0	0	0	0	0	2
Hand Close (III)	1	0	39	1	4	0	1	0
Hand Open (IV)	0	0	1	49	0	0	0	0
Wrist Pronation (V)	0	0	0	0	31	0	0	0
Wrist Supination (VI)	0	0	0	0	0	38	0	0
Wrist Ulnar Deviation (VII)	0	1	0	0	2	0	33	0
Wrist Radial Deviation (VIII)	0	2	0	0	0	0	1	33

- OBSERVATIONS

  – It can be inferred from Table 6.7 that the overall classification rate

Table 6.7: Error in Classification for the MLP classifier using Wavelet Transform features

Hand and Wrist Motion	Error
Wrist Flexion	0.027
Wrist Extension	0.083
Hand Close	0.025
Hand Open	0.020
Wrist Pronation	0.183
Wrist Supination	0.000
Wrist Ulnar Deviation	0.083
Wrist Radial Deviation	0.083
Total Error	0.098

for the MLP classifier for using wavelet transform features is 90.2 %.

- The wrist pronation is again the most poorly classified but the efficiency has improved to 81.58% as seen from Tables 6.7 and 6.6.

- The next poorly classified motion is the wrist extension motion that has a classification rate of 91.7% as seen from Tables 6.7 and 6.6.

It can be concluded from the above observations that the wavelet feature based classifier can classify different hand motions using the MLP classifier better than the time-frequency based classifier. The overall classification rate is 90.2 % and the classification rates for wrist pronation is still the poorest. Wrist ulnar deviation, wrist extension and wrist radial deviation have acceptable error of approximately 8.3 %. and is acceptable for a pattern recognition based MMG classification system. The overall high classification rate is again due to the MLP classifying the wrist supination, hand open and wrist extension motions with better accuracies.

6.4 Empirical Mode Decomposition Feature Extraction and Classification

6.4.1 Feature Extraction using Empirical Mode Decomposition

The Empirical Mode Decomposition (EMD) has been described in detail in Chapter 4. The empirical mode decomposition method is a convenient tool to deal with data from non-stationary and nonlinear processes and is represented by different Intrinsic Mode Function (IMF) with the following denition:

1. In the whole dataset, the number of extrema and the number of zero-crossings must either be equal or differ at the most by one, and

2. At any point, the mean value of the envelope dened by the local maxima and the envelope dened by the local minima is zero.

The EMD algorithm attempts to decompose nearly any signal into a finite set of functions, whose Hilbert transforms give physical instantaneous frequency values. The EMD decomposes the non-stationary signal into narrow-band components with decreasing frequency. The decomposition is complete, local and adaptive. The basis formed by the IMF directly comes from the signal which guarantees the inherent characteristic of signal and avoids the diffusion and leakage of signal energy. The sifting process eliminates riding waves, so each IMF is more symmetrical and is a zero mean signal. By construction, the number of extrema is decreased when going from one residual to the next thus ensuring that there are a finite number of steps for the complete decomposition.

EMD is performed on the MMG signal for the analysis window of 500 ms with a moving window of 250 ms. The number of IMF(s) for each analysis window is fixed at ten. The absolute mean and mean absolute value slope have no significance for EMD as each IMF has zero mean. Hence, two new features are defined for the EMD. Similar to wavelets, using the coefficients of each IMF as features would be a computational disaster. Hence, the following features were defined for each IMF. These features are extracted for motions corresponding to the wrist and hand:

- Hilbert Energy: The Hilbert spectral energy is calculated for each IMF

$$Hil(IMF_{jk}) = \sum_{i=1}^{N} a_i^2 \tag{6.7}$$

  where a_i is the instantaneous amplitude of the i_{th} sample of the j_{th} IMF in the k_{th} time segment containing *'N'* number of samples.

- Median Frequency: The Instantaneous Frequency (IF) in the Hilbert spectrum that divides the spectrum in two equal halves.

$$\sum_{i=0}^{l_{MDF_i}} a_i^2 \approx \frac{1}{2} Hil(IMF_{jk}) \tag{6.8}$$

$$MDF(IMF_{jk}) = \omega_j[l_{MDF_i}] \tag{6.9}$$

  where ω_j represents the sorted values of the IF in the ascending order for the i_{th} IMF in the k_{th} time segment.

- Shannon Entropy: The Shannon entropy of the j_{th} IMF in the k_{th} time segment is

$$H(IMF_{jk}) = -\sum_{j=1}^{N} P(x_i) ln(P(x_i)) \tag{6.10}$$

- Mean Frequency: The mean frequency component in the j_{th} IMF for the k_{th} time segment is

$$MNF(IMF_{jk}) = \frac{\sum x_{ijk}^2 f_{ijk}}{\sum x_{ijk}^2} \tag{6.11}$$

  where f_{ijk} is the i_{th} frequency component in the j_{th} IMF in the k_{th} time segment and x_{ijk} is the corresponding amplitude component.

- Waveform Length: A feature which provides information on the waveform amplitude, frequency and duration. It is the cumulative length of each IMF over each analysis window.

$$WL(IMF_{jk}) = \sum_{i=1}^{N} (x_{ijk} - x_{(i-1)jk}) \tag{6.12}$$

These features, extracted from the MMG signal constitute the feature set of five features per wavelet per channel. Thus, the total number of time-frequency features extracted for each hand motion is one hundred fifty for the three channels of MMG data and ten IMF(s).

Empirical Mode decomposition of the signal in Fig. 6.5 gives the IMFs in Fig.6.10. The first IMF is isolated in Fig. 6.11 and a set of its time domain features are shown in Fig.6.12

- **OBSERVATIONS**
  - It can be observed from Fig. 6.10(a) and the top most two waves of Fig. 6.10(b) that the higher frequency IMF(s) are representative of the MMG signal in this case.
  - It is difficult to draw any conclusion regarding the bottommost two waves in Fig. 6.10(b) and Fig. 6.10(c). Since the basis is

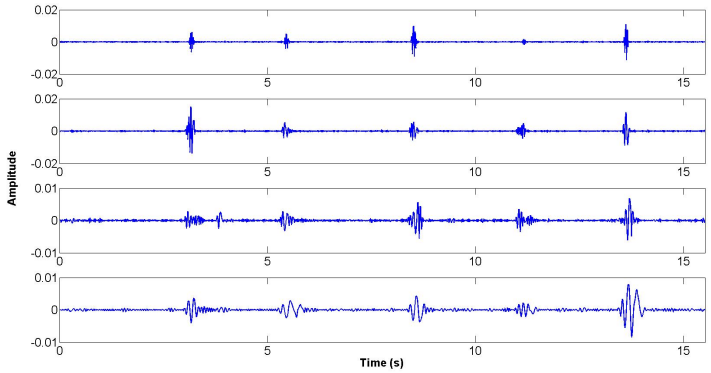

(a)

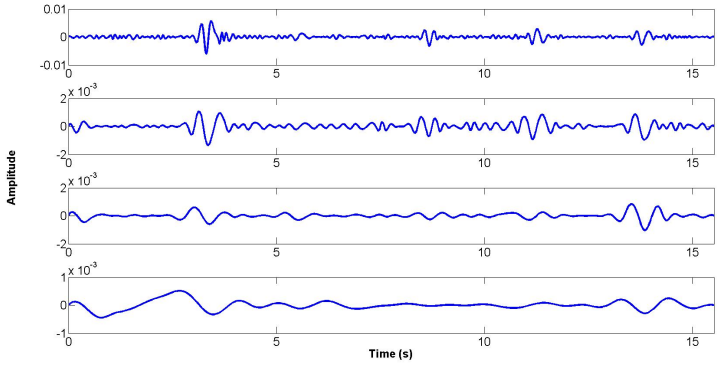

(b)

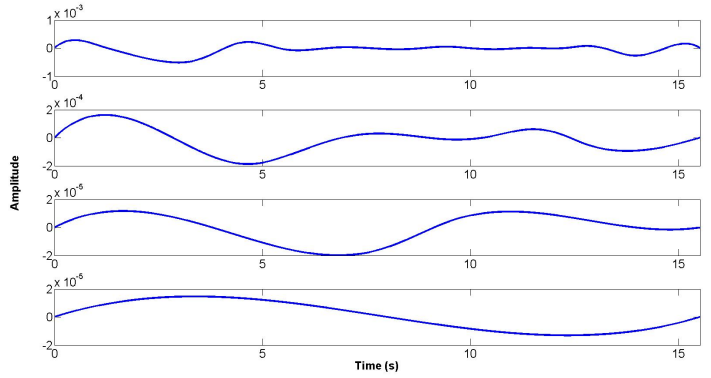

(c)

Figure 6.10: Intrinsic Mode Functions of the MMG Signal in Fig. 6.5

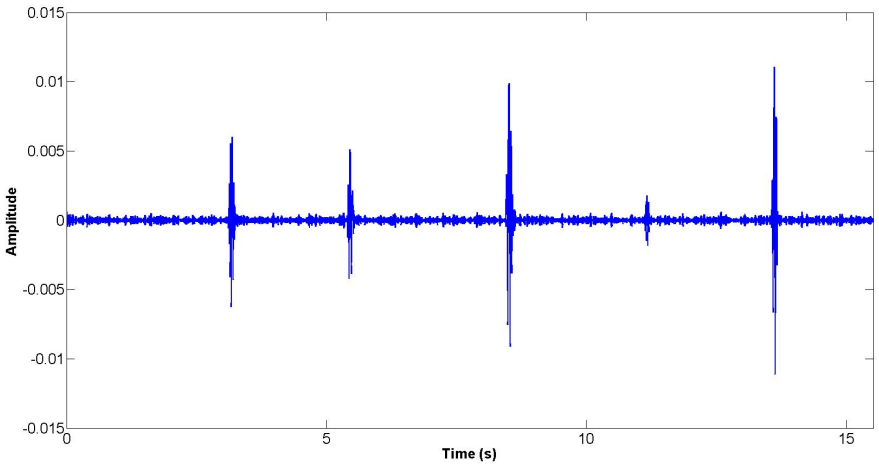

Figure 6.11: The IMF 1 of the EMD of signal in Fig. 6.5

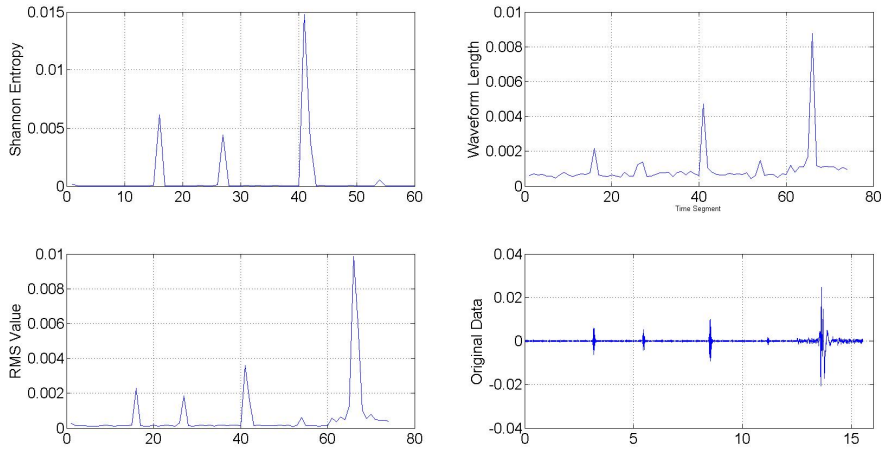

Figure 6.12: Time domain feature set for IMF1 of the MMG Signal at the flexor carpi ulnaris for hand open and close

purely adaptive to the MMG signal, it would be unique to each hand motion. Possible noise due to motion artifact has already been removed by the signal pre-processing detailed in Section 6.1.3

- The Shannon IMF entropy in Fig. 6.12 of the first IMF in Fig. 6.11 is a good indicator of the boundary envelope of the IMF.
- Waveform length, RMS value, and the MAV, look similar. These features along with the Shannon wavelet entropy can be used to distinguish not only the dynamic and the isometric components of the signal but also the different wrist movements.

6.4.2 Classification of EMD features using MLP Classifier

The confusion matrix of the EMD features for classification of the eight hand motions is given in Table 6.8 while Table6.9 shows the error in classification for the different hand motions.

Table 6.8: Confusion Matrix for the the MLP Classifier for the EMD features

Classified Motion	Actual Motion							
	I	II	III	IV	V	VI	VII	VIII
Wrist Flexion (I)	30	0	0	0	0	0	0	2
Wrist Extension(II)	2	36	0	2	0	0	2	0
Hand Close (III)	0	0	39	0	1	0	0	0
Hand Open (IV)	0	0	1	46	1	0	2	0
Wrist Pronation (V)	4	0	0	2	34	0	0	0
Wrist Supination (VI)	0	0	0	0	0	38	0	0
Wrist Ulnar Deviation (VII)	0	0	0	2	2	0	28	2
Wrist Radial Deviation (VIII)	0	0	0	2	0	0	4	30

The following observations can be inferred from Tables 6.8 and 6.9.

- OBSERVATIONS

Table 6.9: Error in Classification for the MLP classifier using Empirical Mode Decomposition features

Hand and Wrist Motion	Error
Wrist Flexion	0.167
Wrist Extension	0.000
Hand Close	0.025
Hand Open	0.080
Wrist Pronation	0.053
Wrist Supination	0.000
Wrist Ulnar Deviation	0.222
Wrist Radial Deviation	0.167
Total Error	0.094

- It can be inferred from Table 6.9 that the overall classification rate for the MLP classifier for using EMD features is 90.65 %.
- The wrist pronation is classified better in this case with an efficiency of 89.47% as seen from Tables 6.9 and 6.8.
- The most poorly classified motion is the wrist ulnar deviation that has a classification rate of 77.78% as seen from Tables 6.9 and 6.8.
- The classification rates for the wrist flexion has dropped to 83.33 % as compared to 97.22 % in the wavelet based classifier as seen from Tables 6.9 and 6.8.

It can be concluded from the above observations that the EMD feature based classifier can classify different hand motions using the MLP classifier better than the time-frequency based classifier. The overall classification rate is slightly better than the wavelet based classifier at 90.65 % while the classification rates for wrist pronation has improved to 89.4 %.The error in classifying wrist ulnar deviation and wrist flexion has dropped and the former is the poorest classified motion. The overall high classification rate is again due to the MLP classifying the wrist supination, hand open and wrist

extension motions with better accuracies as compared to the time-frequency based classifier.

It can be inferred from the above results that the EMD feature based classifier and the wavelet feature based classifier both perform comparatively better while using a MLP classifier as compared to a time-frequency based MLP classifier.

6.5 Discussion

The RMS temporal evolution of the signal at the various muscle sites closely agreed with physiological muscle function. Higher values of the RMS is observed when the muscle site is the primary contributor to the hand motion. While the RMS of MMG signals demonstrated task-specificity, the higher pattern recognition rates attained by wavelet based classifiers and EMD based classifier suggest that there is a complex coding of time and frequency characteristics of the MMG signals during motor tasks.

The EMD algorithm attempts to decompose the MMG signal into a finite set of functions, whose Hilbert transforms give physical instantaneous frequency values. The EMD decomposes the non-stationary signal into narrow-band components with decreasing frequency. The decomposition is complete, local and adaptive. The basis formed by the IMF directly comes from the signal which guarantees the inherent characteristic of signal and avoids the diffusion and leakage of signal energy.

The temporal evolution of the MMG signal studied show that the MMG signal increased from its resting value before the movement was detected by the accelerometer on the participant's hand. The RMS steadily increased, peaked between 250 to 500 ms after the initiation of movement, decayed, and

stabilized after about 1000 ms. Thus it was concluded that the minimum time segment needed for analysis of the MMG signal is 500 ms. To satisfy the threshold of 300 ms for real time processing, an analysis window of 250 ms was chosen with a sliding window of 250 ms for feature extraction and classification. The time-to-peak and the steady-state RMS depended on the hand movement being performed. It can also be observed that that the hand motion directly associated with the corresponding muscle group had a peak RMS earlier and at a higher amplitude compared to other muscle groups.

The MLP classifier performs satisfactorily for both wavelet based feature extraction system and the EMD based feature extraction system. The classification rates for the classifier were 90.2% and 90.65% for the wavelet features and EMD features respectively.

6.6 Summary

This chapter describes the methodology used for MMG signal acquisition and processing for eight different types of forearm movements. These eight forearm movements are first classified based on time-frequency features and a Multilayer Perceptron (MLP) classifier. The temporal evolution of the MMG signal was also studied. The requisite theory is presented and experimental results for classification are computed.

Subsequently, the classification of the eight forearm movements based on wavelet transform features and an MLP classifier is presented and it is found to perform better than the time-frequency based classifier. Finally, EMD features are extracted from the MMG signal for the same set of motions. The requisite theory is presented and two new features based on the EMD and Hilbert spectrum were defined and used in feature extraction. Experimental

results for the same are presented and it is found that the wavelet based feature set and EMD based feature set performed best for classifying movements of hand and wrist using MMG.

7

Conclusions and Future Works

This thesis presents the research work on developing signal processing techniques for upper limb rehabilitation for the elderly, to use in the convenience of their homes. This work was focused at developing signal processing techniques for implementation of an assistive device for the elderly with Electromyography (EMG) and Mechanomyography (MMG). The problem statement is defined in Chapter 1 and current solutions available for the same are evaluated for implementation for elderly rehabilitation. The concept of task-oriented biofeedback has been explained, differentiated it with static biofeedback and stressed its importance in rehabilitation. A review of myoelectric control, different feature extraction methods and the different classifiers used by researchers is carried out and presented.

7.1 Conclusions

The life expectancy of human beings in general, has improved in the last decade throughout the world. With advancing age, the ageing population is likely to be subjected to stroke and neurological degenerative diseases like Parkinsons disease, Dementia or Alzheimers disease and, the agility of the brain to process information critical for going about daily living slows down.

As a result, persons affected by these disorders lose their dexterity, reflexes and speed in performing simple day-to-day tasks. An elderly person is set in his/her ways and would not want to believe that they are losing control of their faculties. They would prefer if the rehabilitative service is available at their homes or nearby their homes. To an elderly person, it would be too troublesome to attach and detach multiple electrodes everyday for measuring biosignals for rehabilitation and they would prefer not to use such a device.

Neuroplasticity is the fundamental issue that supports the scientific basis for treatment of acquired brain injury and dementia with goal-directed experiential therapeutic programs in the context of rehabilitation approaches to the functional consequences of the injury. Physical activity proportionately increases a person's ability to perform physical work. An increasingly repetitive physical activity, known as stressing, can take the form of therapy that includes planned physical conditioning. Stressing is the repetition of a stimulus to produce an analogue effect of faithfully reproduced stimulation. Physiological stressing is the faithful repetition of a stimulus for a significant period of time to produce change in the system.

Rehabilitation robotics exploits this therapeutic effect of neuroplasticity in both in-patient and out-patient rehabilitation. Comprehensive training for basic but necessary tasks for the elderly cannot be given sitting in a clinic or rehabilitation centre. Moreover, these tasks are a closer outlook to the elderly persons actual life; hence, using an assistive robotic system at homes for day-to-day activities could initiate a continuous recovery for the patient instead of only at rehabilitative sessions. Such assistive systems need to be scaled down in terms of the number of the sensors and actuators used, without compromising on the quality of care and end results. This is to ensure that the rehabilitation process doesn't become a burden to the elderly user.

Myoelectric control is the preferred scheme for the control of upper limb prosthesis or orthotic devices. In these systems, the processed EMG signal is used as a control input and the generated result is used to actuate the motor controlling limb movement. To facilitate elderly rehabilitation, the primary aim would be to explore feature extraction and classification methods focussed on the use of a single channel or dual channel EMG or MMG for multi-class hand movement classification.

It is essential to have a good understanding of the measurement protocols to be followed while dealing with different biosignals such as EMG and MMG. Selection of various parameters for EMG measurement such as electrode geometry, shape, size, inter-electrode distance, electrode placement, electrode configuration and skin preparation are essential in ensuring clean and faithful data. For MMG, the accelerometer selection plays a critical role in acquiring the signal and a MMG data acquisition system has been developed in the laboratory for this study. The primary recording sites for EMG and MMG for different motions are identified while keeping the noise levels to a minimum. The use of band-pass filters ensures that only the signal bandwidth is measured. A feedback parameter is important in gauging how well the system is working; hence, different protocols for measuring the EMG-Torque data and the elbow joint angle have been developed.

A pattern classification based system is proposed for distinguishing between six basic hand movements using just two sets of electrodes. Basic time domain features are used with a multilevel perceptron classifier for pattern recognition. The measured EMG data is analysed and the results for classification are not satisfactory. This re-iterates the earlier assumption that the quality of care and end results should not be compromised for using a lesser number of electrodes. A hardware myoelectric glove was built and it fared even worse

than its theoretical counterpart. The EMG signal acquisition was not faithful and large amount of power line interference was present in the data.

While implementing the hardware myoelectric glove, it was observed that the EMG raw signals have a large amount of noise. The signal strength is very low and it is difficult to identify the signal from the raw signal. It was also clear that the noise is predominantly the Power Line Interference (PLI). The magnitude of the power line interference is very high compared to the actual signal strength of the EMG. This is also augmented by the fact that, the signal strength of the elderly person's EMG is much lesser as compared to a young healthy person. The problem with removing the PLI from EMG signal is due to the overlap of the PLI(s) bandwidth with that of the surface EMG signals' bandwidth which lies predominantly in the range of 10 to 350 Hz.

The Hilbert-Huang Transform (HHT) is an attractive solution for the estimation of power line interference in a spectrum of overlapping frequencies. It eliminates the need for an a priori defined functional basis, as is generally required for traditional signal analysis techniques. Being purely data-driven, the HHT precisely determines the most appropriate empirical but adaptive basis. This ability to adapt is crucial, given the individualistic nature of nonlinear systems. Another key feature of the method is that, by utilizing the Hilbert transform, it operates at the scale of one oscillation and is, thus, truly able to track local changes in signals and take into account the variable nature of the power line frequency.

The variable step size of the Least Mean Squares (LMS) algorithm ensures that any changes in the frequency, amplitude and phase of the noise is adapted to using the inputs from the HHT block. An algorithm is designed for estimation of the PLI frequency in the EMG signal using Hilbert-Huang

Transform. Simulations were performed to evaluate the effectiveness of the Hilbert-Huang Transform based Least Mean Squares (HHT-LMS) adaptive filter under different conditions. The HHT-LMS adaptive filter is then applied on experimental data to predict and remove the the PLI component from the measured EMG data.

Feature identification and classification alone is not a robust way for generating control signals for the assistive system as seen while implementing the hardware myoelectric glove. The generation of the control signal for such a case doesn't have any co-relation to the torque that needs to be produced by the actuator. This system is acceptable if the torque required for the movement is not substantial. In other words, smaller joints like the wrists and hand can be actuated using such a control system. But the torque required for the actuation of the joints such as the elbow joint is high and it would be detrimental to use a pattern recognition based system for classifying such motions. The amount of time required to complete a movement is not fixed, and varies from person to person and a pattern recognition based system is unable to predict the in-between states between the initial and final motions. These transient states need to be programmed into the actuator accordingly and there is no surety that it mimics the elderly user's intention.

A hybrid muscle model is designed that combines the muscle physiological model and the neural network to predict the joint torque of the elbow. The predicted results follow the actual joint torque faithfully and the mean square error is minimum of all the different models. Moreover, the time required for executing the hybrid model is directly proportional to the number of iterations required per data point and the constant time required by the neural network for predicting the joint torque. The accuracy of the predicted output is neither just a function of the black box neural network nor dependent on multiple

muscle activation data.

Iterative Learning Control (ILC) is a simple and effective solution to the parameter identification problems of the muscle model which is highly nonlinear and multi-dimensional. ILC method can guarantee the learning process convergence even if the muscle model is partially unknown or difficult to analyze. The use of ILC ensures that that the model doesn't predict unreasonable values for the parameter while simultaneously ensuring that the time required for processing the data is minimized. This is due to the repetitive nature of rehabilitation exercises and the dependency of the predicted output on the previously predicted value and the error calculated. A pointwise ILC is implemented where the data points in the signal are iterated one-by-one till the desired output is the same as the actual system output.

Another method that is useful in assessing activities of skeletal muscles is mechanomyography (MMG) that measures vibrations from contracting muscles. The MMG signals, produced by contracting and vibrating muscle fibers can be interpreted as a mechanical counterpart of EMG signals, as the MMG signal informs about differences in motor units recruitment pattern, degenerative changes in skeletal muscles, and mechanical properties of skeletal muscles (stiffness and vibration) . Despite the different natures of these two signals, each of them gives information about the motor unit recruitment, firing frequency and synchronization that are reflected in the amplitude and frequency of the EMG and MMG signals. However, an apparent advantage of MMG over EMG is that EMG requires meticulous care in attaching the electrodes for measurement while MMG measurements are independent of any such constraints. This could be a boon in elderly rehabilitation as the MMG system can be designed to measure data using accelerometers built into the assistive device itself and, hence, doesn't require any active involvement

of the patient.

A Multilayer Perceptron (MLP) classifier based on time-frequency features is implemented to classify eight different types of forearm movements. Subsequently, the classification of the eight forearm movements based on wavelet transform features and an MLP classifier is presented and it is found to perform better than the time-frequency based classifier. Finally, Empirical Mode Decomposition (EMD) features are extracted from the MMG signal for the same set of motions. The requisite theory is presented and two new features based on the EMD and Hilbert spectrum were defined and used in feature extraction. Experimental results for the same are presented and it is found that the wavelet based feature set and EMD based feature set performed best for classifying movements of hand and wrist using MMG.

Three distinctive methods for processing EMG and MMG were studied and the results are presented in this thesis. The algorithms in this study follow real time constraints for assistive devices while the measurement protocols ensure that the biosignals were broadly representative of that measured from the elderly. Thus, the EMG and MMG signal processing techniques can be used in implementing a sensory system for an upper limb assistive device for the elderly.

7.2 Future Work

The Hill model has many parameters that need to be optimized to get more accurate values of the joint torque with respect to the input single channel EMG signal. Moreover, some of the parameters need to be calculated from existing data and/or derived by iterative methods. An efficient way of estimating the muscle length and the contractile element length using iterative

learning control is currently being implemented. The parameter estimation along with the optimization of the physiological model will give better results for the torque prediction.

Currently, the EMG and MMG sensors are used separately for estimating the different movements, muscle vibrations, the joint angle or the muscle inclination. A fusion of these sensors will ensure that the rehabilitative glove will work in real time. Sensor fusion of the EMG and MMG data along with the angular data can not only eliminate the need to have a higher number of sensors but can also improve upon the classification of different hand movements and the torque prediction of different joints.

A hardware design for the elderly assistive rehabilitation is essential in realising the theories in practice hence, a working prototype needs to be made with adaptive actuator control for implementing the rehabilitative glove in a rehabilitative institute or hospital for clinical trials.

The final aim is total non-dependence on the glove, as it is not intended to act as a substitute for the upper limb. Conducting clinical trials with elderly patients and recording their progress will gauge the time frame required for such independence.

Bibliography

[1] **Report on the Aging Population**. *Committee on Ageing Issues*, 2006.

[2] **The Prevalance of Dementia Worldwide**. *Alzheimer's Disease International*, 2008.

[3] **Health, United States**. *National Center for Health Statistics*, 2011.

[4] **Heart Disease and Stroke Statistics**. *American Heart Association*, 2012.

[5] **World Health Report**. Technical report, 2007.

[6] K.J. Sandin and K.D. Mason. *Manual of Stroke Rehabilitation*. 1996.

[7] M.A. Brown and V.J. Hardman. *Plasticity of vertebrate motoneurons, in Growth and Plasticity of Neural Connections*. Manchester University Press, 1987.

[8] P. Laidler. *Stroke Rehabilitation: Structure and Strategy*. Chapman and Hall, 1996.

[9] P.W. Duncan, L.B. Goldstein, R.D. Horner, P.B. Landsman, G.P. Samsa, and D.B. Matchar. **Similar motor recovery of upper and lower extremity after stroke**. *Stroke*, pages 1181–1188, 1994.

[10] H.S. Jrgensen, H. Nakayama, H.O. Raaschou, J. Vive-Larsen, M. Stier, and Olsen T.S. **Outcome and time course of recovery in**

stroke. *Archives of Physical Medicine and Rehabilitation*, pages 399–405, 1995.

[11] G. Colombo, Wirz M., and Dietz V. **Driven gait orthosis for improvement of locomotor training in paraplegic patients.** *Spinal Cord*, pages 252–255, 2001.

[12] J Hidler, D Nichols, M Pelliccio, K Brady, D.D. Campbell, J.H. Kahn, and T.G. Hornby. **Multicenter randomized clinical trial evaluating the effectiveness of the Lokomat in subacute stroke.** *Neurorehabilitation and Neural Repair,*, pages 5–13, 2009.

[13] K. P. Westlake and C. Patten. **Pilot study of Lokomat versus manual-assisted treadmill training for locomotor recovery post-stroke**. *J Neuroeng Rehabil*, **6**:18, 2009. Westlake, Kelly P Patten, Carolynn England J Neuroeng Rehabil. 2009 Jun 12;6:18.

[14] B.T. Volpe, Krebs H.I., N. Hogan, O.T.R. Edelstein, C. Diels, and M. Aisen. **A novel approach to stroke rehabilitation: Robot-aided sensorimotor stimulation.** *Neurology*, pages 1938–1944, 2000.

[15] M. Thulasidas, G. Cuntai, and J. Wu. **Robust Classification of EEG Signal for BrainComputer Interface.** *IEEE Transactions On Neural Systems And Rehabilitation Engineering*, pages 24–29, 2006.

[16] R Sanchez, Jiayin Liu, S Rao, P Shah, R Smith, T Rahman, S Cramer, J Bobrow, and D Reinkensmeyer. **Automating Arm Movement Training Following Severe Stroke: Functional Exercises With Quantitative Feedback in a Gravity-Reduced Environment**. *Neural Systems and Rehabilitation Engineering, IEEE Transactions on*, **14**(3):378–389, September 2006.

[17] J Stein. **Electromyography-Controlled Exoskeletal Upper-Limb-Powered Orthosis for Exercise Training After Stroke**. *American Journal of Physical Medicine & Rehabilitation*, pages 255–261, 2007.

[18] J.D Moreland, M.A. Thomson, and A.R. FUOCO. **Electromyographic Biofeedback to Improve Lower Extremity Function After Stroke: A Meta-Analysis**. pages 134–140, 1988.

[19] D. Stegeman Moritani, T. and R. Merletti. **Robust Classification of EEG Signal for BrainComputer Interface.** *IEEE Transactions On Neural Systems And Rehabilitation Engineering*, pages 24–29, 2004.

[20] Suzanna M M Martens, Massimo Mischi, S Guid Oei, and Jan W M Bergmans. **An improved adaptive power line interference canceller for electrocardiography.** *IEEE transactions on bio-medical engineering*, **53**(11):2220–2231, November 2006.

[21] S Yacoub and K Raoof. **Noise Removal from Surface Respiratory EMG Signal**. *International Journal of Computer, Information and Systems Science, and Engineering*, **2**(4):226–233, 2008.

[22] J.V. Basmajian and C.J. DeLuca. *Muscles Alive: Their Functions revealed by Electromyography*, pages 59–60. 5th edition, 1985.

[23] Michal Meller Maciej Niedz'wiecki. **New Algorithms for Adaptive Notch Smoothing**. *IEEE Transactions on Signal Processing*, **59**(5), 2011.

[24] Simon Haykin. *Adaptive Filter Theory*. Prentice Hall, 4th edition.

[25] P Heinonen, T Saramaki, J Malmivuo, and Y Neuvo. **Periodic Interference Rejection using Coherent Sampling and Waveform Estimation**. *IEEE Transactions on Circuits and Systems*, **31**(5):438–446, 1984.

[26] A Pomsathit, P Wattanaluk, O Sangaroon, and C Benjagkaprasert. **Variable Step-size Algorithm for Lattice Form Structure Adaptive IIR Notch Filter**. In *Proceedings of IEEE Communications Circuits and Systems*, pages 332–335.

[27] B.C. Taylor S.Acharya, D.H. Mugler. **A Fast Adaptive Fitler for Electrocardiography**. In *Proceedings of IEEE Bioengineering Conference*, pages 106–107.

[28] M Malboubi, F Razzazi, and S.M Aliyari. **Elimination of power line noise from EMG signals using an efficient adaptive Laguerre filter**. In *Signals and Electronic Systems (ICSES), 2010 International Conference on*, pages 49–52, 2010.

[29] Chavdar Levkov, Georgy Mihov, Ratcho Ivanov, Ivan Daskalov, Ivaylo Christov, and Ivan Dotsinsky. **Removal of power-line interference from the ECG: a review of the subtraction procedure**. *BioMedical Engineering OnLine*, **4**(1):50, 2005.

[30] A.-O Boudraa and J.-C Cexus. **EMD-Based Signal Filtering**. *Instrumentation and Measurement, IEEE Transactions on*, **56**(6):2196–2202, 2007.

[31] P. A. Parker, K. B. Englehart, and B. S. Hudgins. *Electromyography: Physiology, Engineering, and Noninvasive Applications*, chapter Control of Powered Upper Limb Prostheses. John Wiley & Sons, Inc., 2005.

[32] J.P. Giuffrida, A. Lerner, R. Steiner, and J. Daly. **Upper-Extremity Stroke Therapy Task Discrimination Using Motion Sensors and Electromyography**. *Neural Systems and Rehabilitation Engineering, IEEE Transactions on*, **16**(1):82 –90, feb. 2008.

[33] J.U Chu. **A Supervised Feature-Projection based Real-Time EMG Pattern Recognition for Multifunction Myoelectric Hand Control**. *IEEE/ASME Transactions on Mechatronics*, pages 282–290, 2007.

[34] B Hudgins, P Parker, and R.N. Scott. **New startergy for multifunction myoelectric control**. *IEEE Transactions on Biomedical Engineering*, pages 82–94, 1993.

[35] K Englehart and B Hudgins. **A robust, real-time control scheme for multifunction myoelectric control**. *IEEE Transactions on Biomedical Engineering*, 2003.

[36] K Englehart, B Hudgins, P Parker, and M Stevenson. **Time-frequency representation for classification of the transient myoelectric signal**. *Engineering in Medicine and Biology Society, 1998. Proceedings of the 20th Annual International Conference of the IEEE*, **5**:2627–2630 vol.5, 1998.

[37] K Englehart, B Hudgins, and P Parker. **A Wavelet Based Continuous Classification Scheme for Multifunction Myoelectric Control**. *IEEE Transactions on Biomedical Engineering*, **48**(3):302–311, 2001.

[38] M Yoshikawa, M Mikawa, and K Tanaka. **Real-Time Hand Motion Estimation Using EMG Signals with Support Vector Machines**. In *International Joint Conference SICE-ICASE*, pages 593–598, 2006.

[39] R Khushaba, A Al-Jumaily, and A Al-Ani. **Novel feature extraction method based on fuzzy entropy and wavelet packet transform for myoelectric Control**. *Communications and Information Technologies, 2007. ISCIT '07. International Symposium on*, pages 352–357, October 2007.

[40] Ali H Al-Timemy, Guido Bugmann, Nicholas Outram, and Javier Escudero. **Single channel-based myoelectric control of hand move-**

ments with Empirical Mode Decomposition. In *Engineering in Medicine and Biology Society,EMBC, 2011 Annual International Conference of the IEEE*, pages 6059–6062, 2011.

[41] B. Hudgins, P. Parker, and R.N. Scott. **A new strategy for multifunction myoelectric control**. *Biomedical Engineering, IEEE Transactions on*, **40**(1):82 –94, jan. 1993.

[42] A.V. Hill. **The heat of shortening and the dynamic constants of muscle.** *Proceedings of Royal Society of London Series B-Biological Sciences.* ., **126**:136–195, 1938.

[43] H Hatze. **A myocybernetic control model of skeletal muscle**. *Biological cybernetics*, **25**(2):103–119, 1977.

[44] H Hatze. **A complete set of control equations for the human musculo-skeletal system**. *Journal of biomechanics*, 1977.

[45] H Hatze. **A three-dimensional multivariate model of passive human joint torques and articular boundaries**. *Clinical Biomechanics*, **12**(2):128–135, 1997.

[46] Herbert Hatze. *Myocybernetic Control Models of Skeletal Muscle: Characteristics and Applications*. University of South Africa, 1981.

[47] A.L. Hof and Jw. Van den Berg. **EMG to force processing I: An electrical analogue of the hill muscle model**. *Journal of Biomechanics*, **14**(11):747 – 758, 1981.

[48] A.L. Hof and Jw. Van den Berg. **EMG to force processing II: Estimation of parameters of the Hill muscle model for the human triceps surae by means of a calfergometer**. *Journal of Biomechanics*, **14**(11):759 – 770, 1981.

[49] A.L. Hof and Jw. Van den Berg. **EMG to force processing III: Estimation of model parameters for the human triceps surae muscle and assessment of the accuracy by means of a torque plate**. *Journal of Biomechanics*, **14**(11):771 – 785, 1981.

[50] A.L. Hof and Jw. Van den Berg. **EMG to force processing IV: Eccentric-concentric contractions on a spring-flywheel set up**. *Journal of Biomechanics*, **14**(11):787 – 792, 1981.

[51] Zajac. **Neuromuscular and Musculoskeletal Control Models for the Human Leg**. In *American Control Conference, 1983*, pages 229–234, 1983.

[52] J M Winters and L Stark. **Analysis of fundamental human movement patterns through the use of in-depth antagonistic muscle models.** *IEEE Transactions on Biomedical Engineering*, **32**(10):826–839, October 1985.

[53] J M Winters and L Stark. **Estimated mechanical properties of synergistic muscles involved in movements of a variety of human joints.** *Journal of biomechanics*, **21**(12):1027–1041, 1988.

[54] R Riener and J Quintern. **Biomechanical model of the human knee evaluated by neuromuscular stimulation**. *Journal of biomechanics*, 1996.

[55] Riener. **Patient-driven control of FES-supported standing up: a simulation study**. *Rehabilitation Engineering, IEEE Transactions on*, **6**(2):113–124, 1998.

[56] Riener. **Patient-driven control of FES-supported standing up and sitting down: experimental results**. *Rehabilitation Engineering, IEEE Transactions on*, **8**(4):523–529, 2000.

[57] K Ullah and Jung-Hoon Kim. **A mathematical model for mapping EMG signal to joint torque for the human elbow joint using non-linear regression**. In *Autonomous Robots and Agents, 2009. ICARA 2009. 4th International Conference on*, pages 103–108, 2009.

[58] K. K. Mankala, S. K. Banala, and S. K. Agrawal. **Novel swing-assist un-motorized exoskeletons for gait training**. *J Neuroeng Rehabil*, **6**:24, 2009. Mankala, Kalyan K Banala, Sai K Agrawal, Sunil K HD38582/HD/NICHD NIH HHS/ R01 HD038582-09/HD/NICHD NIH HHS/ England J Neuroeng Rehabil. 2009 Jul 3;6:24.

[59] G. S. Sawicki and D. P. Ferris. **A pneumatically powered knee-ankle-foot orthosis (KAFO) with myoelectric activation and inhibition**. *J Neuroeng Rehabil*, **6**:23, 2009. Sawicki, Gregory S Ferris, Daniel P England J Neuroeng Rehabil. 2009 Jun 23;6:23.

[60] J.G Hincapie, D Blana, E Chadwick, and R.F Kirsch. **Neural Network Controller for an Upper Extremity Neuroprosthesis**. In *Neural Engineering, 2005. Conference Proceedings. 2nd International IEEE EMBS Conference on*, pages 392–395, 2005.

[61] J.G Hincapie and R.F Kirsch. **Feasibility of EMG-Based Neural Network Controller for an Upper Extremity Neuroprosthesis**. *Neural Systems and Rehabilitation Engineering, IEEE Transactions on*, **17**(1):80–90, 2009.

[62] H H Savelberg and W Herzog. **Prediction of dynamic tendon forces from electromyographic signals: an artificial neural network approach.** *Journal of neuroscience methods*, **78**(1-2):65–74, December 1997.

[63] M M Liu, W Herzog, and H H Savelberg. **Dynamic muscle force predictions from EMG: an artificial neural network approach.** *Journal of Electromyography and Kinesiology*, **9**(6):391–400, December 1999.

[64] Lin Wang and Thomas S Buchanan. **Prediction of joint moments using a neural network model of muscle activations from EMG signals.** *IEEE transactions on neural systems and rehabilitation engineering : a publication of the IEEE Engineering in Medicine and Biology Society*, **10**(1):30–37, March 2002.

[65] J M Winters and L Stark. **Muscle models: What is gained and what is lost by varying model complexity**. *Biological cybernetics*, **55**(6):403–420, March 1987.

[66] Hua Cao, S Boudaoud, F Marin, and C Marque. **Optimization of input parameters of an EMG-force model in constant and sinusoidal force contractions**. In *Engineering in Medicine and Biology Society, 2009. EMBC 2009. Annual International Conference of the IEEE*, pages 4962–4965, 2009.

[67] E.E. Cavallaro, J Rosen, J.C. Perry, and S. Burns. **Real-Time Myoprocessors for a Neural Controlled Powered Exoskeleton Arm**. *IEEE Transactions on Biomedical Engineering*, **53**(11):2387–2396, November 2006.

[68] Cavallaro. **Hill-Based Model as a Myoprocessor for a Neural Controlled Powered Exoskeleton Arm - Parameters Optimization**. In *Robotics and Automation, 2005. ICRA 2005. Proceedings of the 2005 IEEE International Conference on*, pages 4514–4519, 2005.

[69] Weijie Wang. **Selection of optimization methods for estimating muscle parameters during walking**. In *Electronic Measurement Instruments, 2009. ICEMI '09. 9th International Conference on*, pages 4–523 –4–526, aug. 2009.

[70] R.N Khushaba, A Al-Ani, and A Al-Jumaily. **Swarm Intelligence based Dimensionality Reduction for Myoelectric Control**. In *Intel-*

ligent Sensors, Sensor Networks and Information, 2007. ISSNIP 2007. 3rd International Conference on, pages 577–582, 2007.

[71] K Akataki, K Mita, M Watakabe, and K Ito. **Age-related change in motor unit activation strategy in force production: a mechanomyographic investigation.** *Muscle Nerve*, **25**:505–512., 2002.

[72] A Jasko lska, K Kisiel, W Brzenczek, and A. Jaskolski. **EMG and MMG of synergists and antagonists during relaxation at three joint angles.** *Eur J Appl Physiol Occup Physiol*, **90**:58–68., 2003.

[73] C Orizio, F Esposito, I Paganotti, L Marino, B Rossi, and A. Veicsteinas. **Electrically-elicited surface mechanomyogram in myotonic dystrophy.** *Ital J Neurol Sci*, **18**:185190, 1997.

[74] C Orizio, B Diemont, F Esposito, E Alfonsi, G Parrinello, and A. Moglia. **Surface mechanomyogram reflects the changes in the mechanical properties of muscle at fatigue.** *Eur J Appl Physiol Occup Physiol*, **80**:276284, 1999.

[75] T Beck, T Housh, G Johnson, and J Weir. **Mechanomyographic and electromyographic time and frequency domain responses during submaximal to maximal isokinetic muscle actions of the biceps brachii**. *European journal of Applied Physiology*, 2004.

[76] T Beck, T Housh, G Johnson, and J Weir. **Mechanomyographic amplitude and mean power frequency versus torque relationships during isokinetic and isometric muscle actions of the biceps brachii**. *Journal of Electromyography and Kinesiology*, 2004.

[77] Travis W Beck, Terry J Housh, Glen O Johnson, Joseph P Weir, Joel T Cramer, Jared W Coburn, and Moh H Malek. **Comparison of Fourier and wavelet transform procedures for examining**

the mechanomyographic and electromyographic frequency domain responses during fatiguing isokinetic muscle actions of the biceps brachii. *Journal of Electromyography and Kinesiology*, **15**(2):190–199, April 2005.

[78] Travis W Beck, Terry J Housh, Glen O Johnson, Joel T Cramer, Joseph P Weir, Jared W Coburn, and Moh H Malek. **Comparison of the fast Fourier transform and continuous wavelet transform for examining mechanomyographic frequency versus eccentric torque relationships.** *Journal of neuroscience methods*, **150**(1):59–66, January 2006.

[79] Jared W Coburn, Terry J Housh, Moh H Malek, Joseph P Weir, Joel T Cramer, Travis W Beck, and Glen O Johnson. **Mechanomyographic and electromyographic responses to eccentric muscle contractions.** *Muscle & nerve*, **33**(5):664–671, May 2006.

[80] Travis W Beck, Terry J Housh, Andrew C Fry, Joel T Cramer, Joseph P Weir, Brian K Schilling, Michael J Falvo, and Christopher A Moore. **A wavelet-based analysis of surface mechanomyographic signals from the quadriceps femoris.** *Muscle & nerve*, **39**(3):355–363, March 2009.

[81] J Silva, T Chau, and A Goldenberg. **MMG-based multisensor data fusion for prosthesis control**. *Engineering in Medicine and Biology Society, 2003. Proceedings of the 25th Annual International Conference of the IEEE*, **3**:2909–2912 Vol.3, 2003.

[82] J Silva, W Heim, and T Chau. **MMG-based classification of muscle activity for prosthesis control**. *Engineering in Medicine and Biology Society, 2004. IEMBS '04. 26th Annual International Conference of the IEEE*, **1**:968–971, 2004.

[83] J Silva and T Chau. **A mathematical model for source separation of MMG signals recorded with a coupled microphone-accelerometer sensor pair**. *Biomedical Engineering, IEEE Transactions on*, **52**(9):1493–1501, 2005.

[84] A O Posatskiy and T Chau. **The effects of motion artifact on mechanomyography: A comparative study of microphones and accelerometers.** *Journal of electromyography and kinesiology : official journal of the International Society of Electrophysiological Kinesiology*, **22**(2):320–324, 2011.

[85] Natasha Alves and Tom Chau. **Uncovering patterns of forearm muscle activity using multi-channel mechanomyography.** *Journal of electromyography and kinesiology : official journal of the International Society of Electrophysiological Kinesiology*, **20**(5):777–786, October 2010.

[86] Natasha Alves and Tom Chau. **Stationarity distributions of mechanomyogram signals from isometric contractions of extrinsic hand muscles during functional grasping**. *Journal of Electromyography and Kinesiology*, **18**(3):509 – 515, 2008.

[87] Hong-Bo Xie, Yong-Ping Zheng, and Jing-Yi Guo. **Classification of the mechanomyogram signal using a wavelet packet transform and singular value decomposition for multifunction prosthesis control.** *Physiological measurement*, **30**(5):441–457, May 2009.

[88] K Shima and T Tsuji. **An MMG-based human-assisting manipulator using acceleration sensors**. *Systems, Man and Cybernetics, 2009. SMC 2009. IEEE International Conference on*, pages 2433–2438, 2009.

[89] Yong Zeng, Zhengyi Yang, Wei Cao, and Chunming Xia. **Hand-motion patterns recognition based on mechanomyographic signal**

analysis. In *BioMedical Information Engineering, 2009. FBIE 2009. International Conference on Future*, pages 21–24, 2009.

[90] G.L Soderberg. **Recording Techniques, in Selected Topics in Surface Electromyography for Use in the Occupational Setting-**. In *Expert Perspective*, pages 75–82, 1989.

[91] G.L Soderberg. **Recording Techniques.** *Selected Topics in Surface Electromyography for Use in the Occupational Setting*, 1992.

[92] J.R Cram and D Rommen. **Effects of Skin Preparation on Data Collected Using an EMG Muscle-Scanning Procedure**. In *Biofeedback and Self-Regulation*, pages 75–82, 1989.

[93] Moh H. Malek, Terry J. Housh, Jared W. Coburn, Joseph P. Weir, Richard J. Schmidt, and Travis W. Beck. **The effects of interelectrode distance on electromyographic amplitude and mean power frequency during incremental cycle ergometry**. *Journal of Neuroscience Methods*, **151**(2):139 – 147, 2006.

[94] L Mesin, R Merletti, and A Rainoldi. **Surface EMG: The issue of electrode location**. *Journal of Electromyography and Kinesiology*, **19**(5):719–726, October 2009.

[95] **Surface Electromyography: Detection and Recording**. *Delsys Inc.*, 2002.

[96] K Nishihara, H Kawai, T Gomi, M Terajima, and Y Chiba. **Investigation of Optimum Electrode Locations by Using an Automatized Surface Electromyography Analysis Technique**. *IEEE Transactions of Biomedical Engineering*, **55**(2):636–642, 2008.

[97] L Hargrove, K Englehart, and B Hudgins. **A Comparison of Surface and Intramuscular Myoelectric Signal Classification**. *Biomedical Engineering, IEEE Transactions on*, **54**(5):847–853, May 2007.

[98] K Nazarpour. **Surface EMG signals pattern recognition utilizing an adaptive crosstalk suppression preprocessor**. *Computational Intelligence Methods and Applications, 2005 ICSC Congress on*, 2005.

[99] Christian Jutten and Jeanny Herault. **Blind separation of sources, part I: An adaptive algorithm based on neuromimetic architecture**. *Signal Processing*, **24**(1):1–10, July 1991.

[100] D.A Winter, A.J Fuglevand, and S.E Archer. **Crosstalk in Surface Electromyography: Theoretical and Practical Estimates**. *Journal of Electromyography and Kinesiology*, pages 15–26, 1994.

[101] C.D.B Orizio, F Esposito, E Alfonsi, G Parrinello, and A Moglia. **Surface mechanomyogram reflects the changes in the mechanical properties of muscle at fatigue**. *European Journal of Applied Physiology and Occupupational Physiology*, **80**:276–284, June 1999.

[102] M Watakabe, K Akataki, and K Mita. **Mechanical behaviour of condenser microphone in mechanomyography**. *Medical & biological engineering & computing*, **39**(2):195–201, 2001.

[103] M Watakabe, Y Itoh, and K Mita. **Technical aspects of mechanomyography recording with piezoelectric contact sensor**. *Medical & biological engineering & computing*, **36**(5):557–567, 1998.

[104] J.U Rainoldi. **Repeatability of maximal voluntary force and of surface EMG variables during voluntary isometric contraction of quadriceps muscles in healthy subjects**. *Journal of Electromyography and Kinesiology*, pages 425–438, 2001.

[105] R.O. Duda, P. E. Hart, and D. G. Stork. *Pattern Classification.* Wiley, New York, 2001.

[106] B Widrow, J.R. Jr Glover, J.M McCool, J Kaunitz, C.S Williams, R.H Hearn, J.R Zeidler, Jr Eugene Dong, and R.C Goodlin. **Adaptive noise cancelling: Principles and applications**. In *Proceedings of the IEEE*, pages 1692–1716, 1975.

[107] Zhao Zhidong and Ma Chan. **2008 11th IEEE International Conference on Communication Technology**. In *2008 11th IEEE International Conference on Communication Technology (ICCT 2008)*, pages 517–520. IEEE, 2008.

[108] Steven R. Long Manli C. Wu Hsing H. Shih Quanan Zheng Nai-Chyuan Yen Chi Chao Tung Henry H. Liu Norden E. Huang, Zheng Shen. **The empirical mode decomposition and the Hilbert spectrum for nonlinear and non-stationary time series analysis**. *Proceeding of R.Soc.Lond.A*, **454**:903–995, 1998.

[109] Daniel N Kaslovsky and Francois G Meyer. **Noise Corruption of Empirical Mode Decomposition and Its Effect on Instantaneous Frequency**. *arXiv.org*, **physics.data-an**, August 2010.

[110] S Acharya, D.H Mugler, and B.C Taylor. **A fast adaptive filter for electrocardiography**. In *Bioengineering Conference, 2004. Proceedings of the IEEE 30th Annual Northeast*, pages 106–107, 2004.

[111] M Malboubi, F Razzazi, M.A Sh, and A Davari. **Power line noise elimination from EMG signals using adaptive Laguerre filter with fuzzy step size**. In *Biomedical Engineering (ICBME), 2010 17th Iranian Conference of*, pages 1–4, 2010.

[112] Razzazi F. & Aliyari S. M. Malboubi, M. **Elimination of power line noise from EMG signals using an efficient adaptive Laguerre filter.** In *International Conference on Signals and Electronic Systems (ICSES)*, pages 49–52.

[113] P Flandrin, G Rilling, and P Goncalves. **Empirical mode decomposition as a filter bank**. *Signal Processing Letters, IEEE*, **11**(2):112–114, 2004.

[114] Norden E Huang. *Hilbert-Huang Transform and its Applications*, chapter HHT and problems. World Scientific Publishing, 2005.

[115] Z Wu and N.E. Huang. **A study of the characteristics of white noise using the empirical mode decomposition method**. *Proceedings to Royal Society of London*, **460**:1597–1611, 2004.

[116] Herbert Hatze. **A teleological explanation of Weber's law and the motor unit size law**. *Bulletin of Mathematical Biology*, **41**(3):407–425, May 1979.

[117] H Hatze. **The fundamental problem of myoskeletal inverse dynamics and its implications**. *Journal of biomechanics*, **35**(1):109–115, 2002.

[118] Kurt Manal, Roger V Gonzalez, David G Lloyd, and Thomas S Buchanan. **A real-time EMG-driven virtual arm.** *Computers in biology and medicine*, **32**(1):25–36, January 2002.

[119] Kurt Manal and Thomas S Buchanan. **A one-parameter neural activation to muscle activation model: estimating isometric joint moments from electromyograms.** *Journal of biomechanics*, **36**(8):1197–1202, August 2003.

[120] J. M. Winters and L. Stark. **Analysis of fundamental human movement patterns through the use of in-depth antagonistic muscle models**. *IEEE Transactions on Biomedical Engineering*, **32**:826–839, 1985.

[121] WM Murray and SL Delp. **Variation of muscle moment arms with elbow and forearm position**. *Journal of Biomechanics*, **28**(5):513–525, 1995.

[122] B A Garner and M G Pandy. **A Kinematic Model of the Upper Limb Based on the Visible Human Project (VHP) Image Dataset.** *Computer methods in biomechanics and biomedical engineering*, **2**(2):107–124, 1999.

[123] Mary D. Klein Breteler, Cornelis W. Spoor, and Frans C.T. Van der Helm. **Measuring muscle and joint geometry parameters of a shoulder for modeling purposes**. *Journal of Biomechanics*, **32**(11):1191 – 1197, 1999.

[124] Iain W. Charlton and Garth R. Johnson. **Application of spherical and cylindrical wrapping algorithms in a musculoskeletal model of the upper limb**. *Journal of Biomechanics*, **34**(9):1209 – 1216, 2001.

[125] B A Garner and M G Pandy. **The Obstacle-Set Method for Representing Muscle Paths in Musculoskeletal Models.** *Computer methods in biomechanics and biomedical engineering*, **3**(1):1–30, 2000.

[126] B A Garner and M G Pandy. **Musculoskeletal model of the upper limb based on the visible human male dataset.** *Computer methods in biomechanics and biomedical engineering*, **4**(2):93–126, February 2001.

[127] J Rosen. **Performances of Hill-Type and Neural Network Muscle Models—Toward a Myosignal-Based Exoskeleton**. *Computers and Biomedical Research*, **32**(5):415–439, October 1999.

[128] H. Huang, S. L. Wolf, and J. He. **Recent developments in biofeedback for neuromotor rehabilitation**. *Journal of Neuroengineering Rehabilitation*, **3**:11, 2006. Huang, He Wolf, Steven L He, Jiping N01-HD 3-3353/HD/NICHD NIH HHS/ England J Neuroeng Rehabil. 2006 Jun 21;3:11.

[129] Jian-Xin Xu and Zenn Z. Bien. **Iterative learning control**. chapter The frontiers of iterative learning control, pages 9–35. Kluwer Academic Publishers, Norwell, MA, USA, 1998.

[130] Jian-Xin Xu, Tong Heng Lee, and Heng-Wei Zhang. **Analysis and comparison of iterative learning control schemes**. *Engineering Applications in Artificial Intelligence*, **17**(6):675–686, September 2004.

[131] T D'Alessio. **Analysis of a Digital EMG Signal Processor in Dynamic Conditions**. *Biomedical Engineering, IEEE Transactions on*, (1):78–82, 1985.

[132] Jing-Yi Guo, Yong-Ping Zheng, Hong-Bo Xie, and Xin Chen. **Continuous monitoring of electromyography (EMG), mechanomyography (MMG), sonomyography (SMG) and torque output during ramp and step isometric contractions.** *Medical Engineering and Physics*, **32**(9):1032–1042, November 2010.

[133] J Weir, K Ayers, and J Lacefield. **Mechanomyographic and electromyographic responses during fatigue in humans: influence of muscle length**. *European journal of Applied Physiology*, 2000.

[134] Liping Qi, James M Wakeling, and Martin Ferguson-Pell. **Spectral properties of electromyographic and mechanomyographic signals during dynamic concentric and eccentric contractions of the human biceps brachii muscle.** *Journal of electromyography and kinesiology :*

official journal of the International Society of Electrophysiological Kinesiology, **21**(6):1056–1063, December 2011.

[135] Fabio Esposito, Emiliano Ce, Susanna Rampichini, and Arsenio Veicsteinas. **Acute passive stretching in a previously fatigued muscle: Electrical and mechanical response during tetanic stimulation.** *Journal of sports sciences*, **27**(12):1347–1357, October 2009.

[136] Fabio Esposito, Eloisa Limonta, and Emiliano Ce. **Time course of stretching-induced changes in mechanomyogram and force characteristics.** *Journal of electromyography and kinesiology : official journal of the International Society of Electrophysiological Kinesiology*, **21**(5):795–802, October 2011.

[137] Shi-Liu Tian, Yu Liu, Li Li, Wei-Jie Fu, and Chien-Hua Peng. **Mechanomyography is more sensitive than EMG in detecting age-related sarcopenia**. *Journal of biomechanics*, **43**(3):551–556, 2010.

[138] W Jeffrey Armstrong. **Wavelet-based intensity analysis of mechanomyographic signals during single-legged stance following fatigue.** *Journal of Electromyography and Kinesiology*, October 2011.

[139] P Parker and R Merletti. **Surface Mechanomyogram**. *Electromyography:Physiology, Engineering, and Non-Invasive Applications*, pages 305–322, 2005.

Publications

Published

Conference Proceedings:

1. **Sasidhar Sangit, Panda, S.K., Xu, J**., *Design of a Myoelectric Glove for Upper Limb Stroke Rehabilitation*, ICREATE, April 2009.

2. **Sasidhar Sangit, Panda, S.K., Xu, J**., *A Real Time Control Algorithm for a Myoelectric Glove for the Rehabilitation of Wrist and Elbow of stroke Patients*, ICCA, June 2010.

Book Chapter:

1. **Y.K. Tan and Sangit Sasidhar**, "*Engineering Better Electric-Powered Wheelchairs To Enhance Rehabilitative and Assistive Needs of Disabled and Aged Populations*", Rehabilitation Engineering, I-Tech Education and Publishing KG, ISBN 978-953-7619-37-4, 2010.

Submitted for Review

1. **Sasidhar Sangit, Panda, S.K., Xu, J**., *Feature Extraction and Classification of forearm muscle Mechanomyography using Empirical Mode Decomposition.* , submitted for review to IEEE Transactions in Biomedical Engineering.

2. **Sasidhar Sangit, Panda, S.K., Xu, J**., *A modified Hilbert-Huang Transform based Adaptive Filter for Elimination of Power line Interference from Surface Electromyography* , submitted for review to Journal of Electromyography and Kinesiology.

3. **Sasidhar Sangit, Panda, S.K., Xu, J**., *An Iterative Learning Predictor for the parameter estimation of a Hybrid Muscle Model* , submitted for review to Computer Methods and Programs in Biomedicine.